lower than in our own measurements (it should be emphasized that our values were controlled by different methods). Also the numerous measurements at Mainz show no decrease with very good visibility. According to measurements by LOEHLE and FOITZIK and the theoretical investigations by JUNGE ([6]), the decrease of α_{vis} with visibility- ranges below 2 km in Mainz is only found with relative humidities greater than 97 per cent; in Fig. 5 such cases are not considered.

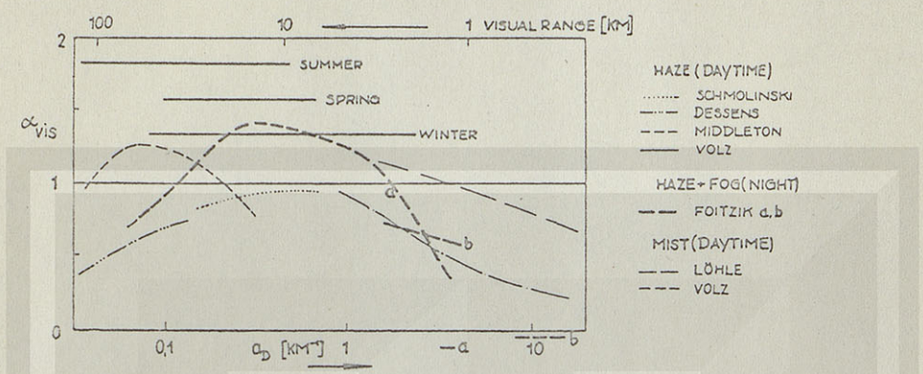

Fig. 5 - ÅNGSTRÖM *exponents of visibility according to some authors* ([5]).

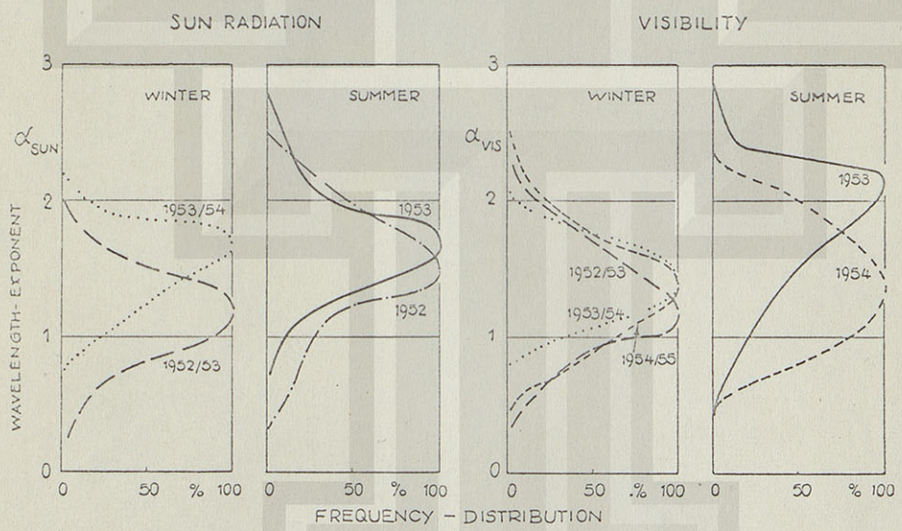

Fig. 6 - *The relative frequency of the* ÅNGSTRÖM *exponents* α_{sun} *and* α_{vis} *for winter and summer in different years.*

The results for α_{sun} and α_{vis} for three years are summarized in Fig. 6 by a frequency distribution. The annual variation seems to be more significant for α_{vis} than for α_{sun}. No influence of the sky-light scattering types or the meteorological situation could be found.

On many days γ_{vis} and γ_{sun} are measured at the same time. The results are shown in Fig. 7, the mean ratio of both values is 1.

How can we explain these results? According to the relation $\alpha = \nu - 2$, the nuclei distribution (at least in the range of optical efficiency) would have an annual variation. The mean power law should be $r^{-3.5}$ in winter and in summer $r^{-3.5}$ to r^{-4}. This occurs especially near the earth's surface, but also in the ground layer and perhaps in the whole atmosphere. Until now neither the measurements of JUNGE nor the analyses of scattered sky-light give a basis for this conclusion. On the contrary, the author has the suspicion that $\alpha = \nu - 2$ is not exactly valid. This may be caused by an annual variation of the absorption

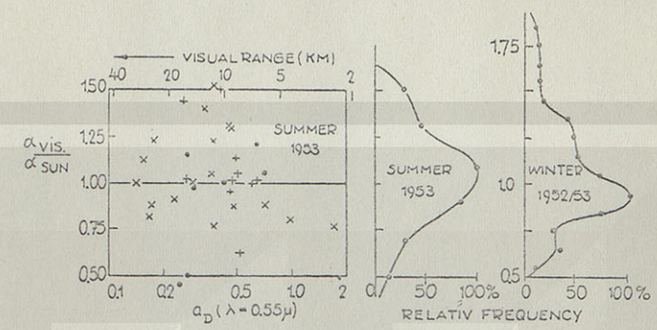

Fig. 7 - *The relation ship between α_{vis} and α_{sun}, measured at the same time.*

of light by the aerosol, but this assumption is improbable, because the absorption very probably is small and not essential. It may be noticed that it is also difficult to explain the reason of the anomal extinction of haze in the near UV, which has been measured sometimes by GOETZ (7), DUNKELMAN (8) and now at Mainz (9). By the optical theory, the anomal haze extinction requires that a sharp maximum of the nuclei distribution exists near 0.2μ radius. It is not known, that this is possible with normal turbidity circumstances.

The previous discussion of the results shows that still many problems in the optics of the atmospheric aerosol are to be clarified. Simultaneous measurements of the nuclei distribution and the optical effects are highly desirable.

LITERATURE

(1) JUNGE, CHR., Tellus 5, 1, (1953). — (2) VOLZ, F., Ber. Dtsch. Wetterd. 2, Nr. 13 (1954). — (3) SCHUEPP, W., Archiv. Met. Geoph. Biokl. B, 1, 257 (1949). — (4) WEMPE, J., Astron. Nachr. 275, 1 (1947). — (5) SCHMOLINSKI, F., Met. Zeitschr., 61, 199 (1944). DESSENS, H., Ann. Geoph. 2, 68 (1946); MIDDLETON, W. E. K., Beitr. Geophys., 44, 358 (1935); FOITZIK, L., & ZSCHAECK, H., Zs. Meteor., 7, 1 (1953); FOITZIK, L., Wiss. Abh. Reichsamt Wetterd. 4, Nr. 5 (1938); LOEHLE, F., Zs. Phys., 45, 199 (1944). — (6) JUNGE, CHR., Journ. Met., 12, 24 (1955). — (7) GOETZ, F. W. P., Met. Zs., 51, 472 (1934). — (8) DUNKELMAN, L., Nav. Res. Lab. Washington D. C., NRL Rep. 4031, (1952). — (9) MICHLOWISKI, J., Diplomarbeit Mainz 1955 (unpublished).

JOURNAL OF GEOPHYSICAL RESEARCH VOLUME 60, No. 3 SEPTEMBER, 1955

DAY SKY BRIGHTNESS TO 220 KM

BY OTTO E. BERG

United States Naval Research Laboratory, Washington 25, D.C.

(Received March 15, 1955)

ABSTRACT

The brightness of the daytime sky has been measured using rocket-borne stereocameras. An upper limit of 0.0075 candle/ft^2 was found for the brightness at altitudes ranging from 80 to 220 km. This limit is consistent with the brightness being due entirely to Rayleigh scattering. No evidence of high altitude clouds was found.

INTRODUCTION

During the past few years, experiments have been conducted for the purpose of determining the brightness of the daytime sky at high altitudes. The principal point in question was whether the emission by the upper atmosphere could be explained as chiefly Rayleigh scattering by air molecules, or whether there were, in addition, strong emissions due to resonance radiation, and perhaps scattering by extremely high altitude particles and noctilucent clouds.

This paper presents the techniques and results of a recent rocket-borne photographic investigation of the daytime sky in the altitude range of 80 to 220 km. These results showed that the daytime sky at high altitudes did not have brightness in excess of that expected from Rayleigh scattering alone, and also that sunlight scattered from gas and material emanating from the rocket may have contributed to the high value reported by Miley [see 1 of "References" at end of paper].

As corroboration of statements made in this paper, series of pictures are presented in the appendix showing the sensitivity and validity of the stereoscopic system and the effects of scattered sunlight.

PAST MEASUREMENTS

Photometric measurements made by Teele [2] from the stratosphere balloon-flight of 1935 (*Explorer II*) indicate a linear relationship between atmospheric pressure and sky brightness to 72,000 feet. This linear relationship is just that expected on the basis of the sky brightness being due to Rayleigh scattering alone and is reproduced in Figure 1. The lower portion of the curve, of course, is an extrapolation. An altitude scale based on the Rocket Panel standard atmosphere [3] has been added for convenience in computing sky brightness for altitudes corresponding to those of rockets.

In a series of investigations using high altitude rockets as the transport laboratory, H. A. Miley, *et al.* [1], recently reported new and high values of the day sky brightness at high altitudes. They used photomultipliers and found a brightness

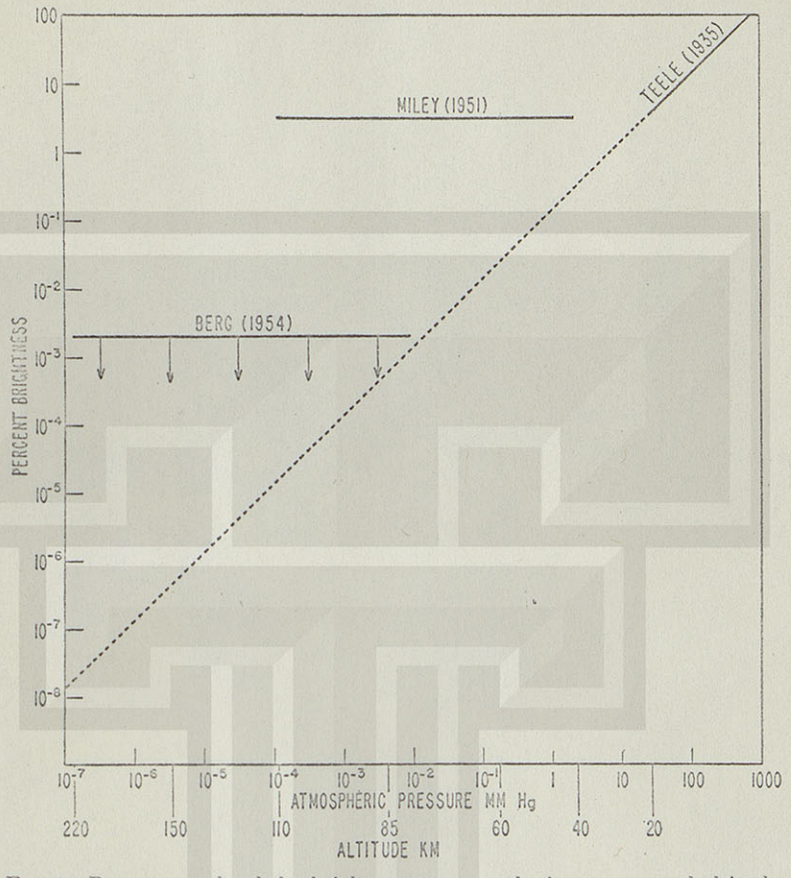

FIG. 1—Per cent sea-level sky brightness *vs* atmospheric pressure and altitude

of nearly a constant three per cent of the sea-level value for altitudes of from 40 to 130 km. Their measurement is included in Figure 1. The sky brightness predicted from Rayleigh scattering alone at these respective levels can be seen from Figure 1 to range from 0.3 per cent to 10^{-4} per cent of sea-level brightness.

Included in Miley's report are interesting photographs of overhead clouds of some sort taken on one flight at 70 km with a 16-mm camera operating at 6.67 frames per second. The exposure was 1/400 second at F/4.5 on Eastman Linagraphic film. These he interpreted to be true clouds of the noctilucent type and were thought to be associated with the high recorded sky brightness.

PURPOSE AND EXPERIMENTAL PROCEDURE

A simple photographic experiment was designed to investigate sky brightness at high altitudes. The four objectives of the experiment were as follows:

(1) To record, photographically, the brightness of the sky at known points in the sky during flight

(2) To take stereophotographs of any high-altitude cloud formations in order to determine their proximity to the rocket

(3) To determine, by comparison of photographs taken through red and blue filters, whether the clouds were of large particles and scattered neutrally, or whether they were of very small particles and scattered like the sky itself
(4) To determine whether the light from the clouds and sky was polarized or not, since, if not, the explanation of the clouds would lie in scattering by large particles or a true airglow emission, rather than Rayleigh scattering by air molecules and small particles

Figure 2 shows the unit assembled and ready for flight. It comprises two modified and armored 16-mm GSAP gun cameras, mechanically interconnected

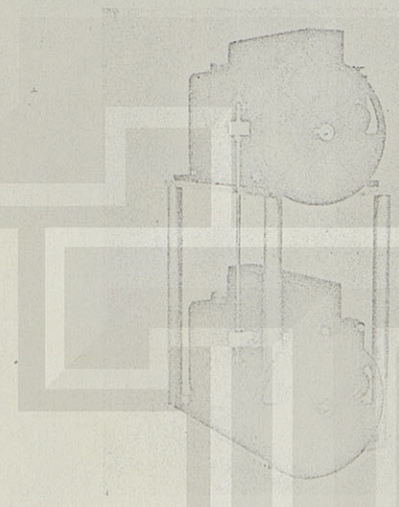

FIG. 2—Day sky stereoscopic unit

and synchronized, and mounted in stereoposition, one foot apart, with axes parallel. The one-inch F/1.5 lenses shot pictures through revolving disks, each having eight filters (Fig. 3) rotating at about 2 rpm. The camera mechanism was modified to transport 4.8 frames per second, or about 150 frames per revolution of the filter disk. The effective exposure was 1/20 second at F/1.5 on Eastman Super XX film. In each case, the film was developed in a high-speed developer, which doubled the ASA rating. The filters were Wratten Nos. 23A and 47, selected for their transmittance characteristics in red and blue, respectively. The Polaroid screen was of optical quality and oriented as shown in Figure 3.

The cameras were mounted in the forward instrument section in a position perpendicular to the rocket axis. Since the rocket was deliberately programmed to to roll after peak with its axis parallel to the earth's surface, the cameras alternately photographed the earth and the sky. The angular position of the photographed area with respect to the earth or the sky was determined by reference to data from an aspect camera.

The camera-film-filter combination was calibrated by exposures to the sky at ground-level on a very clear day. Film densities ranging from 0 to 2.0 were obtained by attenuating the sky brightness with two crossed Polaroid filters, and photometering each brightness.

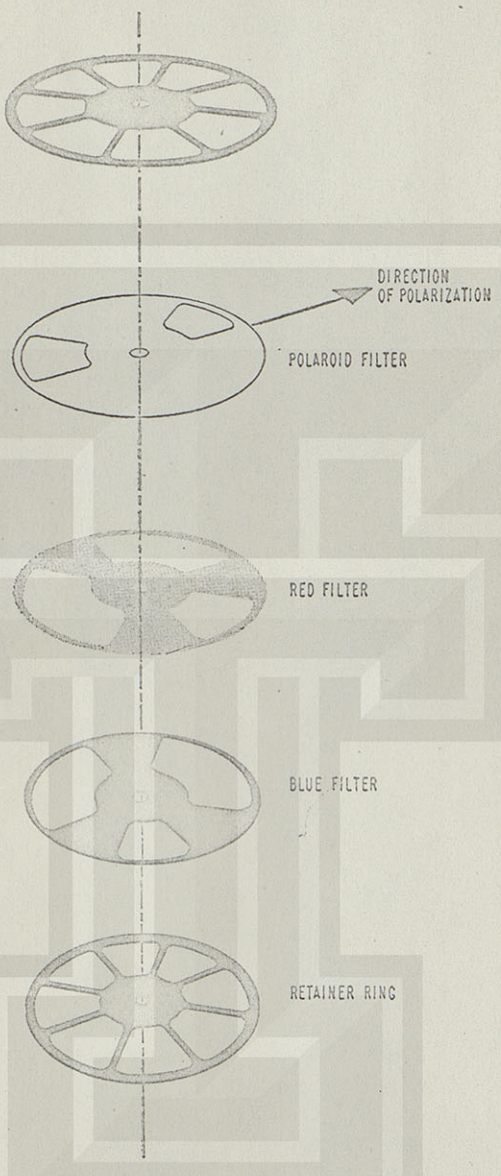

FIG. 3—Exploded view of filter disk showing orientation and assembly of filters and Polaroid

RESULTS

Since there were no true clouds observed during this flight, the remainder of this paper will be concerned with only the first of the four experimental objectives listed, namely: To record photographically the brightness of the sky at known points in the sky during flight.

In view of the many obstacles to rocket-borne sky-brightness measurements and the complex nature of scattered sunlight, the author is of the opinion that

any value assigned to sky brightness at any particular angular distance from the sun can only represent an upper limit. In this investigation, the minimum measurable brightness was determined by the sensitivity of the film. Sky brightness values assigned from this experiment are based on exposures made through the no filter-no Polaroid sections of the filter disk (see sketch, Fig. 3). Exposures made during ascent while the rocket axis was vertical were excluded from this study, since they contained obvious evidence of considerable reflection from the earth into the optical system. Only those frames were selected which were exposed as the camera aimed toward the sky and away from the sun while the rocket was rolling in a horizontal position. A total of 13 exposures were made in each camera while thus oriented. These occurred during the rocket descent from 220 to 80 km. Densitometer readings on these 13 frames showed no density above normal background density. In other words, the sensitivity of the film was not sufficient to record the brightness at this altitude range, and it can only be said that the sky brightness in this range was below a certain value.

Referring then to the calibration film, for a ground-level sky brightness of 380 candles/ft^2, the least exposure which produced a readable density above normal background density was 1/200 second at F/16 with a sky attenuation of 40 (refer to paragraph on calibration). This is equivalent to an exposure of 1/8,000 second at F/16.

A study of the above exposures—1/20 second at F/1.5 for the day sky unit and 1/8,000 second at F/16 for the calibration film— gives a ratio of 1:51,000 between the day sky brightness in the region from 80 to 220 km to that at sea-level. Or in terms of percentage, the day sky brightness from 80 to 220 km is less than 0.002 per cent of sea-level brightness. In absolute values, this represents a maximum brightness of 0.0075 candle/ft^2.

DISCUSSION OF RESULTS

It can be seen from Figure 1 that the measured upper limit for the day sky brightness is consistent with an extrapolation of the results of Teele. It can be seen that the present results are in marked disagreement with those of Miley. A possible explanation for this discrepancy is that Miley's high recorded brightness and clouds were caused by sunlight scattered from clouds of gas and particles blowing out of the rocket. This explanation is supported by the fact that the recorded brightnesses were the same at all three wavelength bands—a normal distribution if the clouds were of relatively large particles such as might be ejected from the rocket. Further support for this explanation is given by the "cloud" pictures included in the appendix.

An article entitled "Theoretical considerations regarding the dayglow," by Bates and Dalgarno [4], has recently appeared, which would also seem to refute the day sky values reported by Miley, *et al.* Bates and Dalgarno survey various possible sources of high altitude illumination and conclude that "the tenuous air at altitudes greater than 135 km cannot extract enough energy from the incoming solar radiation to supply a source having a photon intensity of some 10^{14} cm^{-2} sec" (as inferred by Miley). Their theoretical approach substantiates, in effect, the day sky-brightness values reported in this paper.

SUMMARY

The density of the stereocamera films indicated an upper limit of 0.0075 candle/ft^2 for the brightness of the daytime sky at altitudes ranging from 80 to 220 km. This value is based on 26 exposures made while the cameras were aimed away from the sun and the earth, and is consistent with values based on Rayleigh scattering alone. There were no true clouds in space recorded by the stereoscopic unit.

ACKNOWLEDGMENTS

In conclusion, the author desires to record his grateful thanks to Dr. R. Tousey, Dr. R. J. Havens, and Mr. M. Koomen for their stimulating interest and advice in the preparation of this paper.

PHOTOGRAPHIC EXHIBIT

Whenever a movie-film exposed in a rocket-borne camera is viewed frame by frame, a number of exposures occur which exhibit strange images and effects. Normally, there is no choice but to assign their origin to one of several common phenomena involving either film-processing technique or extraneous optical effects. In a calibrated stereoscopic system as was flown in this rocket, however, it is relatively simple to distinguish positively between images due to real objects in the camera field of view and images due to processing errors or extraneous optical effects—the latter image types being betrayed by either (1) their presence in one film only, (2) their unrelated geometry and dimension, or (3) their unrelated traversal across the field of view in the two films.

Shown below are stereopictures selected as a sample exhibit of objects and effects encountered in this rocket flight.

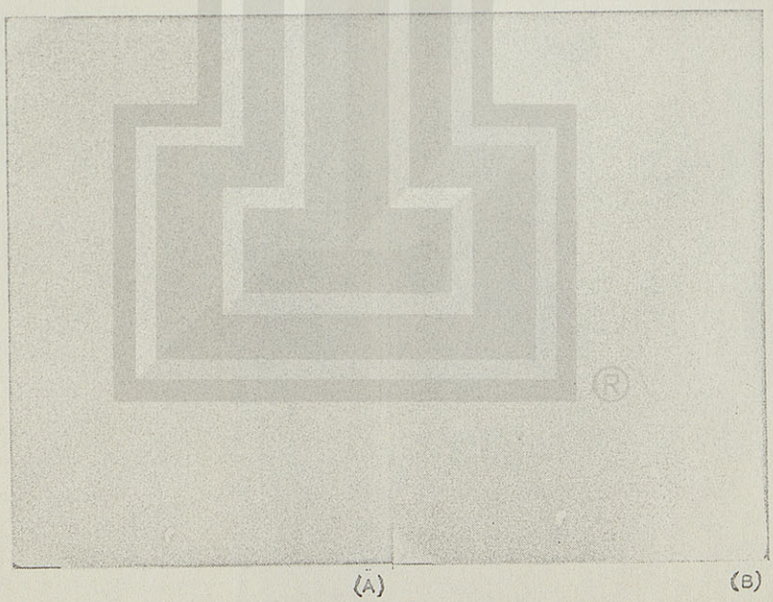

FIG. 4—A set of stereoexposures of the moon

Figure 4—A set of stereoexposures of the moon. These are included to validate the accuracy of the investigation as to image quality or reproduction and to the position of the object with respect to the rocket. The rocket to object distance is given by a comparison of the image within the frame on both stereofilms and reference to a calibration chart. Here, of course, the distance is essentially infinity.

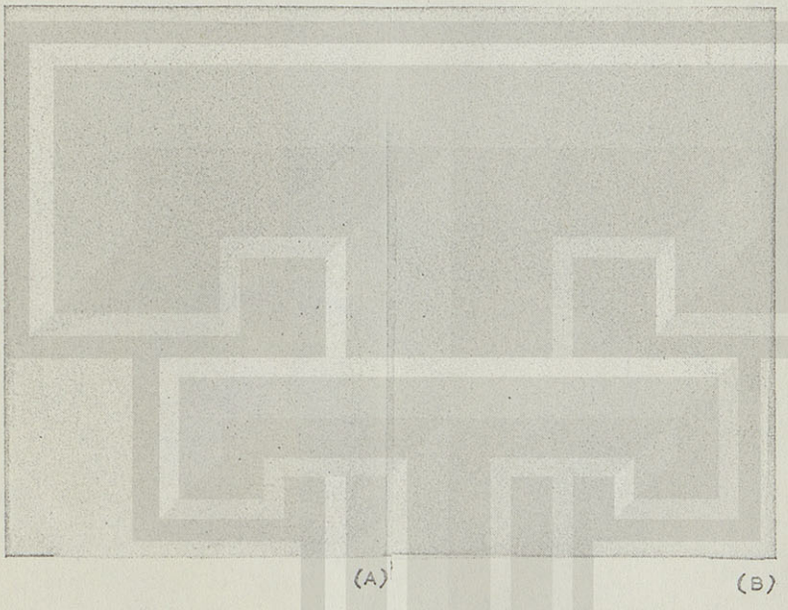

FIG. 5—Images resembling clouds or sunlit aurorae

Figure 5—Images resembling clouds or sunlight auroras, but actually optical scatter as the camera field of view approached the direction of the sun. These are not true stereopictures, since the upper and lower exposures were not taken at the same time by the two cameras, but are separated by one frame or about one-fifth second. The matching exposures from the upper and lower stereocameras that do correspond in time show an over-all, readable density, but no clouds or such effects. These are included in support of a previous suggestion in this paper that the clouds recorded by Miley's single camera may have been produced by a similar effect, or more likely by scattered sunlight in the gaseous envelope of the rocket.

References

[1] H. A. Miley, E. H. Cullington, and J. F. Bedinger, Trans. Amer. Geophys. Union, 34, 680-694 (1953).
[2] R. P. Teele, Nation. Geog. Soc., Contrib. Tech. Papers, Stratosphere Ser., No. 2, 133-138 (1936).
[3] The Rocket Panel, Phys. Rev., 88, 1027-1032 (1952).
[4] D. R. Bates and A. Dalgarno, J. Atmos. Terr. Phys., 5, 329-344 (1954).

F

EXTRAIT DES

ANNALES DE GÉOPHYSIQUE

Tome 17, 1961

Extrait des ANNALES DE GÉOPHYSIQUE
Tome 17, N° 3. — Juillet-Septembre 1961.

THE INTENSITY DISTRIBUTION IN THE ULTRAVIOLET SOLAR SPECTRUM [1]

By C. R. Detwiler, D. L. Garrett, J. D. Purcell and R. Tousey.
(U. S. Naval Research Laboratory Washington 25, D. C., U. S. A.)

Résumé. — *La distribution énergétique du spectre ultraviolet solaire est donnée en valeur absolue de* 2600 Å *à* 850 Å (*pour des intervalles de* 50 Å). *L'intensité des raies les plus intenses du spectre entre* 1900 Å *et* 835 Å *est également donnée. La courbe spectrale représentant l'émission solaire part du niveau d'émission du corps noir à* 5000 °*K pour* 2085 Å, *tombe rapidement à* 4900 °*K pour* 1800 Å *et à* 4750 °*K environ pour* 1500 Å. *Le continuum de Lyman peut être assimilé à l'émission d'un corps noir à* 6600 °*K.*

Abstract. — *Spectral intensities of the ultraviolet solar spectrum are given in absolute units from* 2600 Å *to* 850 Å *including continuum and lines in* 50 Å *intervals. The intensity produced by the strongest solar emission lines between* 1900 Å *and* 835 Å *are also given. The solar curve falls slowly from a* 5000 °*K black body level at* 2085 Å, *to* 4900 °*K at* 1800 Å *and to about* 4750 °*K at* 1500 Å. *The Lyman continuum follows a* 6600 °*K black body curve.*

Резюме. — Энергетическое распределение ультрафиолетового солнечного спектра дано в абсолютной величине от 2600 Å до 850 Å (для промежутков в 50 Å). Дается также интенсивность самых сильных линий спектра между 1900 Å и 835 Å. Спектральная кривая представляющая солнечное излучение берет начало на уровне излучения чёрного тела при 5000° К для 2085 Å, быстро падает до 4900° К для 1800 Å и до 4750° К для 1500 Å. Континуум Лимана может быть приравнен к излучению чёрного тела при 6600° К.

Introduction

From the point of view of Aeronomy, the most important aspect of the spectrum of the sun is the distribution of intensity with wavelength. Spectral intensities outside the earth's atmosphere must be known in absolute units before satisfactory theories of the photochemical processes taking place in the atmosphere of the earth can be developed. Experimentally, the measurement of absolute intensities in the extreme ultraviolet is more difficult and far less precise than the determination of wavelengths. There are difficulties of several kinds. First, there is the technical problem of calibration. Both the relative spectral speed of the spectrograph and film and the absolute speed in terms of incident energy must be determined. This is made difficult by the lack of any radiation standards in the extreme ultraviolet part of the spectrum. The second problem concerns the transparency of the atmosphere between the spectrograph and the sun. Ideally, the spectrograph should be flown to an altitude such that there is no absorbing gas within the optical path. So far, experiments have been flown in Aerobee-High Rockets and the peak altitude attained has been about 235 km. Even at this altitude, absorption by N_2 is strong at certain wavelengths. Gas desorption from the rocket and within the instrument presents another problem. Finally, there is the variability of the sun itself. The emission from the sun is neither constant in time, nor uniform over its surface. In the visible portion of the spectrum variations in time are very small, but in the X-ray end of the spectrum, the changes are tremendous. Throughout the extreme ultraviolet there have been too few measurements to establish the magnitude of the time variations in solar output. Although the variations of emission over the solar disc are important in the astrophysics of the solar atmosphere, it is mainly the radiation from the entire sun which is of interest in aeronomy.

The photographic experiments have not usually led to a direct determination of the integrated emission from the disc, because the spectrum is photographed from certain specific places on the sun. To derive the integrated emission precisely is difficult, because the emission varies greatly over the sun in the extreme ultraviolet, and the variation depends upon the particular emission under consideration. For example, from the disc

[1] Communication présentée au Colloque d'Aéronomie (Copenhague, juillet 1960), tenu sous les auspices du Comité de la Haute Atmosphère de l'Association Internationale de Géomagnétisme et d'Aéronomie.

photographs of the sun obtained in the wavelength of Lyman-α [13], it is known that Lyman-α is emitted from plage regions with five or more times greater intensity than from the quiet portions of the sun. Spectra obtained in 1960 [4], show that this is true to a greater or lesser extent for all emissions in the extreme ultraviolet. There is evidence that the variation between plage and quiet regions may be increased for radiations originating higher in the solar atmosphere than Lyman-α, for example, for the lines of O VI at 1031.9, 1037,6 Å.

In spite of these various difficulties, fairly satisfactory data are now available to about 850 Å with reasonably high resolution. From 1300 to about 60 Å, data have been obtained by HINTEREGGER [6] with a photoelectric scanning monochromator. These results are of lower resolution than the photographic spectra, but have the advantage of applying to the radiation from the entire disc.

THE NEAR ULTRAVIOLET

The spectral intensity distribution in the solar spectrum is known with high resolution and reasonably good accuracy from the visible to about 2000 Å. For many years, however, there was considerable disagreement over the wavelength range 3000 to 4000 Å. The measurements of DUNKELMAN and SCOLNIK [5] from Mount Lemmon, Arizona were undertaken to resolve this confusion. They apply to the entire solar disc. In our opinion, they are the best data available at the present time.

The absolute energy scale for the Mount Lemmon data was set by JOHNSON [7]. In a paper dealing with a revision of the solar constant, JOHNSON reconsidered the Smithsonian Institution results of many years, taking into account the newly published explanation of the absolute scale [1], making a new correction for the infrared absorption by the atmosphere, and revising the ultraviolet correction with the aid of the relative curve of DUNKELMAN and SCOLNIK [5] and the rocket results. This value of solar constant, 2.00 ± 0.04 cal cm^{-2} min^{-1}, we believe to be the best available. It is against this value that the absolute scale of the curve of DUNKELMAN and SCOLNIK [5] was adjusted.

The rocket spectrum has been published by WILSON et al [17] for the wavelength range 2990 to 2635 Å, and by MALITSON et al [9] from 2635 to 2085 Å. Curves are given on an absolute energy scale, at a resolution of the order of 1/2 Å. The absolute energy scale over this entire region was set by adjusting the long wavelength end of the distribution to agree with the Mount Lemmon curve over the range 3000 to 3300 Å where the rocket data and the ground observations overlap.

Numerical data for the intensities from the visible to 2200 Å were published by JOHNSON [7] who averaged the available data over a wavelength interval of 100 Å in order to obtain values at low resolution, which are more convenient for aeronomical calculations. These data are nearly the same as our most recent result to 2400 Å, but at shorter wavelengths they are low by a factor reaching 2 at 2200 Å. The change at the short wavelength end is caused by new measurements of the intensity distribution in the radiation from the carbon arc used to calibrate the rocket spectrographs [8]. In addition, other small changes have been introduced from a rocket spectrum obtained on February 21, 1954, with a low resolution spectrograph especially designed for photometric purposes, which accepted the light from the entire disc. The most recent results are presented in Table I.

THE EXTREME ULTRAVIOLET

The region of the spectrum from 2000 to 500 Å has been studied by means of normal incidence grating spectrographs with photographic recording of the spectrum. The instrument used is shown in Figure 1. Basically it consists of a 40 cm radius, 600 lines per mm diffraction grating, used in the first order close to normal incidence. Previous to 1960, light was gathered by means of a concave mirror and an image of the sun was projected on the slit. On April 19, 1960 we flew a spectrograph in which a diffraction grating, arranged as in Figure 1, was used in place of the mirror. This grating was similar to the grating inside the spectrograph, but was oriented so that the spectrum was dispersed along the slit. As a result of this pre-dispersion, the stray light from the intense visible and near ultraviolet portions of the solar spectrum was rejected from the spectrograph. With the double-dispersing spectrograph the spectrum has been photographed to 499 Å and its intensity distribution has been determined from 1550 Å to 850 Å. From 2000 Å to 1700 Å the intensity distribution was derived from spectrograms obtained with the earlier spectrograph where the pre-disperser was not employed.

Portions of two of the exposures obtained on

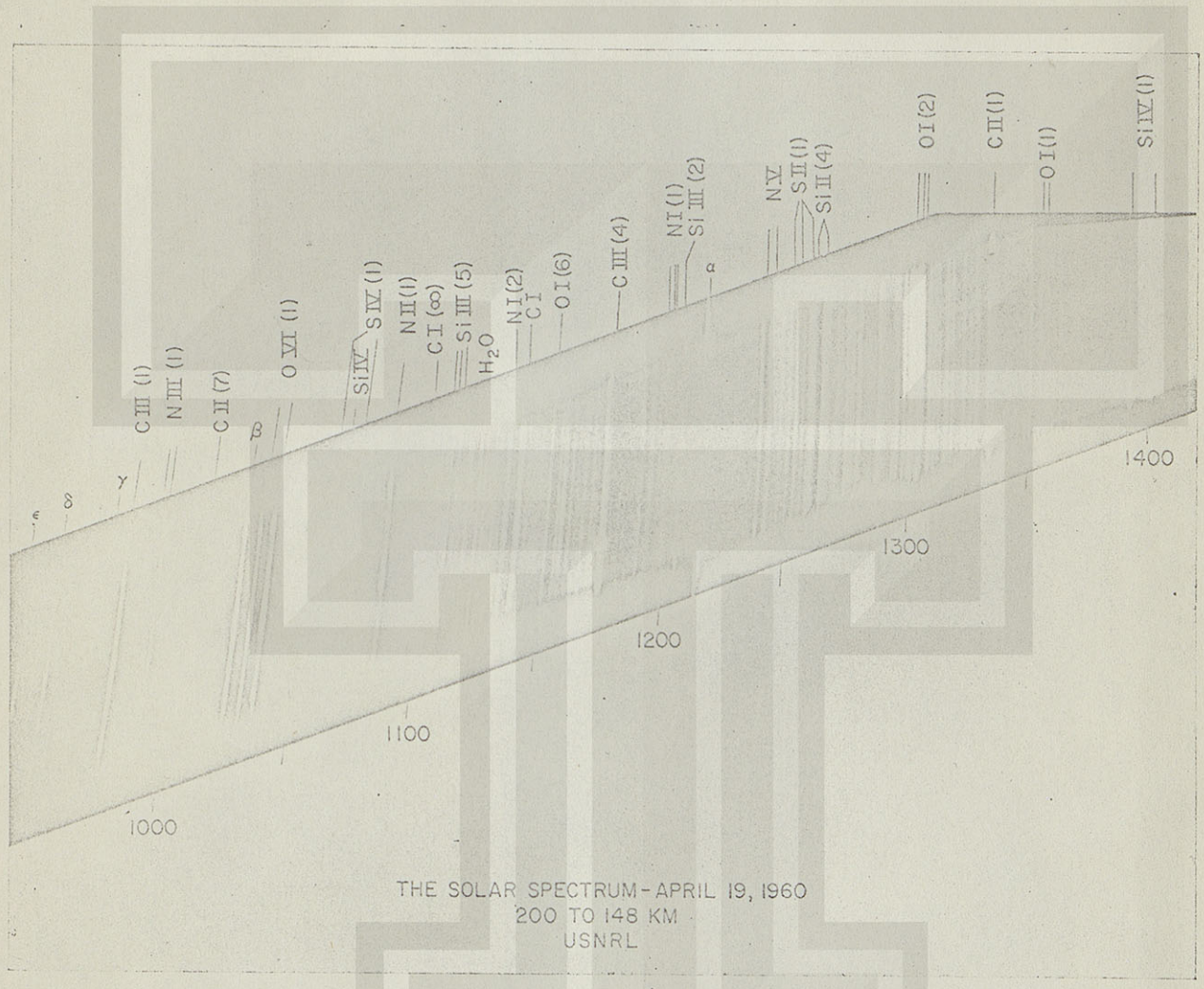

FIG. 2. -- The solar spectrum, photographed from an Aerobee-High rocket, 19 April 1960, altitude 206.8-157.2 km, a 60-second exposure on DC-3 film.

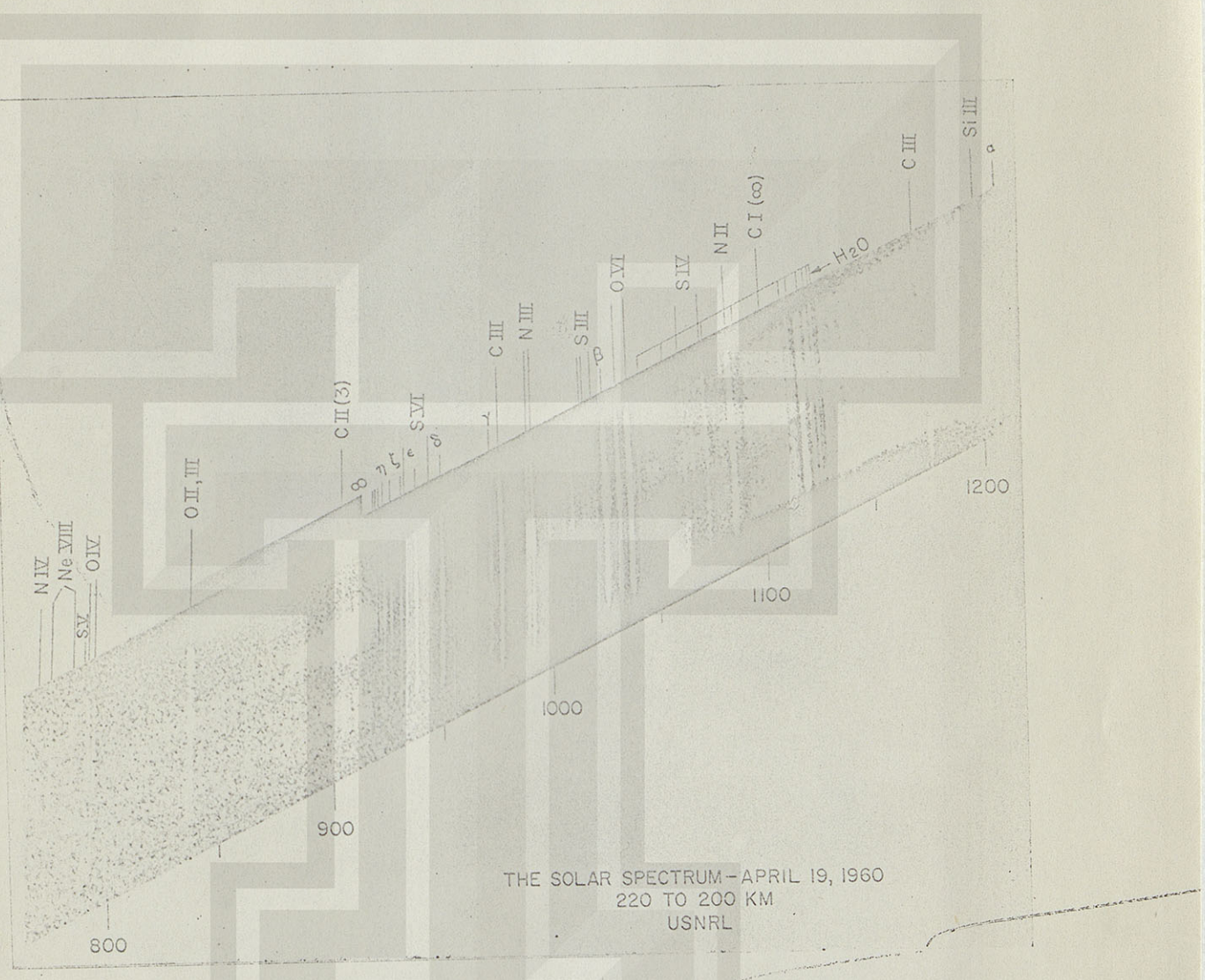

FIG. 3. — The solar spectrum, photographed from an Aerobee-high rocket, April 19, 1960. A 60-second exposure on SC-4 film from 222,4 km, over peak at 222.9 km to 206.8 km.

April 19, 1960 with the double-dispersing spectrograph are reproduced in Figures 2 and 3. The external grating was distorted mechanically so as to compensate for the astigmatism of the second grating, thus a stigmatic spectrum was produced. Therefore, points along a spectrum line correspond to points in a slice along a diameter of the sun, and plage regions show in the spectrum with enhanced intensity. Since a curved slit was used, the portions of the sun producing the spectrum line changed slowly from wavelength to wavelength ; for example, in Figure 2 the central plage region disappears at wavelengths longer than Lyman-α.

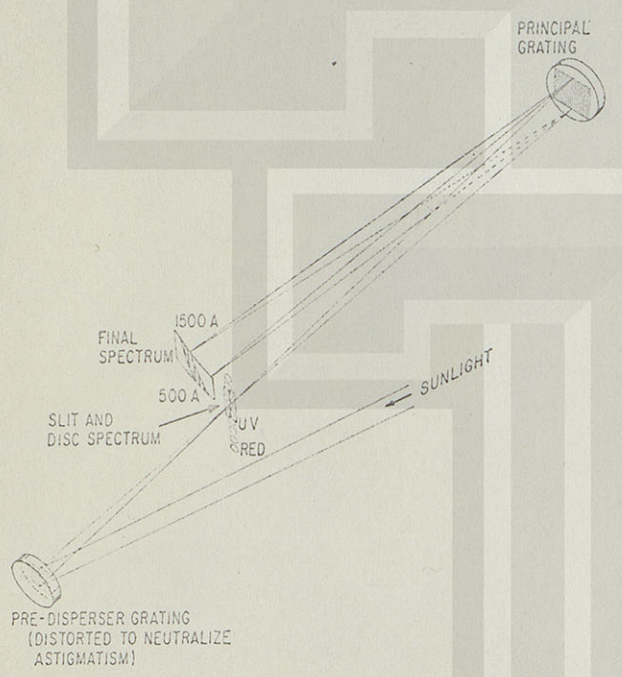

FIG. 1. — The double-dispersion, normal-incidence, grating spectrograph flown on April 19, 1960.

In these spectra it is possible for the first time to distinguish the true continuum of the sun and to determine its intensity distribution from 1550 Å, the wavelength limit of this particular spectrograph, to 942 Å. Between 942 and 920 Å only a faint trace of the continuum could be seen. Below the Lyman limit, 912 Å. the Lyman continuum was detectable to 800 Å, and its intensity was determined to 850 Å.

The spectra were reduced by the usual procedures of photographic photometry, with characteristic curves determined in the laboratory using sectored discs to reduce the intensity. Three types of film produced by Kodak-Pathé were employed : SWR-C, DC-3, and SC-4. The speed of the spectrograph as a function of wavelength was determined from measurements of the efficiency of the two diffraction gratings, and of the relative spectral response of the photographic materials.

The absolute level of the spectrum was referred to Lyman-α, whose intensity was measured during flight with an NO-filled LiF-windowed ion chamber attached to the spectrograph housing. This detector received light from the entire sun and responded to the spectrum from 1075 to 1275 Å, which is, for the most part, Lyman-α. A correction of 15 % for the contribution of the continuum and lines other than Lyman-α was derived from the final intensity curve and the spectral response curve of the ion chamber. In the 1959 spectrum, a sufficiently short exposure was made to obtain an easily measurable photographic image of Lyman-α, which served as a standard reference line. In 1960, however, because all images of this line were over-exposed, Lyman-β was used as a standard reference line ; it was assumed that the ratio of Lyman-α to Lyman-β was the same in 1960 as was determined from the short exposure in 1959.

TABLE I

THE INTENSITY OF THE SOLAR SPECTRUM, (CONTINUUM AND LINES), IN 50 Å INTERVALS, AT A DISTANCE OF 1 A. U.

$\lambda \pm 25$ Å	erg cm^{-2} sec^{-1} (50 Å)$^{-1}$	$\lambda \pm 25$ Å	erg cm^{-2} sec^{-1} (50 Å)
—	—	—	—
2600	700	1700	8.2
2550	560	1650	5.0
2500	380	1600	3.2
2450	390	1550	1.7
2400	340	1500	0.95
2350	320	1450	0.50
2300	360	1400	0.26
2250	350	1350	0.26
2200	310	1300	0.18
2150	240	1250	0.15
2100	145	1200	5.7
2050	90	1150	0.08
2000	70	1100	0.06
1950	55	1050	0.10
1900	41	1000	0.18
1850	28	950	0.15
1800	19	900	0.25
1750	12	850	0.11

A source of error lies in the method of adjusting the rocket curve to apply to the light from the entire sun. The ion chamber measures the Lyman-α radiation from the entire disc. The 1959 ratio of Lyman-β to Lyman-α was determined not for the whole sun, but for a rather quiet portion of the sun away from the limb. In 1960, the spectra from 1550 to 1100 Å were reduced for a quiet portion of the disc ; but from 1100 Å to shorter wavelengths the intensity was not sufficient to work with a quiet portion of the disc and a plage region was used. The plage region in the continuum at 1100 Å was three times more intense than the quiet portion of the disc. It was assumed that the same factor of 3 applied at all wavelengths below 1100 Å, including Lyman-β, though it is unlikely that this is exactly true. It is possible that further study of the 1960 exposures will throw light on the validity of this procedure.

An independent check on the method of determining the absolute intensity by reference to the Lyman-α ion chamber measurement, was made by comparing the density of the Lyman-α line image with the spectrum near 2000 Å. Both were present on one of the exposures obtained in 1959. The agreement was within 20 %, which was considered quite satisfactory.

Within the continuum strong absorption bands can be seen. The most conspicuous are from 1110 Å to 1140 Å, near 1060 Å, and close to Lyman alpha and beta. These were identified as bands of H_2O, indoubtedly carried with the rocket. An attempt had been made to free the spectrograph itself from water by evacuating it in the laboratory before installation in the rocket, and then filling it with helium, as has been done for some years. During installation and until firing, helium was maintained within the spectrograph at a positive pressure in order to prevent air and water vapor entering the spectrograph from outside. Evidently this procedure was not wholly successful.

It was necessary to correct the 1960 spectra for water vapor absorption in order to obtain the true solar spectral intensity distribution. Using the published values of the absorption coefficients of H_2O [15] it was found that a good fit to the observed absorption could be obtained over the strongest bands for a total water vapor content within the light path of 4.6×10^{16} molecules cm^{-2} col^{-1}. The entire spectrum was then corrected using this value of the total amount of water vapor. In certain regions absorption coefficients were obtained at greater spectral resolution than those of Watanabe by study of plates exposed by Price [12] and from data of Bell and Walsh [1].

The intensity data presented at the Copenhagen Symposium were obtained using an assumption that the water vapor lay entirely outside the rocket, and therefore applying a correction factor of 2 to the ion chamber Lyman alpha value. It now seems more likely that most of the water was within the spectrograph and that no correction to the ion chamber value should be made. Therefore the values of intensity presented in this paper for wavelengths below 1550 Å are about one-half as great as those given earlier and published in the report of the meeting [3]. The use in 1960 of the Lyman-β/α ratio from 1959 is not affected by H_2O attenuation, because the absorption coefficients at these two wavelengths happen to be nearly equal.

The correction for water vapor absorption cannot be regarded as precise until more complete laboratory data are obtained on its absorption spectrum. The absorption cross sections of Watanabe [15] and coworkers were measured using the molecular spectrum of hydrogen as the light source. Hence they apply to specific wavelengths or groups of wavelengths which do not necessarily coïncide with the line emissions to which corrections must be applied. Measurements of the absorption coefficients of water vapor are required at higher resolving power and using a continuous spectrum light source. The same situation exists for N_2.

The spectral intensity curves

The spectral intensity distribution curves obtained after reduction of the 1960 spectra are shown in Figure 4(*a-c*). Intensities are given in erg cm^{-2} sec^{-1} $Å^{-1}$. If it is desired to separate emission lines from the continuum, this is best done by integrating under the line and subtracting the continuum contribution. However, since the slit was equivalent in width to 1 Å, for unblended narrow lines, such as O VI, 1031.9 Å, the peak value minus the continuum level gives the intensity directly. These curves were derived from the final 60-second exposure, obtained after about 5 minutes of in-flight evacuation, and covering the altitude range 206.8 to 157.2 km. Since the half-way point in time was 185 km, the curves apply to an altitude not less than 185 km, and in spectral regions of strong N_2 absorption, they apply to a somewhat greater altitude.

The curves of Figures 4(*a-c*) have been adjusted

to apply to the radiation from the entire disc. Corrections for absorption by H_2O and N_2 have not been applied, but the correction curves are reproduced in the Figures. The H_2O curve applies to 4.6×10^{16} molecules cm^{-2} col^{-1}, the value determined as described previously. The N_2 curve was computed for 3×10^{16} molecules cm^{-2} col^{-1}, a value derived from the absorption features within the Lyman continuum. Since the absorption is plotted as transmittance on the same logarithmic scale as the spectrum, the corrections can be made by adding curves. In several regions, however, the absorption features in the solar curve show more detail than is present in the log T curve, which was obtained from laboratory data having less resolution, for example, H_2O at 1120-1140 Å.

Figure 5 is a solar intensity distribution curve of low resolution, corrected for all absorption effects, and applying to the radiation from the entire sun. The ordinate is ergs cm^{-2} sec^{-1} within a 10 Å wavelength interval and at a distance of 1 A. U. from the sun. A resolution of 10 Å was chosen in order to reduce the detail to a degree more nearly that required in most aeronomical calculations, and to facilitate comparison with data obtained by HINTEREGGER [6] at about 10 Å resolution. The reduction to 10 Å resolution was accomplished by averaging the 1 Å resolution curves of Figures 4(*a-c*) over a 10 Å interval. Also shown are black body curves for 4500 °K-7000 °K. From 2000-1700 Å the curve was obtained from March 13, 1959 flight. The range 1700-1520 Å was obtained by interpolation, because the 1959 spectra had too great a stray light level below 1700 Å.

The solar curve falls slowly from a 5000 °K black body level at 2085 Å, to 4900 °K at 1800 Å, to about 4750 °K at 1500 Å, then follows a minimum level of 4700 °K from 1450 to 1280 Å. The many strong emission lines superimposed on the continuum are not separated at 10 Å resolution, but combine to produce irregularities. These result in raising the level of the curve of Figure 5 above the lowest level shown in the high resolution curves in several places. Below 1280 Å

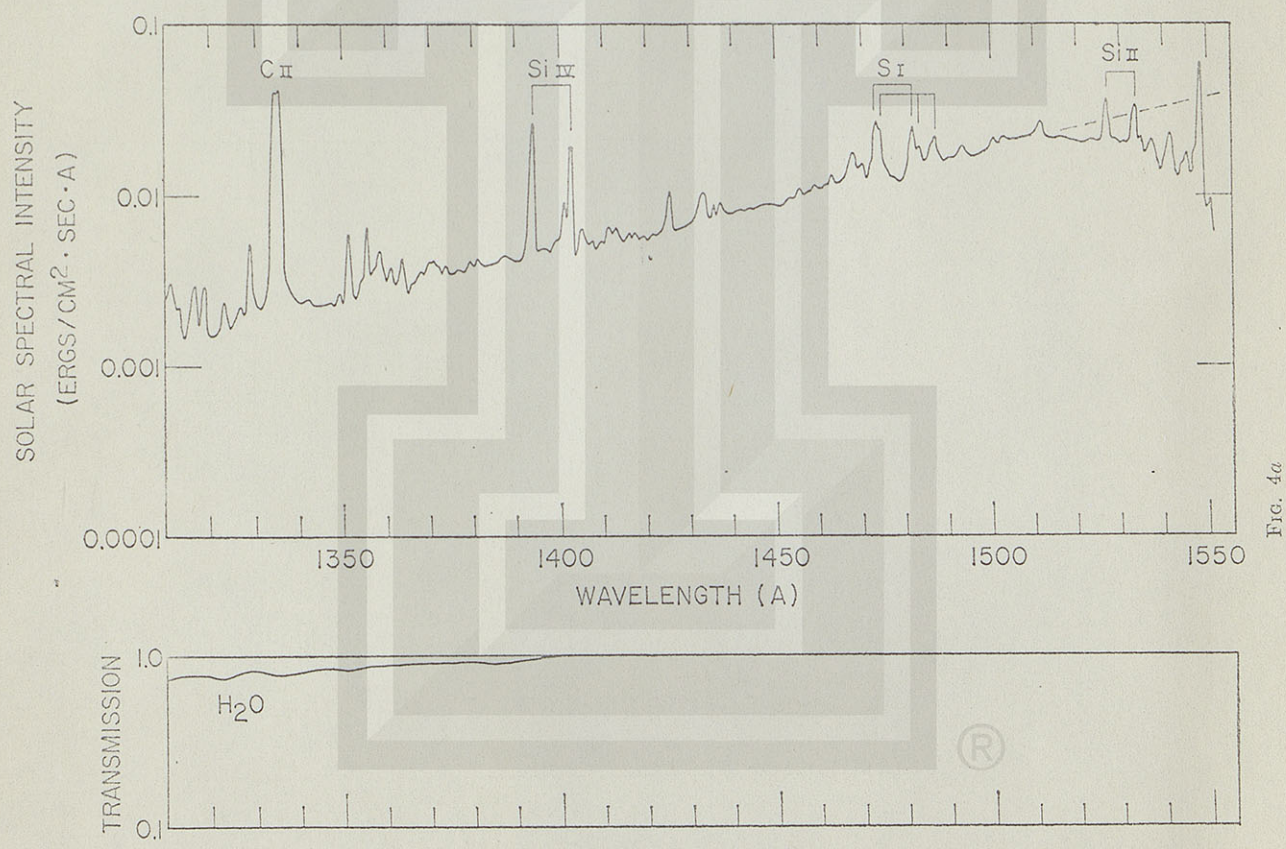

FIG. 4a

FIG. 4. — The spectral intensity as measured from a spectrum photographed over the altitude range 206.8 tol 57.2 km on April 19, 1960. The correction for absorption by 4.6×10^{16} molecules cm^{-2} col^{-1} of H_2O in the light path is shown. Also given in (*c*) is the curve for absorption by 3×10^{16} molecules cm^{-2} col^{-1} of N_2. The peak of Lyman-α on (*b*) reaches 5.1 erg cm^{-2} sec^{-1}, after correction for H_2O absorption.

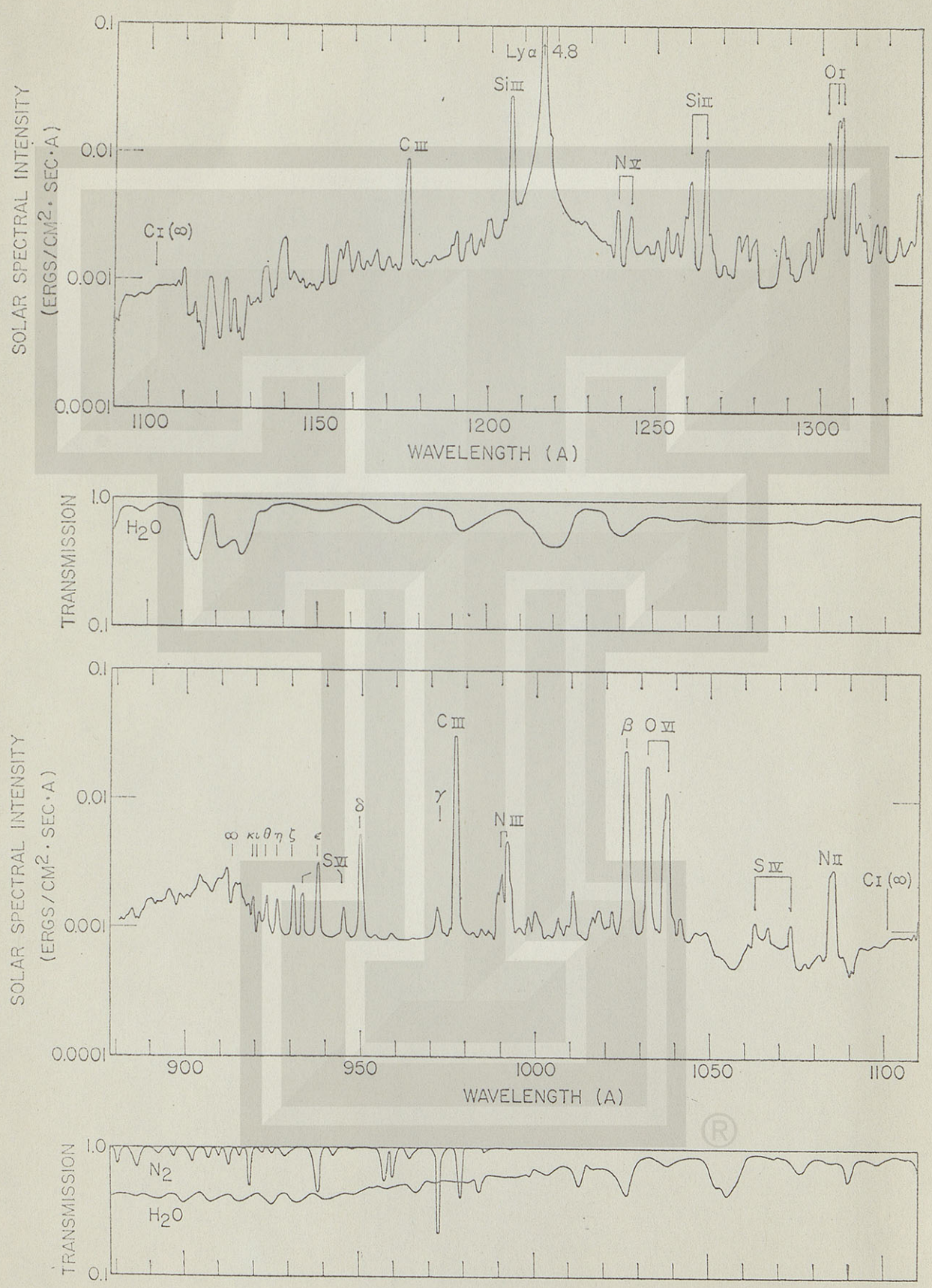
SOLAR SPECTRAL INTENSITY
(ERGS/CM2 · SEC · A)
0.1
0.01
0.001
0.0001
Lyα 4.8
Si III
C III
N V
Si II
O I
C I (∞)
1100
1150
1200
1250
1300
WAVELENGTH (A)
TRANSMISSION
1.0
0.1
H2O
SOLAR SPECTRAL INTENSITY
(ERGS/CM2 · SEC · A)
0.1
0.01
0.001
0.0001
C III
γ
δ
β
O VI
N III
S VI
S IV
N II
C I (∞)
900
950
1000
1050
1100
WAVELENGTH (A)
TRANSMISSION
1.0
0.1
N2
H2O

FIG. 4b

FIG. 4c

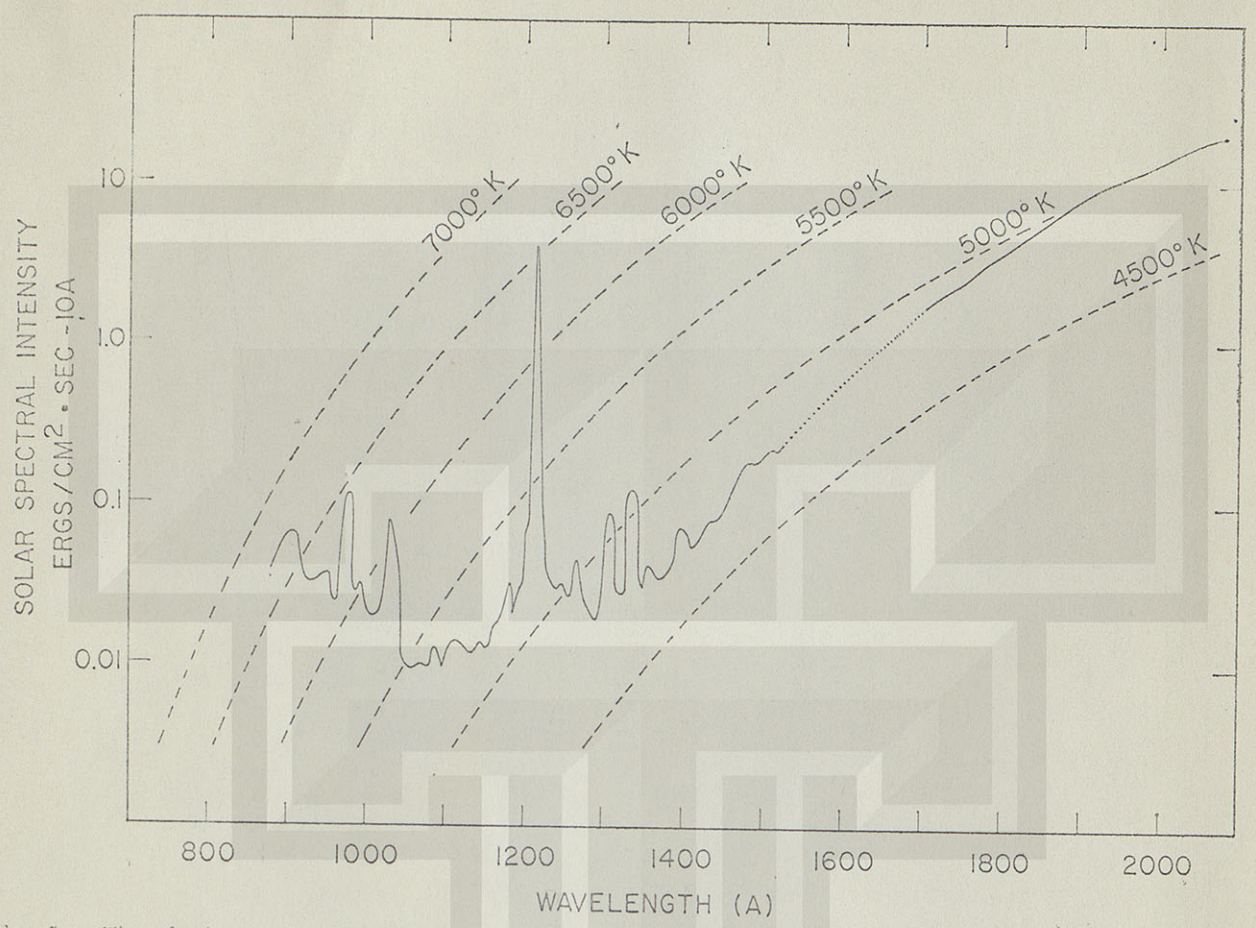

FIG. 5. — The solar intensity distribution at 10 A resolution, at 1 astronomical unit from the sun. The curve is obtained from Figure 4(*a*-*c*) by making the corrections for absorption by H_2O and N_2, and averaging over a 10 A interval. Note that the intensity is given for a spectral band of 10 A width.

the continuum increases rapidly as Lyman-α is approached. On the short wavelength side of Lyman-α the continuum falls to a temperature level of 5200 °K, then stays constant in energy to 1040 Å, but with the temperature level rising gradually to 5500 °K. From 1040 to 912 Å the 10 Å resolution curve is mainly the Lyman series and other lines, with the continuum contribution taken from an upper limit over the region 940-925 Å, where it was just barely detectable. The Lyman continuum extending shortward of 912 Å, follows a 6600 °K black body curve. Although the spectra extend to 499 Å, reliable values of intensity could not be derived below about 850 Å because of the presence of a trace of stray light from a light leak, opened during flight.

Measurements of the intensity distribution in the spectrum emitted by the entire sun have been made by HINTEREGGER [6] with a photoelectric scanning monochromator employing a diffraction grating at grazing incidence with a resolution of the order of 10 Å. The spectral range covered was 1300 to 300 Å, with one instrument, and 312 Å to 60 Å with a second. These data, obtained in January 1960 and reported at the Symposium on Aeronomy, Copenhagen [3] are considerably above the curve of Figure 5. New results obtained by HINTEREGGER in August 1960 (private communication), are much lower than the January 1960 data, and are in reasonably good agreement with Figure 5.

The NRL solar data are assembled in numerical form in Table I. A wavelength interval of 50 Å was chosen, extending 25 Å on either side of λ. The intensities include both continuum and lines. In Table II are listed the intensities of the principal emission lines. All these values have been corrected for absorption effects and apply to the radiation from the entire sun at a distance of 1 A. U.

It can be seen that Lyman-α is by far the most intense emission in the extreme ultraviolet. The

intensity within the 1 Å wide interval containing most of the line is about 5.1 erg cm^{-2} sec^{-1}. The Lyman-α ion chamber, which accepted the spectrum principally between 1075 and 1275 Å, recorded 6.0 erg cm^{-2} sec^{-1}, of which 0.9 erg cm^{-2} sec^{-1} belonged to the wings of Lyman-α, and other emission lines. The intensity of Lyman-α is equal, very approximately, to the integrated intensity within the entire remainder of the spectrum from X-rays to about 1500 Å. The higher members of the Lyman series total about 0.12 erg cm^{-2} sec^{-1}, whereas the Lyman continuum, below 912 Å, contains about 0.24 erg cm^{-2} sec^{-1}. The emission lines, commencing at 1892.0 Å, although conspicuous, contain considerably less energy than the continuum all the way to 1100 Å.

TABLE II

INTENSITY AT ONE ASTRONOMICAL UNIT (A. U.) PRODUCED BY THE STRONGEST SOLAR EMISSION LINES

λ (Å)	IDENTIFICATION	erg cm^{-2} sec^{-1}
1892.03	Si III (1)	0.10
1817.42*	Si II (1)	0.45
1808.01	Si II (1)	0.15
1670.81	Al II (2)	0.08
1657.00*	C I (2)	0.16
1640.47	He II (12)	0.07
1561.40*	C I (3)	0.09
1550.77	C IV (1)	0.06
1548.19	C IV (1)	0.11
1533.44	Si II (2)	0.041
1526.70	Si II (2)	0.038
1402.73	Si IV (1)	0.013
1393.73	Si IV (1)	0.030
1335.68	C II (1)	0.050
1334.51	C II (1)	0.050
1306.02	O I (2)	0.025
1304.86	O I (2)	0.020
1302.17	O I (2)	0.013
1265.04	Si II (4)	0.020
1260.66*	Si II (4)	0.010
1242.78*	N V	0.003
1238.80	N V	0.004
1215.67	H Ly-α	5.1
1206.52	Si III (2)	0.030
1175.70*	C III (4)	0.010
1139.89*	C I (20-23)	0.003
1085.70*	N II (1)	0.006
1037.61*	O VI (1)	0.025
1031.91	O VI (1)	0.020
1025.72	H Ly-β	0.060
991.58*	N III (1)	0.010
989.79*	N III (1)	0.006
977.03	C III (1)	0.050
949.74	H Ly δ	0.010
937.80	H Ly ϵ	0.005
835 *	O II, III	0.010

The value for Lyman-α applies to the intensity within the 1 Å wide central part of the line ; the ion-chamber reading was 6.0 erg cm^{-2} sec^{-1}.

The Lyman continuum follows a 6600° K black body ; its total intensity is 0.24 erg cm^{-2} sec^{-1}.

* indicates that the line is a blend of lines of other elements, or is an unresolved multiplet.

The multiplet numbers and wavelengths are from MOORE [11], with the exception of Si III (1) [14].

The accuracy of these intensity data is difficult to estimate. In the region 2000 Å to 1400 Å we believe that the accuracy is better than ± 20 %, and are fairly sure that there are no errors greater than a factor of ± 1.5. Below 1300 Å there is the possibility of errors as great as a factor of ± 2, and in places perhaps more. The question of solar variability is of course still open.

ATMOSPHERIC ABSORPTION EFFECTS

Spectra at different altitudes, obtained on April 19, 1960, show clearly absorption produced by H_2O, O_2 and N_2. In Figure 6 there is reproduced the wavelength range 1150 to 1350 Å from four exposures taken with several types of photographic film at mean altitudes ranging from 106 km to 217 km.

Effects of water vapor absorption can be seen in all four exposures and they are present to the same degree, approximately in each. Especially noticeable are the bands on the short side of and between the NV emission lines 1238.80, 1242.78 Å. Clearly visible also are three bands between 1190 and 1200 Å, and one at 1172 Å.

Changing O_2 absorption as a function of altitude is apparent in Figure 6. The band centered at 1243 Å is the most intense of all those within the extreme ultraviolet. Its effect is particularly striking because it absorbs the NV, 1242.78 Å line but not the other member of the NV pair, at 1238.80 Å. The exponential absorption coefficient of O_2 per cm, measured by WATANABE [15], is less than 10 from 1212 Å to 1242.0 Å, then rises suddenly to 400 at 1242.8 Å, and to a maximum of about 1000 at 1243.0 Å. This results in the

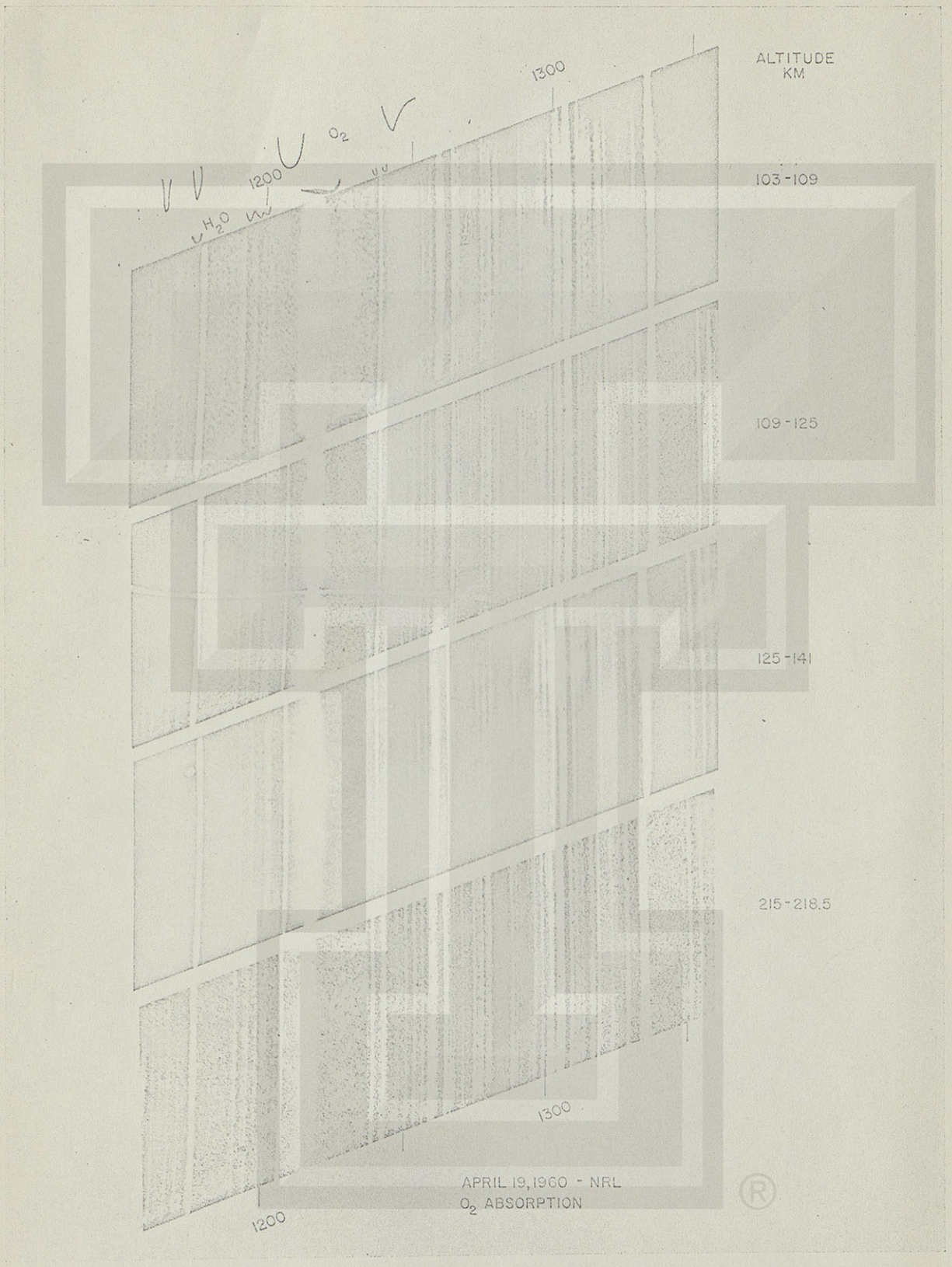

FIG. 6. — Spectra exposed at different altitudes on April 19, 1960, selected to show absorption bands of H_2O and O_2.

attenuation of NV 1242.78 Å to zero, 0.3, 0.9 and not at all, very approximately, at the altitudes of the four exposures reproduced in Figure 6, respectively. The situation is similar for Si III 1206.5 Å, where the coefficient is 460 cm^{-1}. It may be noted, however that the NV 1242.78 line seems still to be present in the lowest exposure, whereas the si III line is absent. Careful measurement shows that the remaining line is actually an unidentified faint line at 1241.9 Å, where the O_2 absorption still remains low. This component causes the diffuse appearance of the NV line in the highest exposure. Other regions excluded by O_2 absorption at 103-109 km, can be seen at 1163 Å, 1172 Å, and in the region of continuous absorption near 1350 Å.

Absorption by N_2 is strong, even for the exposure made above the peak, 222.9 km, reproduced in Figure 3. The absorption bands produce most of the channelled structure within the Lyman continuum. A strong narrow band can be seen near the head of the Lyman series, greatly weakening Lyman-ι, and another strong band causes Lyman-γ to be of low intensity.

An attempt to compare the absorption observed in these spectra with the absorption calculated from various model atmospheres is in progress. There are several difficulties ; first, the absorption cross sections of N_2 are not known with sufficiently great spectral resolution, nor are the temperature and pressure conditions of the upper atmosphere ; second, our exposures cover a wide range of altitudes ; third, in the case of Lyman-γ and ι the emission line profiles are not known.

At the present writing, the absorption within the Lyman continuum for the exposure covering the altitude range 206.8 to 157.2 km is reasonably well accounted for by 3×10^{16} molecules cm^{-2} col^{-1} of N_2. The zenith angle of the sun was 69° and the time 7.15 AM M. S. T. A stepwise calculation of the absorption for this exposure, based on the atmosphere of Minzner, Ripley and Condron [10] resulted in about twice greater absorption than was observed, suggesting that the actual atmosphere was less dense above 160 km and cooler than the model.

The absorption of Lyman-γ and ι is of interest, although not as well suited for comparison with the atmospheric model as is the Lyman continuum. In the 1959 spectrum, obtained at 195.8 km to peak at 199.0 km to 198.9 km altitude, though there was a very faint line at about 971.5 Å, Lyman-γ 972.5 Å was not detected. In the 1960 flight, Lyman-γ was clearly present. This was a result of the greater altitudes attained, and partly because of the elimination of instrumental stray light. On the exposure over the peak, 222.9 km, Lyman-γ was weaker than Lyman-δ ; for the exposure from 206.8 to 157.2 km, whose intensity curve is shown in Figure 4-*c*, Lyman-γ was less than 1/7 the intensity expected by interpolation between Lyman-β and δ.

The attenuation of Lyman-γ is caused by an intense band of N_2 with head at 972.1 Å (Worley, 1943), maximum absorption near 972.5 Å, and degraded toward the red. A value of absorption coefficient at Lyman-γ as high as 7600 cm^{-1} has been measured, [16]. As a result, in Figure 4-*c* there is present only a weak line near Lyman-γ. Some of this line may be the wing of Lyman-γ, and some is probably He II, 972.1 Å, whose center lies at the band head, but whose width also is unknown. Since the observed line in this exposure was centered at 971.7 Å it may be largely some line other than Lyman-γ or He II. In the exposure over peak, however, reproduced in Figure 3, Lyman-γ is definitely present, and at the proper wavelength, although weaker than Lyman-δ. Alongside it, is a faint component at 971.7 Å, which must be the line that remains at the lower altitude. Thus the quantitative interpretation of the attenuation of Lyman-γ is impossible at present.

The absorption of Lyman-ι is similar to that of Lyman-γ. There is a strong band of N_2 with head at 920.04 Å [18], degraded to the red and only about 1 Å wide. This produces the narrow absorption line seen in Figure 3. Lyman-ι, 920.96 Å, is greatly weakened by this band, though it is beyond the region of strongest absorption, as can be seen, in Figure 4-*c*.

Conclusions

The solar intensity distribution is now fairly well known throughout the extreme ultraviolet. Much more work needs to be done, to increase the accuracy of the measurements, especially below 900 Å, to determine the magnitude of time variations in the solar spectrum, to improve the corrections for attenuation that are required at the peak altitudes attainable by Aerobes-High rockets, and to be certain that the results are not affected by water vapor and possibly other gases released during flight.

Manuscrit reçu le 14 *avril* 1961.

REFERENCES

[1] ALDRICH L. B. and HOOVER W. H., 1952, *Science*, 116, 3.

[2] BELL. S. and WALSH A. D., 1960, private communication.

[3] COPENHAGEN, 1960, *Trans. Am. Geophys. Union*, 41, 622.

[4] DETWILER C. R., PURCELL J. D. and TOUSEY R., Proceedings of the International Astrophysical Symposium of 1960 [Mém. Soc. R. Sc., Liège, V, ser. vol. IV p. 253, 1961].

[5] DUNKELMAN L. and SCOLNIK R., 1959, *J. Opt. Soc. Am.*, 49, 356.

[6] HINTEREGGER H. E., 1960, *Astrophys. J.*, 132, 801.

[7] JOHNSON F. S., 1959, *J. Meteorol.*, 11, 431.

[8] JOHNSON F. S., 1956, *J. Opt. Soc. Am.*, 46, 101.

[9] MALITSON H. H., PURCELL J. D., TOUSEY R. and MOORE C. E., 1960, *Astrophys. J.*, 132, 746.

[10] MINZNER R. A., RIPLEY W. S. and CONDRON T. P., 1958, U. S. Extension to the ICAO Standard Atmosphere, Superintendent of Documents, Washington D. C.

[11] MOORE C. E., 1950, An Ultraviolet Multiplet Table, Circular 488, National Bureau of Standards, Washington, D. C.

[12]. PRICE W. C., 1936, We are greatly indebted to Dr. PRICE for the loan of his original plates. *J. Chem. Phys.*, 4, 147.

[13] PURCELL J. D., PACKER D. M. and TOUSEY R., 1959, *Nature*, 184, 8.

[14] TORESSON Y. G., 1960, *Arkiv for Fysik*, 18, 389.

[15] WATANABE K. 1958 *Advances in Geophysics*, Ed. H. E. Landsberg and J. Van Miegham, Academic Press, New York, vol. 5, 154.

[16] WATANABE K., 1960, private communication.

[17] WILSON N., TOUSEY R., PURCELL J. D., JOHNSON F. S. and MOORE C. E., 1954, *Astrophys. J.*, 119, 590.

[18] WORLEY R. E., 1943, *Phys. Rev.*, 64, 207.

Imprimerie TAFFIN-LEFORT, à Lille (France). — *Published in France.*

THE SOLAR SPECTRUM FROM 2635 TO 2085 A

H. H. MALITSON, J. D. PURCELL, R. TOUSEY,
AND C. E. MOORE

Reprinted for private circulation from
THE ASTROPHYSICAL JOURNAL
Vol. 132, No. 3, November 1960

THE SOLAR SPECTRUM FROM 2635 TO 2085 A

H. H. MALITSON, J. D. PURCELL, AND R. TOUSEY
U.S. Naval Research Laboratory, Washington 25, D.C.
AND
C. E. MOORE
National Bureau of Standards, Washington 25, D.C.
Received June 9, 1960

ABSTRACT

Solar ultraviolet spectra obtained from rockets flown on December 15, 1952, February 21, 1955, and June 4, 1956, are presented and analyzed over the wave-length range 2635–2085 A, together with an absolute spectral intensity-distribution-curve. In all, 538 absorption features were observed, and 949 atomic lines are listed as contributing to the observed spectrum.

I. INTRODUCTION

Analyses of solar ultraviolet spectra obtained from rockets have been published by Durand, Oberley, and Tousey (1949), by Hopfield and Clearman (1948), and by Clearman (1953) for the range 3000–2200 A; by Wilson, Tousey, Purcell, Johnson, and Moore (1954) for 2990–2635 A; and by Kachalov, Pavlenko, and Yakovleva (1958) for 2635–2417 A, and (1959) for 2937–2636 A. The present paper continues the analysis of Wilson *et al.* (1954), and extends it to 2085 A. At this wave length the intensity drops suddenly to a level near the bottoms of the Fraunhofer lines, thus placing a natural limit to the spectral range to be covered. Below 2085 A, Fraunhofer lines can still be seen, but they are weak.

II. THE SPECTRA

The spectra upon which the analysis is based were obtained from three rocket flights: Viking 6, December 15, 1952; Aerobee-29, February 21, 1955; and Aerobee-46, June 4, 1956. The various exposures were obtained at different altitudes, but all were sufficiently high to be free from absorption by ozone. The major portion of the analysis was carried out with spectra from the two earlier flights. Aerobee-46, however, gave several spectra of considerably higher resolution. Therefore, the final list was increased somewhat, by addition of lines from this flight, but only lines which were visible in two or more exposures.

All spectrographs employed a 600 lines/mm-, 40 cm-radius, aluminized diffraction-grating. The principal differences lay in the method of illuminating the slit.

In the Viking 9 spectrograph, a "mirror-jawed" slit was employed to expand the field of view, as described by Johnson, Purcell, Tousey, and Watanabe (1952). The instrument was not pointed at the sun but was mounted rigidly in the rocket nose. The spectrograph contained two cameras, the one photographing the first-order spectrum on one side of the central image and the other the second-order spectrum on the opposite side. The spectrum used in the present analysis was a very dense first-order exposure on Eastman IV-O-UV film. A reproduction of this spectrum has been published by Tousey (1953*a*, *b*). The resolution was about 0.6 A.

The designs of the spectrographs flown in Aerobee-29 and Aerobee-46 are shown in Figure 1. The housing, in each case, contained two instruments. The entire unit was pointed at the sun during flight by means of the biaxial pointing control of the University of Colorado (Stacey, Stith, Nidey, and Pietenpol 1954). The lower instrument, described by Johnson, Malitson, Purcell, and Tousey (1958), was the one which gave the spectra

from Aerobee-29, used in the present paper. Several good exposures were obtained, but the resolution, because of the use of a 25 μ slit, was only about 1 A.

The best spectra were obtained from the flight of Aerobee-46, by using the upper spectrograph of Figure 1. This likewise employed a 600 lines/mm-, 40 cm-grating, but a plane aluminized mirror was introduced to fold the light-path so as to fit the instrument into the space available in the housing. The sun's image was focused on the slit with a lithium fluoride lens. A wave-length range of 3000 A to about 1100 A was covered; however, wave lengths below 1700 A were weak because of the reduced reflectance of the two aluminum surfaces and the low transmittance of the lithium fluoride lens. Some reduction in the intensity of long-wave-length stray light was effected by focal isolation. This was accomplished by positioning the lens so that the image was in focus for 1300 A. The dispersion of the LiF caused the visible and near-ultraviolet to be greatly out of focus and consequently reduced in intensity. These wave lengths were further reduced in intensity by blocking off the center of the lens with a mask.

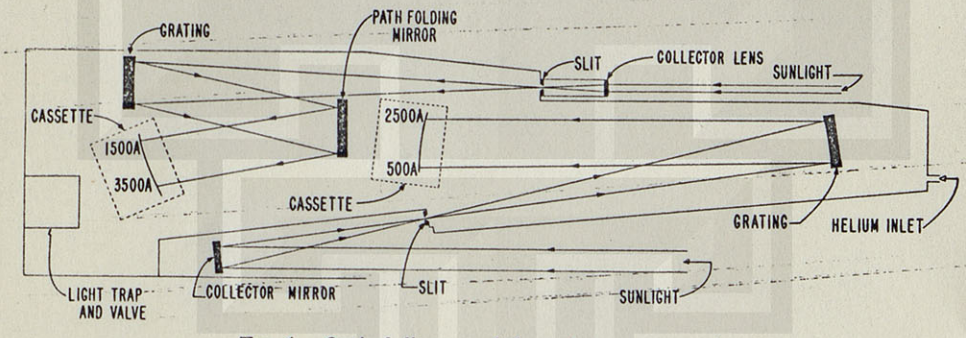

FIG. 1.—Optical diagram of the rocket spectrographs

Five excellent spectra were obtained with the Aerobee-46 spectrograph on IV-O-UV film. The resolution was limited by the slit width to a value of about 0.6 A. One of these spectra is reproduced in Figure 2. Vertical variation in density is not solar but was caused by the focal-isolation slit illumination. The same spectrum is shown in Figure 3 but printed with the paper moving parallel to the lines, so as to reduce the effects of graininess and make the fainter lines easier to see. Both are positive prints, absorption being reproduced as dark.

All these spectra suffer, of course, from both instrumental and natural blending. The discussion of the blending problem presented in the first paper by Wilson *et al.* (1954) applies. In brief, it was shown by comparison of the rocket spectrum, obtained with a 0.65 A equivalent slit width and the intensity-curve of the Utrecht *Atlas* (Minnaert, Mulders, and Houtgast 1940) averaged over a 0.65 A interval, that the observed solar lines should not be expected to match perfectly the spectrum synthesized from a list of probable contributors. For example, a solar absorption line may differ in wave length by as much as 0.3 A from the strongest contributor, because of the influence of other nearby contributors which are not resolved by the spectrograph.

III. WAVE LENGTHS

Forty of the least-blended strong spectral lines were selected for use as wave-length standards in determining the dispersion for each film. The lines used as standards are shown in Table 1. Five lines are included that are blends of two closely spaced lines in the same spectrum.

A linear dispersion equation, with corrections as great as ± 0.2 A in certain regions

and ±0.4 A near 2100 A, was found to describe each spectrum with sufficient accuracy. The small variations between spectra were attributed to erratic dimensional changes in the film. Wave-length measurements are considered accurate to ±0.1 A.

IV. INTENSITIES

The curve of spectral intensity reproduced in Figure 4 was determined from the spectra of Aerobee-46. Density-curves of the films were first recorded with a microdensitometer. The density traces were reduced to relative intensity-curves by means of an optical-mechanical device describe by Purcell (1954). This device contact-printed the trace as it and a piece of sensitized paper were caused to move at different rates past a long illuminated slit running parallel to the wave-length axis. The motions of the

TABLE 1

STANDARD LINES

Multiplet No.	Spectrum	Laboratory Wave Length (A)	Multiplet No.	Spectrum	Laboratory Wave Length (A)
1	Fe II	2628.291	2	Fe II	2388.629
1	Fe II	2621.669	3	Fe II	2364.825
1	Fe II	2613.820	35	Fe II	2354.884
64	Fe II	2591.542	3	Fe II	2332.798
64	Fe II	2582.582	3	Fe II	2327.391
64	Fe II	2566.908	11	Ni II	2316.034
177, 177	Fe II	2555.26	10	Ni I	2310.952
7	Fe I	2522.848	14	Fe I	2287.248
1	Si I	2516.109	73	Fe I	2255.861
1	Si I	2514.315	70	Fe I	2248.858
7	Fe I	2510.833	3	Si I	2216.670
7	Fe I	2501.130	3	Si I	2207.972
9	Fe I	2488.143	21, 21	Fe I	2186.84
9	Fe I	2483.270	24	Fe I	2171.292
9	Fe I	2479.775	21	Fe I	2166.769
9	Fe I	2447.708	24	Fe I	2138.589
2	Fe II	2413.308	48	Si I	2124.111
2	Fe II	2406.660	33, 81	Fe I	2113.00
2	Fe II	2399.237	31, 33	Fe I	2106.32
2, 2	Fe II	2395.53	33	Fe I	2093.660

trace and paper were controlled by cams whose shapes were determined by the characteristic curves of the flight film at different wave lengths. These curves were found from exposures made on the same batch of film with a carbon-arc source just before flight and were developed with the rocket exposures. Although showing detail accurately, the resulting intensity traces were subject to error over a wide wave-length range because of the extreme dependence of the focal-isolation slit illumination device on the accuracy with which the spectrograph was pointed at the sun during flight. A correction was made by adjusting the trace to match in intensity the data obtained from a subsequent rocket experiment which was designed specifically to measure the intensity distribution under the best possible photometric conditions but without high resolution. The principal features of the latter experiment were the use of a wide slit (8 A) and a quartz diffusing screen before the slit to insure that the system was illuminated in the same way at all wave lengths, regardless of pointing errors. Calibration was accomplished with a carbon arc as described in our earlier paper. The carbon-arc measurements of Packer and Lock (1951) and of Johnson (1956) were used to establish the relative intensity–distribution-

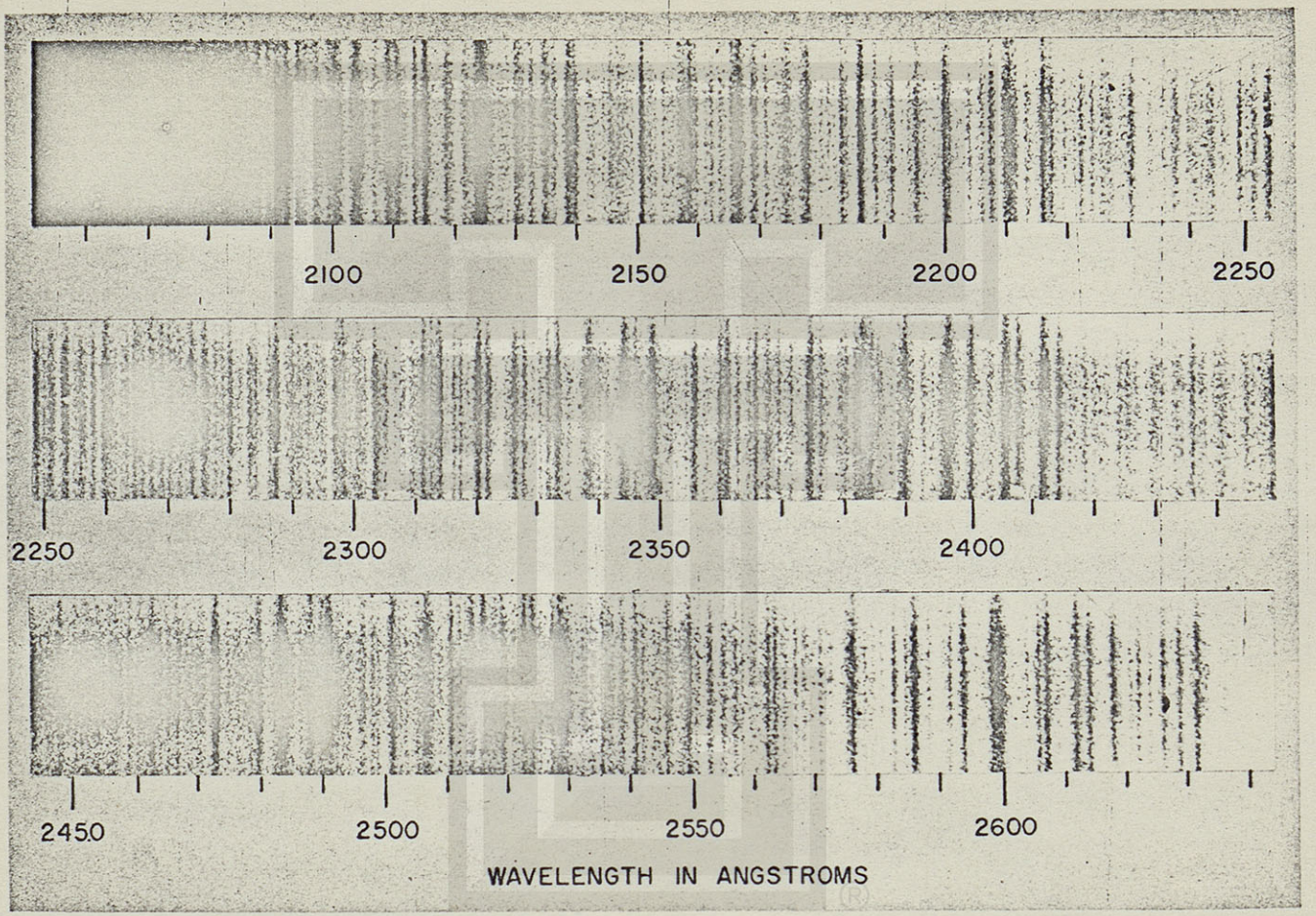

FIG. 2.—A solar spectrum photographed from Aerobee-46, June 4, 1956

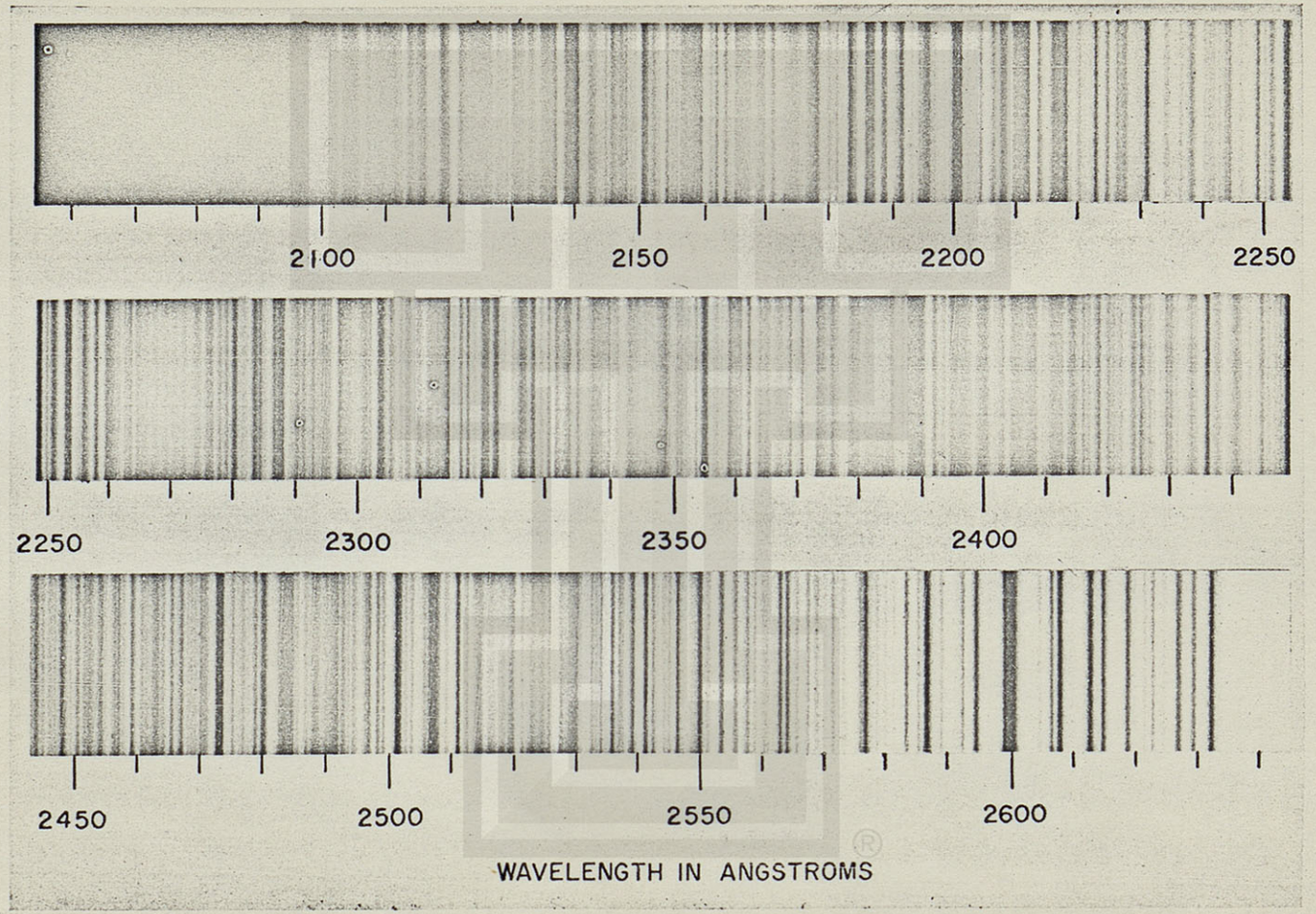

FIG. 3.—The spectrum of Fig. 2 printed with motion introduced parallel to the lines

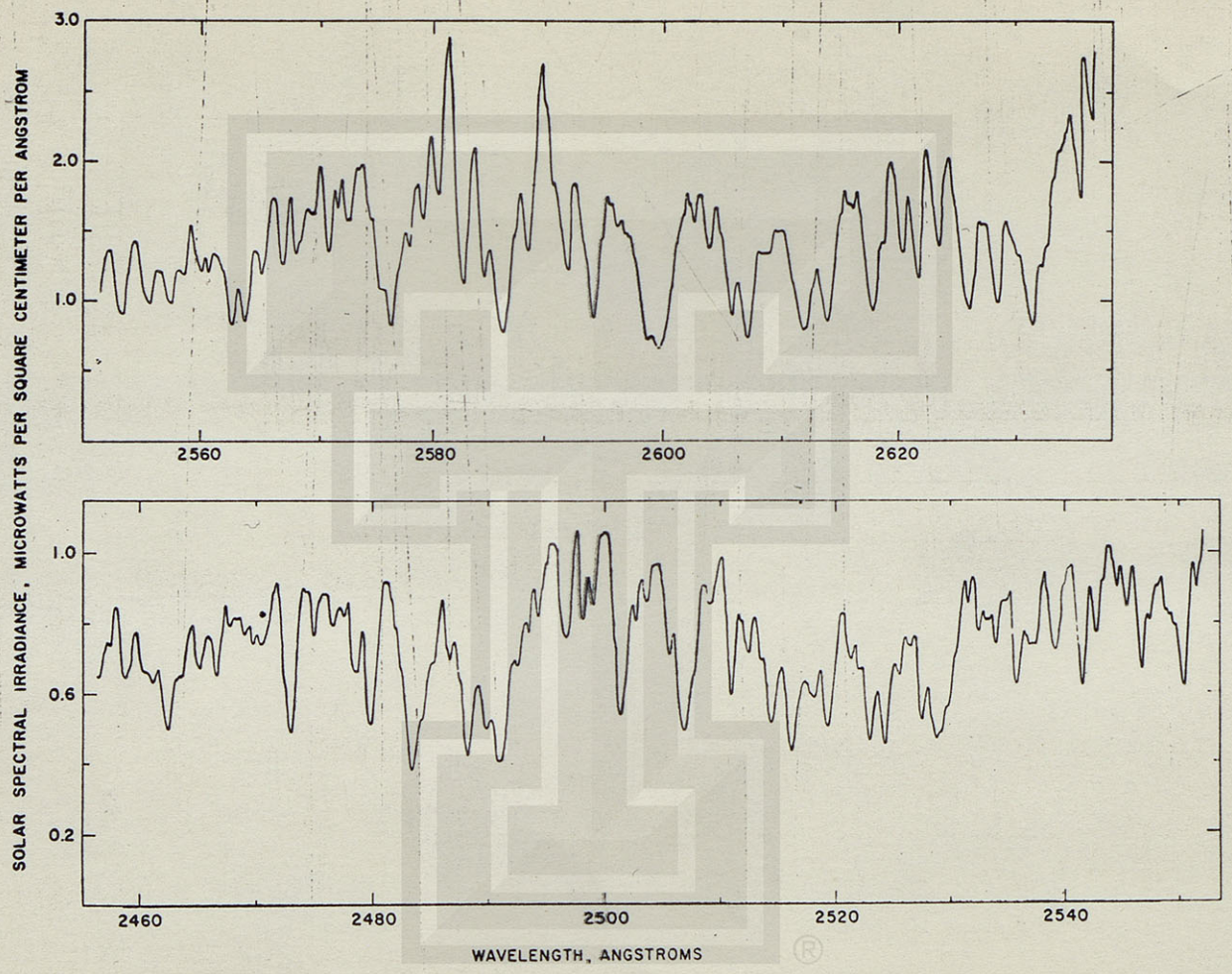

FIG. 4*a*.—The spectral intensity distribution of integrated sunlight

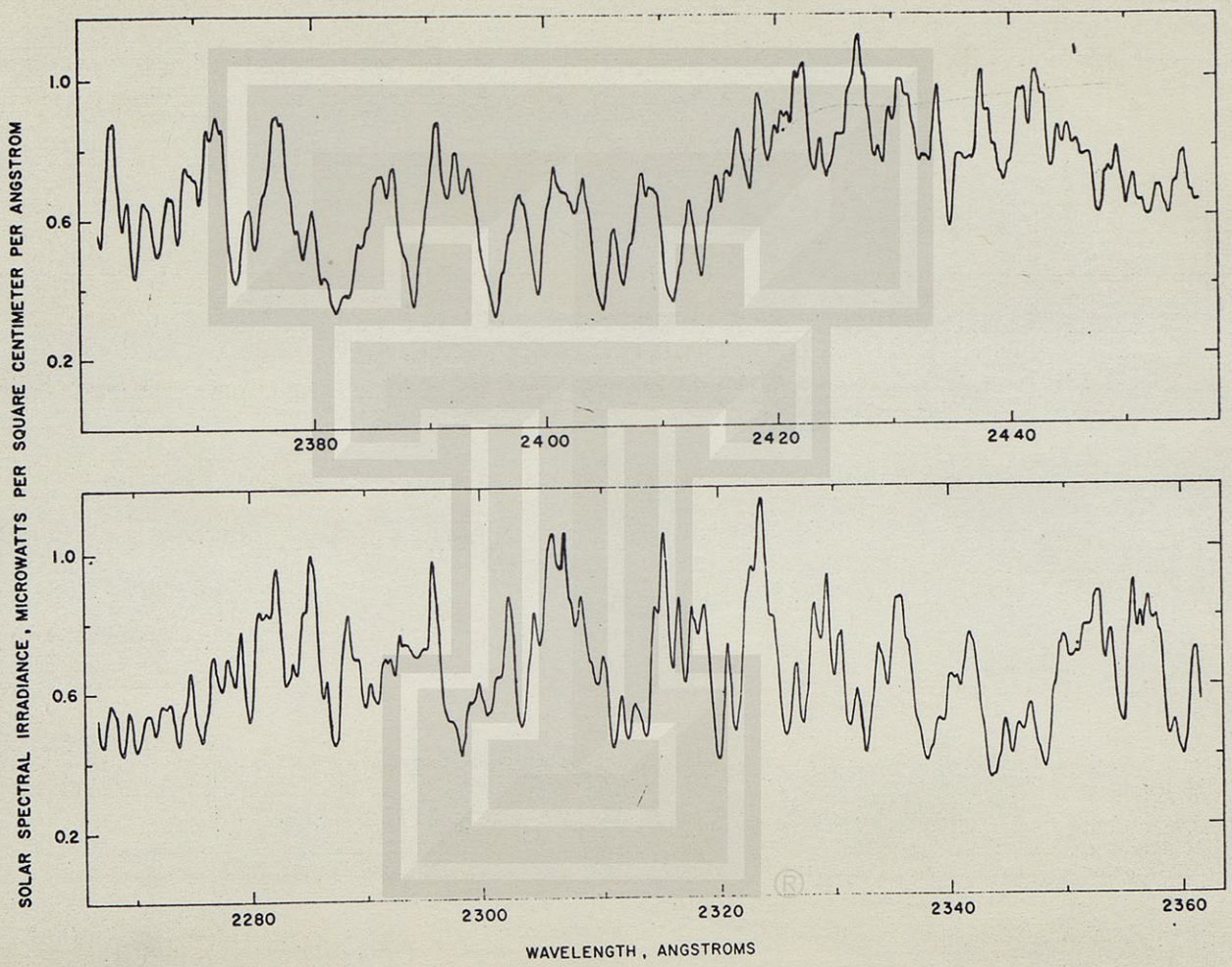

FIG. 4*b*.—The spectral intensity distribution of integrated sunlight

curve for the solar spectrum. The relative intensity-curve was adjusted to an absolute scale by fitting it at 3200 A to the absolute solar intensity distribution-curve as determined by Dunkelman and Scolnik (1959).

The spectral intensity-curve of Figure 4 does not agree exactly at wave lengths below 2300 A with preliminary curves published by Tousey (1953) and by Johnson, Purcell, and Tousey (1954). This change results from the use of the new data for the carbon arc.

V. THE IDENTIFICATION TABLE

In Table 2 is presented a list of the observed absorption features and the probable contributing atomic lines. The form used is that of an expanded linear wave-length scale, with columns 20 A long. As in the earlier paper by Wilson *et al.* (1954), the spectral intensity distribution-curve is presented instead of visual intensity estimates. This curve is a highly expanded version of Figure 4.

The first column of Table 2 presents the measured wave lengths, taken from the Aerobee-46 spectra. The remaining columns contain data from the *Ultraviolet Multiplet Table* of Moore (1950, 1952) concerning those atomic lines considered to contribute most heavily to the observed absorption spectrum. Column 2 presents the laboratory wave lengths, entered in their proper positions on the scale. A dash preceding the wave length indicates the line which is considered to be the predominant contributor to an absorption feature. The third column gives the estimated laboratory intensities, assembled by Moore (1950, 1952) from many different references. Intensities should be used with caution in any comparisons except within a single multiplet. In the fourth column are listed the multiplet numbers assigned by Moore; an asterisk in front indicates blending with another line in the same spectrum, and in this case only the lower multiplet number is given. The selection of contributors follows the procedure described by Wilson *et al.* (1954).

Over the common range, 2635–2300 A, the spectrum described by Table 2 lists approximately four times more lines than were present in the earlier spectra described by Durand, Oberley, and Tousey (1949) and in the spectrum of Hopfield and Clearman (1948), as revised by Clearman (1953). This is, of course, a result of the somewhat greater resolution and denser exposure.

The spectrum reported by Kachalov *et al.* (1958), over the range 2635–2471 A, obtained with a 1-meter radius-, 600 lines/mm-grating, is more highly resolved than the present spectrum and shows about half again more lines. The agreement is excellent, however, and many of their recorded weak lines that we have not observed visually show as slight dips in our intensity trace. Wave lengths are not always in exact agreement for the faint lines, but this is to be expected because of the effect of low resolving power and blends. The identifications differ mainly in details and in the selection of principal contributors. This is largely a matter of judgment and is, of course, strongly influenced by the degree of resolution of the particular spectrum.

VI. IDENTIFICATIONS

Beryllium Z=4.—As noted by Wilson *et al.* (1954), Be I is represented by the six lines of multiplet (2) at about 2650 A, which are unresolved. The three lines of Be I (3) at 2494.6 A appear to be present with low intensity but are unresolved in both the spectrum of Kachalov *et al.* (1958) and ours. The raie ultime, 2348.612 A, is masked by Fe II (3) 2348.300 A, all nine of whose components are present with great intensity. Thus Be I is regarded as present.

Boron Z=5.—The raie ultime, 2497.724 A, is not present, nor is 2496.773 A.

Carbon Z=6.—The two lines (60) and (61) of C I listed in this region by Moore (1950, 1952) are entered in Table 1 but are not considered to be significant contributors to the observed features. Three lines of C II (14) near 2510 A are masked and probably have low intensity because of the high excitation potential, 13.66 e.v.

Table 2. The solar spectrum from 2635 to 2085 A.
(Intensities in microwatts cm^{-2} A-1)

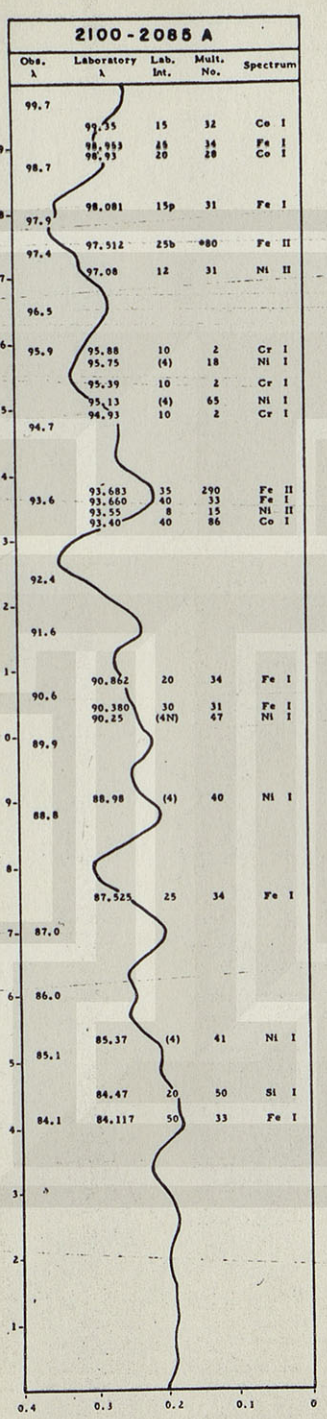

Table 2-Continued

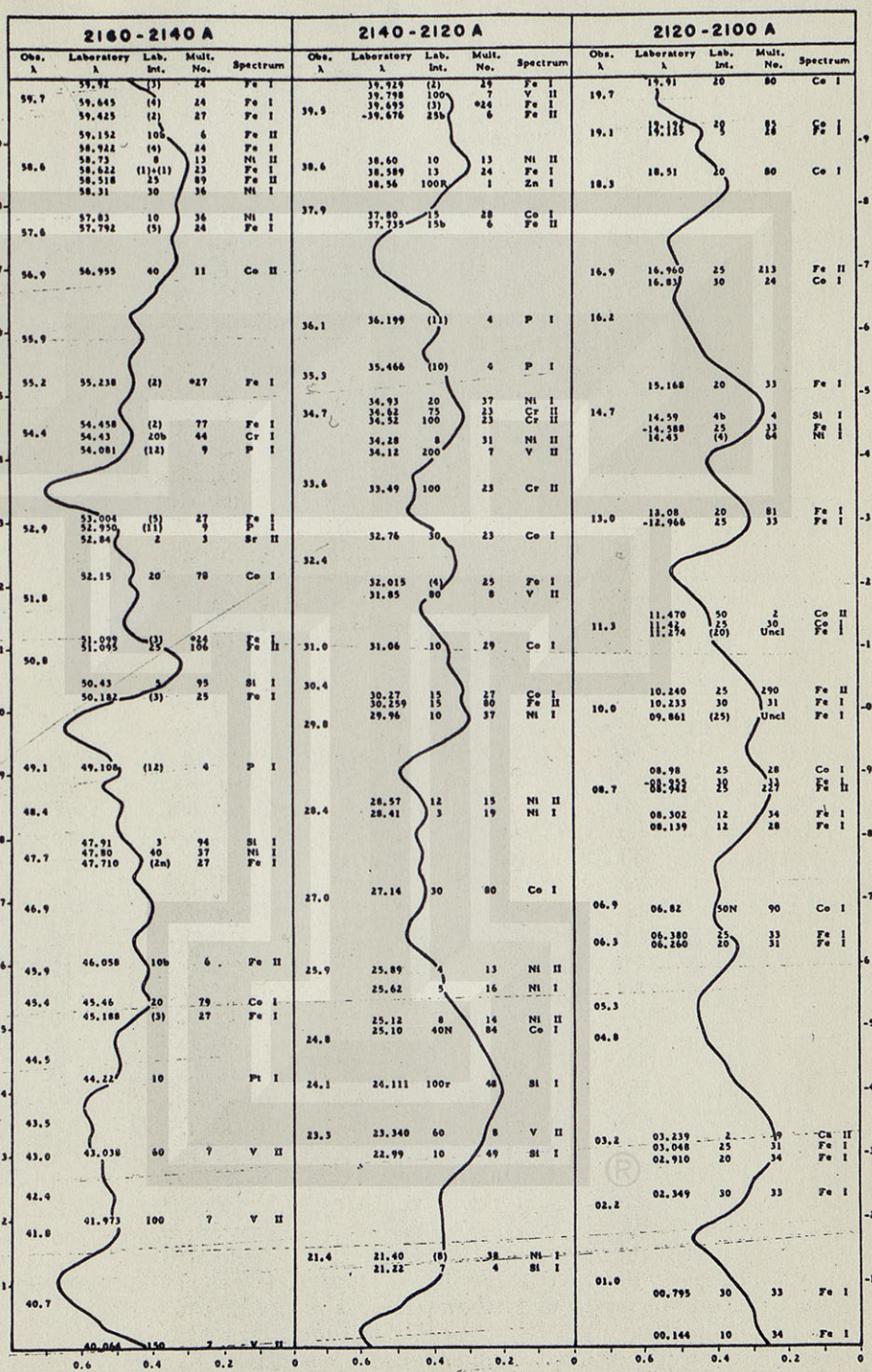

Table 2-Continued

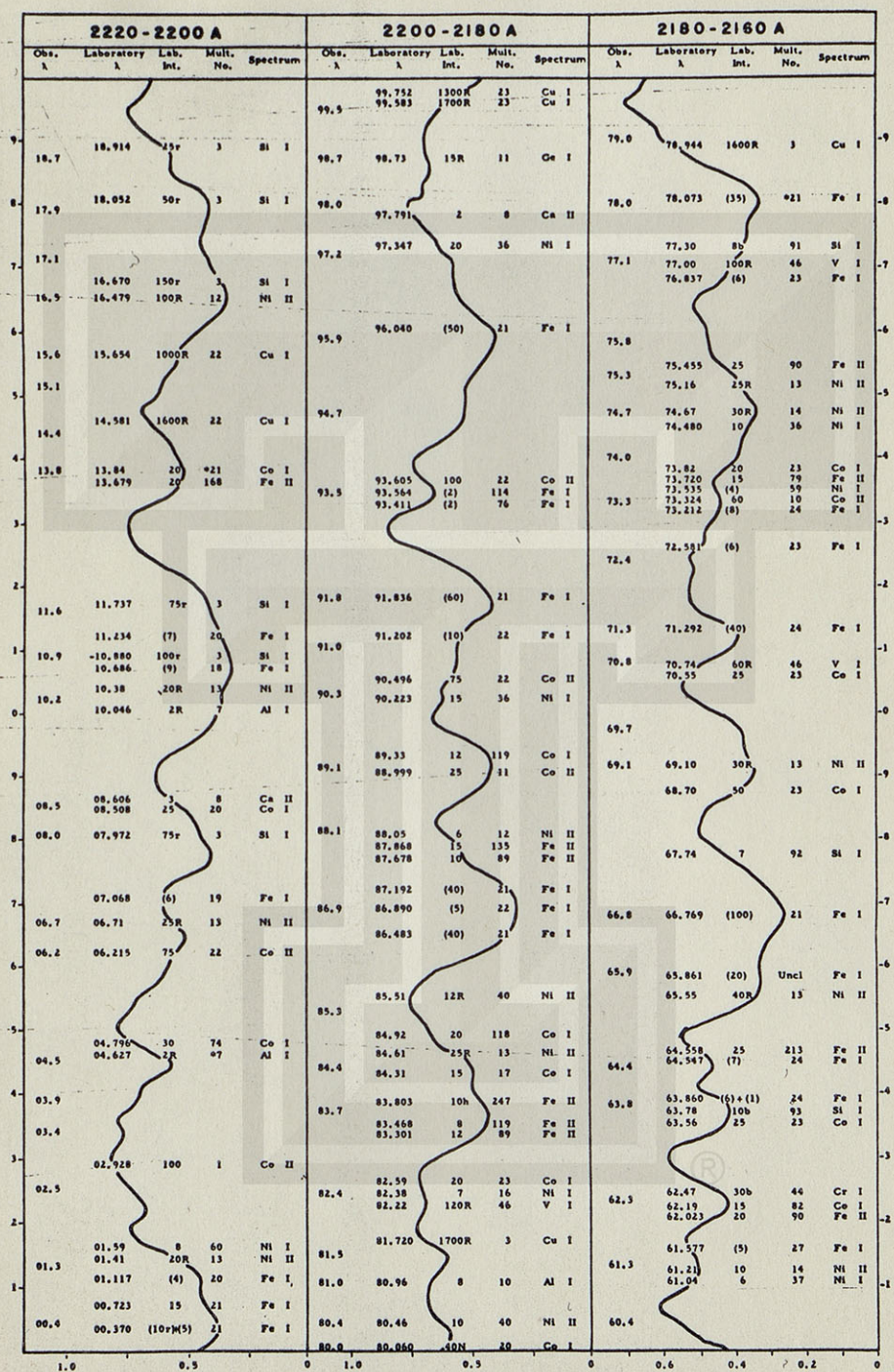

Table 2-Continued

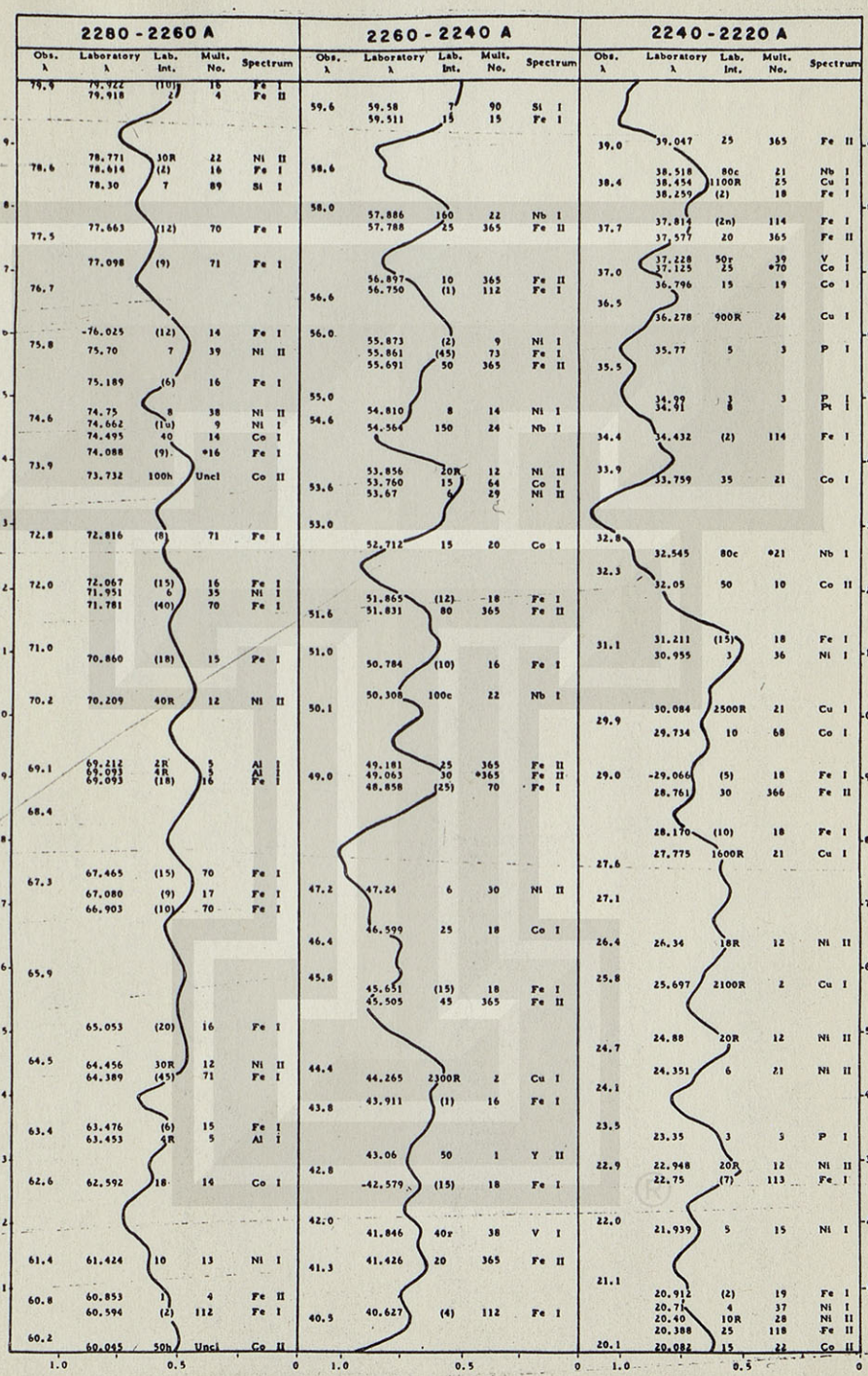

2280 - 2260 A					2260 - 2240 A					2240 - 2220 A				
Obs. λ	Laboratory λ	Lab. Int.	Mult. No.	Spectrum	Obs. λ	Laboratory λ	Lab. Int.	Mult. No.	Spectrum	Obs. λ	Laboratory λ	Lab. Int.	Mult. No.	Spectrum
79.9	79.922	(10)	16	Fe I										
	79.918	2	4	Fe II										
					59.6	59.58	7	90	Si I					
						59.511	15	15	Fe I					
										39.0	39.047	25	365	Fe II
	78.771	30R	22	Ni II							38.518	80c	21	Nb I
78.6	78.614	(2)	16	Fe I	58.6					38.4	38.454	1100R	25	Cu I
	78.30	7	89	Si I							38.259	(2)	18	Fe I
					58.0	57.886	160	22	Nb I					
	77.663	(12)	70	Fe I		57.788	25	365	Fe II	37.7	37.814	(2n)	114	Fe I
77.5											37.577	20	365	Fe II
	77.098	(9)	71	Fe I							37.228	50r	39	V I
						56.897	10	365	Fe II	37.0	37.125	25	*70	Co I
76.7					56.6	56.750	(1)	112	Fe I		36.796	15	19	Co I
										36.5				
	-76.025	(12)	14	Fe I	56.0						36.278	900R	24	Cu I
75.8	75.70	7	39	Ni II		55.873	(2)	9	Ni I					
						55.861	(45)	73	Fe I		35.77	5	3	P I
	75.189	(6)	16	Fe I		55.691	50	365	Fe II	35.5				
					55.0						34.99	3	3	P I
	74.75	8	38	Ni II		54.810	8	14	Ni I		34.91	8		Pt I
74.6	74.662	(1u)	9	Ni I	54.6	54.564	150	24	Nb I					
	74.495	40	14	Co I						34.4	34.432	(2)	114	Fe I
	74.088	(9)	*16	Fe I										
73.9						53.856	20R	12	Ni II	33.9				
	73.732	100h	Uncl	Co II	53.6	53.760	15	64	Co I		33.759	35	21	Co I
						53.67	6	29	Ni II					
					53.0									
72.8	72.816	(8)	71	Fe I		52.712	15	20	Co I	32.8				
											32.545	80c	*21	Nb I
										32.3				
72.0	72.067	(15)	16	Fe I							32.05	50	10	Co II
	71.951	6	35	Ni I		51.865	(12)	-18	Fe I					
	71.781	(40)	70	Fe I	51.6	51.831	80	365	Fe II					
										31.1	31.211	(15)	18	Fe I
71.0					51.0						30.955	3	36	Ni I
	70.860	(18)	15	Fe I		50.784	(10)	16	Fe I					
70.2	70.209	40R	12	Ni II		50.308	100c	22	Nb I		30.084	2500R	21	Cu I
					50.1					29.9				
											29.734	10	68	Co I
	69.212	2R	5	Al I										
69.1	69.093	4R	5	Al I		49.181	25	365	Fe II					
	69.093	(18)	16	Fe I	49.0	49.063	30	*365	Fe II	29.0	-29.066	(5)	18	Fe I
						48.858	(25)	70	Fe I		28.761	30	366	Fe II
68.4														
											28.170	(10)	18	Fe I
											27.775	1600R	21	Cu I
	67.465	(15)	70	Fe I						27.6				
67.3	67.080	(9)	17	Fe I	47.2	47.24	6	30	Ni II	27.1				
	66.903	(10)	70	Fe I										
					46.4	46.599	25	18	Co I					
										26.4	26.34	18R	12	Ni II
65.9					45.8					25.8				
						45.651	(15)	18	Fe I		25.697	2100R	2	Cu I
	65.053	(20)	16	Fe I		45.505	45	365	Fe II					
	64.456	30R	12	Ni II							24.88	20R	12	Ni II
64.5	64.389	(45)	71	Fe I	44.4	44.265	2300R	2	Cu I	24.7				
											24.351	6	21	Ni II
					43.8	43.911	(1)	16	Fe I	24.1				
63.4	63.476	(6)	15	Fe I						23.5				
	63.453	4R	5	Al I							23.35	3	5	P I
						43.06	50	1	Y II					
					42.8									
62.6	62.592	18	14	Co I		42.579	(15)	18	Fe I	22.9	22.948	20R	12	Ni II
											22.75	(7)	113	Fe I
					42.0									
						41.846	40r	38	V I	22.0				
											21.939	5	15	Ni I
61.4	61.424	10	13	Ni I	41.3	41.426	20	365	Fe II					
										21.1				
60.8	60.853	1	4	Fe II							20.912	(2)	19	Fe I
	60.594	(2)	112	Fe I	40.5	40.627	(4)	112	Fe I		20.71	4	37	Ni I
											20.40	10R	28	Ni II
60.2											20.388	25	118	Fe II
	60.045	50h	Uncl	Co II						20.1	20.082	15	22	Co II

Table 2-Continued

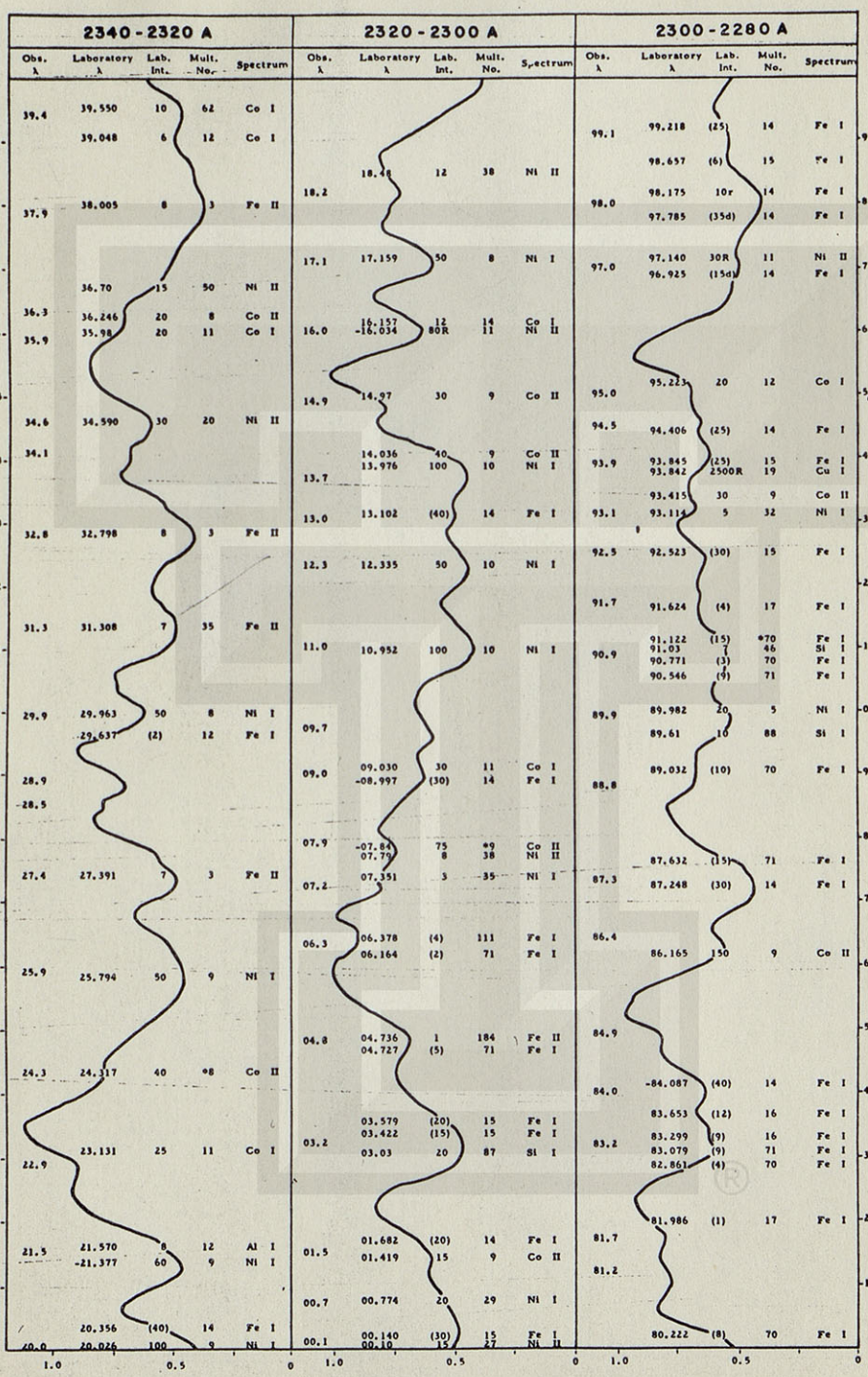

2340 - 2320 A					2320 - 2300 A					2300 - 2280 A				
Obs. λ	Laboratory λ	Lab. Int.	Mult. No.	Spectrum	Obs. λ	Laboratory λ	Lab. Int.	Mult. No.	Spectrum	Obs. λ	Laboratory λ	Lab. Int.	Mult. No.	Spectrum
39.4	39.550	10	62	Co I										
	39.048	6	12	Co I						99.1	99.218	(25)	14	Fe I
						18.48	12	38	Ni II		98.657	(6)	15	Fe I
37.9	38.005	8	3	Fe II	18.2					98.0	98.175	10r	14	Fe I
											97.785	(35d)	14	Fe I
					17.1	17.159	50	8	Ni I	97.0	97.140	30R	11	Ni II
	36.70	15	50	Ni II							96.925	(15d)	14	Fe I
36.3	36.246	20	8	Co II										
35.9	35.98	20	11	Co I	16.0	16.157 16.034	12 80R	14 11	Co I Ni II					
											95.223	20	12	Co I
					14.9	14.97	30	9	Co II	95.0				
34.6	34.590	30	20	Ni II						94.5	94.406	(25)	14	Fe I
34.1						14.036	40	9	Co II					
						13.976	100	10	Ni I	93.9	93.845 93.842	(25) 2500R	15 19	Fe I Cu I
					13.7									
											93.415	30	9	Co II
					13.0	13.102	(40)	14	Fe I	93.1	93.114	5	32	Ni I
32.8	32.798	8	3	Fe II										
					12.3	12.335	50	10	Ni I	92.5	92.523	(30)	15	Fe I
										91.7	91.624	(4)	17	Fe I
31.3	31.308	7	35	Fe II										
					11.0	10.952	100	10	Ni I		91.122	(15)	*70	Fe I
										90.9	91.03	?	46	Si I
											90.771	(3)	70	Fe I
											90.546	(9)	71	Fe I
29.9	29.963	50	8	Ni I						89.9	89.982	20	5	Ni I
	29.637	(2)	12	Fe I	09.7						89.61	10	88	Si I
						09.030	30	11	Co I					
28.9					09.0	08.997	(30)	14	Fe I	88.8	89.032	(10)	70	Fe I
28.5														
					07.9	07.84	75	*9	Co II					
						07.79	8	38	Ni II		87.632	(15)	71	Fe I
27.4	27.391	7	3	Fe II	07.2	07.351	3	35	Ni I	87.3	87.248	(30)	14	Fe I
										86.4				
					06.3	06.378	(4)	111	Fe I		86.165	150	9	Co II
						06.164	(2)	71	Fe I					
25.9	25.794	50	9	Ni I										
										84.9				
					04.8	04.736	1	184	Fe II					
						04.727	(5)	71	Fe I					
24.3	24.317	40	*8	Co II							-84.087	(40)	14	Fe I
										84.0				
						03.579	(20)	15	Fe I		83.653	(12)	16	Fe I
						03.422	(15)	15	Fe I		83.299	(9)	16	Fe I
	23.131	25	11	Co I	03.2	03.03	20	87	Si I	83.2	83.079	(9)	71	Fe I
22.9											82.861	(4)	70	Fe I
											81.986	(1)	17	Fe I
						01.682	(20)	14	Fe I	81.7				
21.5	21.570	8	12	Al I	01.5	01.419	15	9	Co II					
	-21.377	60	9	Ni I						81.2				
					00.7	00.774	20	29	Ni I					
	20.356	(40)	14	Fe I										
20.0	20.026	100	9	Ni I	00.1	00.140 00.10	(30) 15	15 27	Fe I Ni II		80.222	(8)	70	Fe I

Table 2-Continued

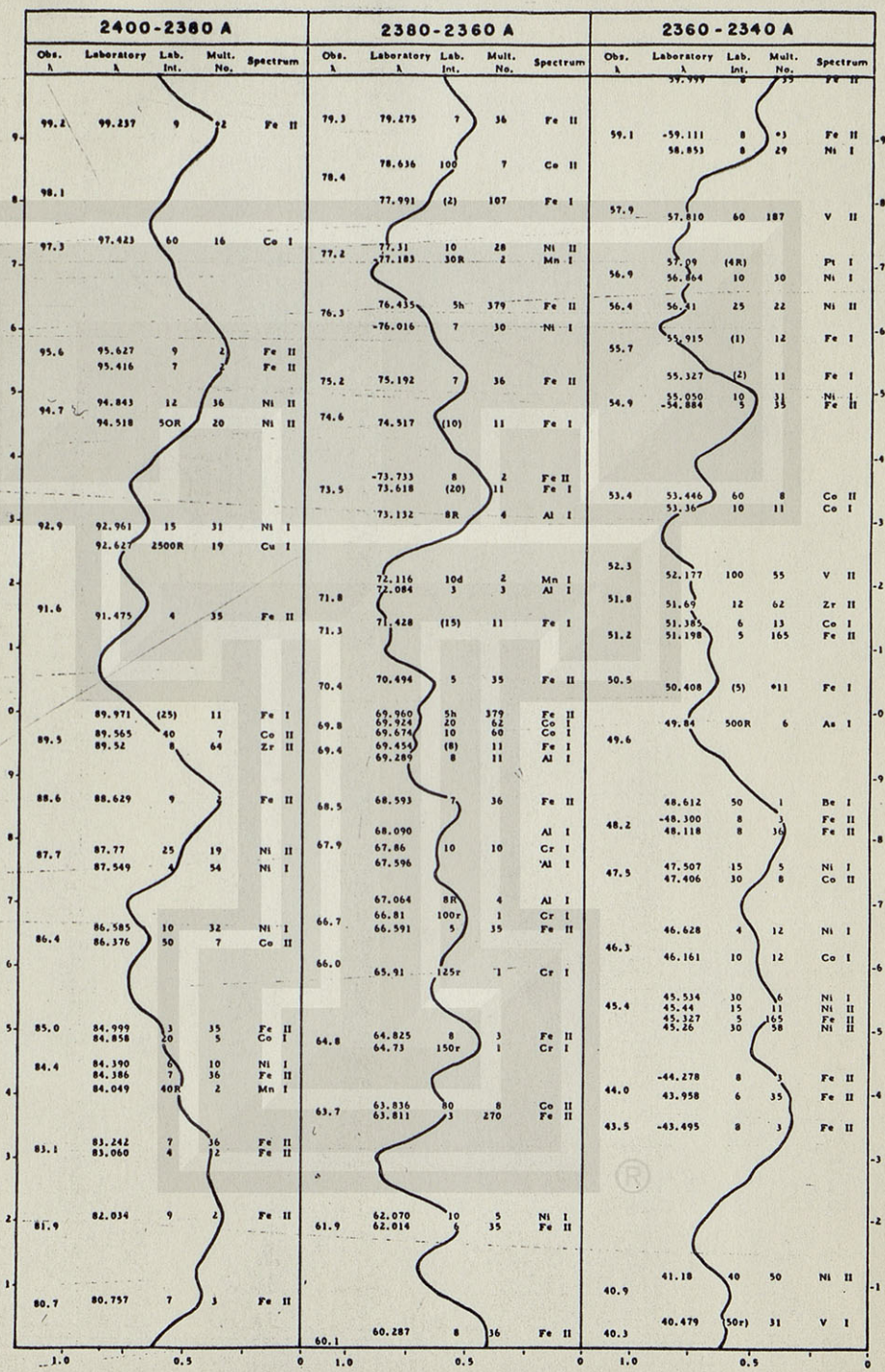

2400-2380 A					2380-2360 A					2360-2340 A				
Obs. λ	Laboratory λ	Lab. Int.	Mult. No.	Spectrum	Obs. λ	Laboratory λ	Lab. Int.	Mult. No.	Spectrum	Obs. λ	Laboratory λ	Lab. Int.	Mult. No.	Spectrum
											59.999	8	35	Fe II
99.2	99.237	9	42	Fe II	79.3	79.275	7	36	Fe II	59.1	-59.111	8	•3	Fe II
											58.853	8	29	Ni I
						78.636	100	7	Co II					
98.1					78.4									
						77.991	(2)	107	Fe I	57.9				
											57.810	60	187	V II
97.3	97.423	60	16	Co I		77.31	10	28	Ni II					
					77.2	77.183	30R	2	Mn I		57.09	(4R)		Pt I
										56.9	56.864	10	30	Ni I
						76.435	5h	379	Fe II	56.4	56.41	25	22	Ni II
					76.3	-76.016	7	30	Ni I					
95.6	95.627	9	2	Fe II						55.7	55.915	(1)	12	Fe I
	95.416	7	2	Fe II										
					75.2	75.192	7	36	Fe II		55.327	(2)	11	Fe I
94.7	94.843	12	36	Ni II							55.050	10	31	Ni I
	94.518	50R	20	Ni II	74.6	74.517	(10)	11	Fe I	54.9	-54.884	5	35	Fe II
						-73.733	8	2	Fe II					
					73.5	73.618	(20)	11	Fe I	53.4	53.446	60	8	Co II
						73.132	8R	4	Al I		53.36	10	11	Co I
92.9	92.961	15	31	Ni I										
	92.627	2500R	19	Cu I						52.3				
						72.116	10d	2	Mn I		52.177	100	55	V II
						72.084	3	3	Al I					
					71.8					51.8	51.69	12	62	Zr II
91.6	91.475	4	35	Fe II							51.385	6	13	Co I
					71.3	71.428	(15)	11	Fe I	51.2	51.198	5	165	Fe II
					70.4	70.494	5	35	Fe II	50.5				
											50.408	(5)	•11	Fe I
	89.971	(25)	11	Fe I		69.960	5h	379	Fe II					
	89.565	40	7	Co II	69.8	69.924	20	62	Co I		49.84	500R	6	As I
89.5	89.52	8	64	Zr II		69.674	10	60	Co I	49.6				
					69.4	69.454	(8)	11	Fe I					
						69.289	8	11	Al I					
88.6	88.629	9	2	Fe II							48.612	50	1	Be I
					68.5	68.593	7	36	Fe II		-48.300	8	3	Fe II
						68.090			Al I	48.2	48.118	8	36	Fe II
87.7	87.77	25	19	Ni II	67.9	67.86	10	10	Cr I					
	87.549	4	54	Ni I		67.596			Al I		47.507	15	5	Ni I
										47.5	47.406	30	8	Co II
						67.064	8R	4	Al I					
						66.81	100r	1	Cr I					
	86.585	10	32	Ni I	66.7	66.591	5	35	Fe II		46.628	4	12	Ni I
86.4	86.376	50	7	Co II						46.3				
											46.161	10	12	Co I
					66.0	65.91	125r	1	Cr I					
											45.534	30	6	Ni I
85.0	84.999	3	35	Fe II						45.4	45.44	15	11	Ni II
	84.858	20	5	Co I							45.327	5	165	Fe II
					64.8	64.825	8	3	Fe II		45.26	30	58	Ni II
84.4	84.390	6	10	Ni I		64.73	150r	1	Cr I					
	84.386	7	36	Fe II										
	84.049	40R	2	Mn I							-44.278	8	3	Fe II
										44.0	43.958	6	35	Fe II
					63.7	63.836	80	8	Co II					
						63.811	3	270	Fe II	43.5	-43.495	8	3	Fe II
	83.242	7	36	Fe II										
83.1	83.060	4	12	Fe II										
	82.034	9	2	Fe II		62.070	10	5	Ni I					
81.9					61.9	62.014	6	35	Fe II					
											41.18	40	50	Ni II
80.7	80.757	7	3	Fe II						40.9				
											40.479	50r)	31	V I
						60.287	8	36	Fe II	40.3				
					60.1									

Table 2-Continued

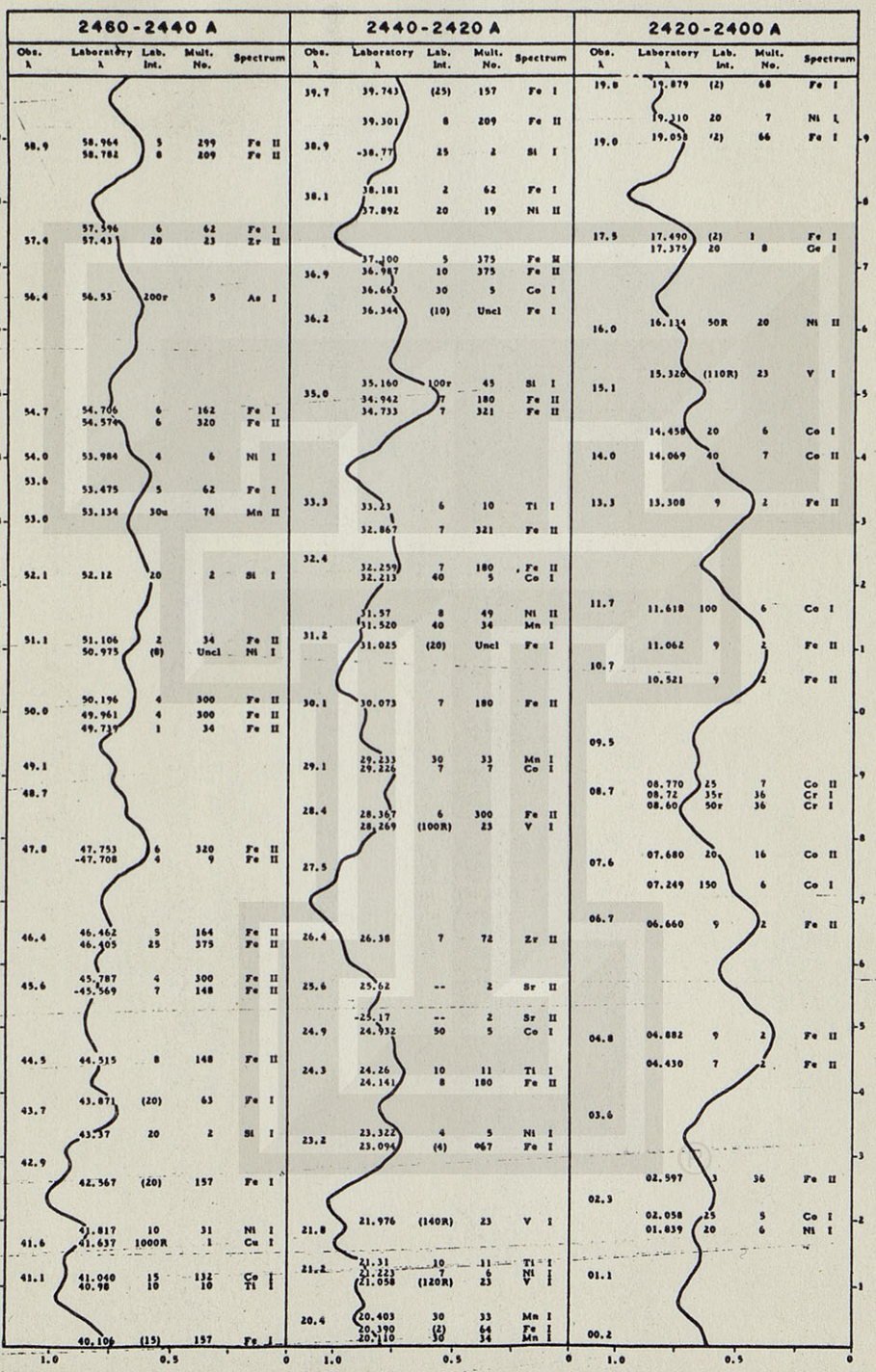

2460 - 2440 A					2440 - 2420 A					2420 - 2400 A				
Obs. λ	Laboratory λ	Lab. Int.	Mult. No.	Spectrum	Obs. λ	Laboratory λ	Lab. Int.	Mult. No.	Spectrum	Obs. λ	Laboratory λ	Lab. Int.	Mult. No.	Spectrum
					39.7	39.743	(25)	157	Fe I	19.8	19.879	(2)	68	Fe I
						39.301	8	209	Fe II		19.210	20	7	Ni I
58.9	58.964	5	299	Fe II	38.9	38.77	25	2	Si I	19.0	19.058	(2)	66	Fe I
	58.782	8	209	Fe II										
					38.1	38.181	2	62	Fe I					
	57.596	6	62	Fe I		37.892	20	19	Ni II					
57.4	57.43	20	23	Zr II						17.5	17.490	(2)	1	Fe I
						37.100	5	375	Fe II		17.375	20	8	Ce I
					36.9	36.987	10	375	Fe II					
56.4	56.53	200r	5	As I		36.663	30	5	Co I					
						36.344	(10)	Uncl	Fe I					
					36.2					16.0	16.134	50R	20	Ni II
						35.160	100r	45	Si I		15.326	(110R)	23	V I
					35.0	34.942	7	180	Fe II	15.1				
54.7	54.706	6	162	Fe I		34.733	7	321	Fe II					
	54.574	6	320	Fe II							14.456	20	6	Co I
54.0	53.984	4	6	Ni I						14.0	14.069	40	7	Co II
53.6														
	53.475	5	62	Fe I										
53.0	53.134	30u	74	Mn II	33.3	33.23	6	10	Ti I	13.3	13.308	9	2	Fe II
						32.867	7	321	Fe II					
					32.4									
						32.259	7	180	Fe II					
52.1	52.12	20	2	Si I		32.213	40	5	Co I					
						31.57	8	49	Ni II	11.7	11.618	100	6	Co I
						31.520	40	34	Mn I					
51.1	51.106	2	34	Fe II	31.2	31.025	(20)	Uncl	Fe I		11.062	9	2	Fe II
	50.975	(8)	Uncl	Ni I						10.7				
											10.521	9	2	Fe II
	50.196	4	300	Fe II	30.1	30.073	7	180	Fe II					
50.0	49.961	4	300	Fe II										
	49.739	1	34	Fe II						09.5				
49.1						29.233	30	33	Mn I					
					29.1	29.226	7	7	Co I					
48.7											08.770	25	7	Co II
					28.4	28.367	6	300	Fe II	08.7	08.72	35r	36	Cr I
						28.269	(100R)	23	V I		08.60	50r	36	Cr I
47.8	47.753	6	320	Fe II										
	47.708	4	9	Fe II	27.5					07.6	07.680	20	16	Co II
											07.249	150	6	Co I
										06.7				
	46.462	5	164	Fe II							06.660	9	2	Fe II
46.4	46.405	25	375	Fe II	26.4	26.38	7	72	Zr II					
	45.787	4	300	Fe II	25.6	25.62	--	2	Sr II					
45.6	45.569	7	148	Fe II										
						25.17	--	2	Sr II					
					24.9	24.932	50	5	Co I	04.8	04.882	9	2	Fe II
44.5	44.515	8	148	Fe II							04.430	7	2	Fe II
					24.3	24.26	10	11	Ti I					
						24.141	8	180	Fe II					
43.7	43.871	(20)	63	Fe I						03.6				
	43.37	20	2	Si I	23.2	23.322	4	5	Ni I					
						23.094	(4)	967	Fe I					
42.9														
	42.567	(20)	157	Fe I							02.597	3	36	Fe II
										02.3				
											02.058	25	5	Co I
	41.817	10	31	Ni I	21.8	21.976	(140R)	23	V I		01.839	20	6	Ni I
41.6	41.637	1000R	1	Cu I										
						21.31	10	11	Ti I					
					21.2	21.223	7	6	Ni I					
41.1	41.040	15	132	Co I		21.058	(120R)	23	V I	01.1				
	40.98	10	10	Ti I										
						20.403	30	33	Mn I					
					20.4	20.390	(2)	64	Fe I					
	40.106	(15)	157	Fe I		20.110	30	34	Mn I	00.2				

Table 2-Continued

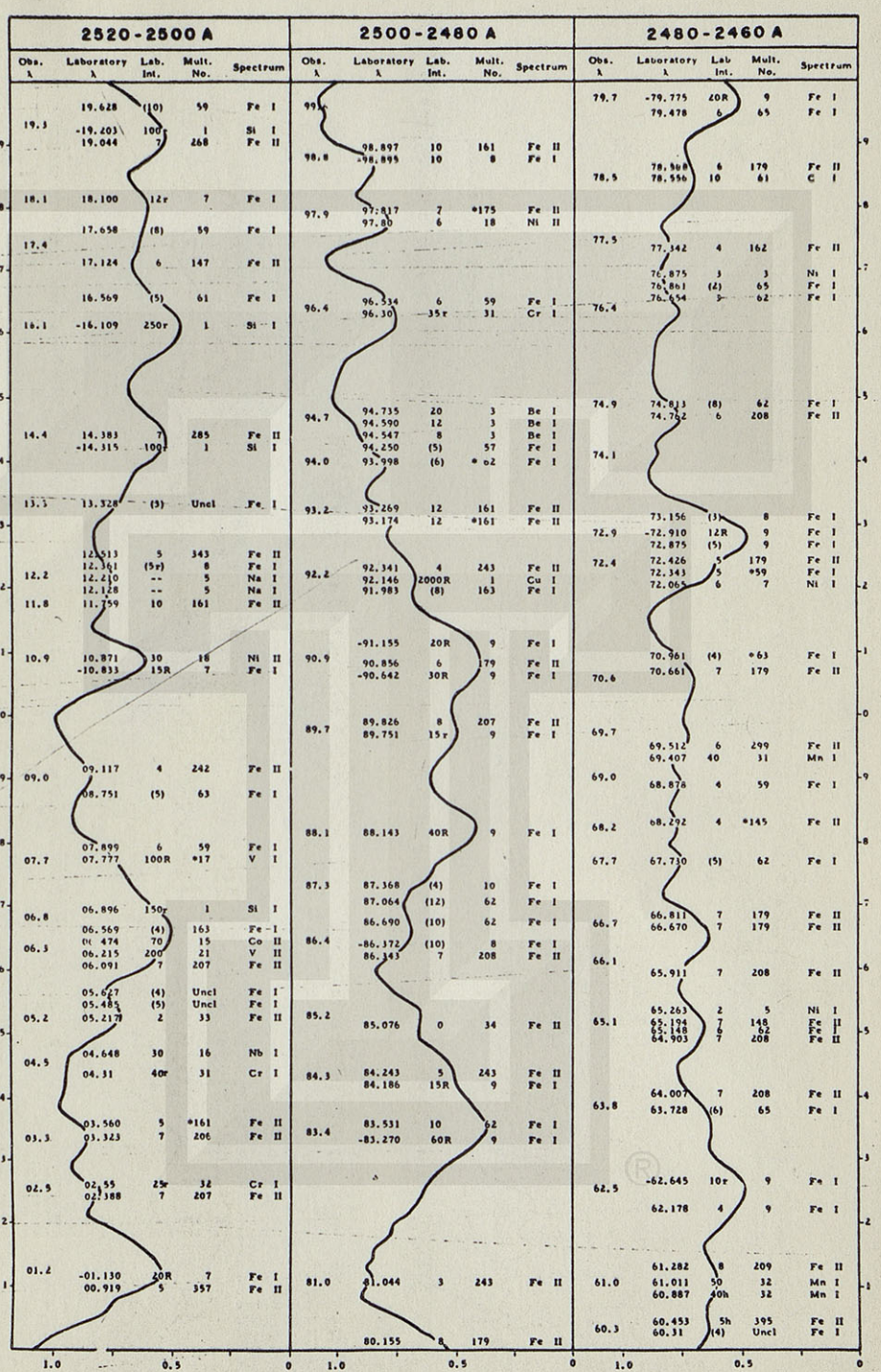

2520 - 2500 A					2500 - 2480 A					2480 - 2460 A				
Obs. λ	Laboratory λ	Lab. Int.	Mult. No.	Spectrum	Obs. λ	Laboratory λ	Lab. Int.	Mult. No.	Spectrum	Obs. λ	Laboratory λ	Lab Int.	Mult. No.	Spectrum
	19.628	(10)	59	Fe I	99.x					79.7	-79.775	40R	9	Fe I
19.3	-19.403	100r	1	Si I							79.478	6	65	Fe I
	19.044	7	268	Fe II		98.897	10	161	Fe II					
					98.8	98.895	10	8	Fe I		78.988	6	179	Fe II
										78.5	78.556	10	61	C I
18.1	18.100	12r	7	Fe I										
					97.9	97.817	7	*175	Fe II					
	17.658	(8)	59	Fe I		97.80	6	18	Ni II					
17.4										77.5				
	17.124	6	147	Fe II							77.342	4	162	Fe II
											76.875	3	3	Ni I
											76.861	(4)	65	Fe I
	16.569	(5)	61	Fe I							76.654	5	62	Fe I
					96.4	96.334	6	59	Fe I	76.4				
16.1	-16.109	250r	1	Si I		96.30	35r	31	Cr I					
						94.735	20	3	Be I	74.9	74.813	(8)	62	Fe I
					94.7	94.590	12	3	Be I		74.762	6	208	Fe II
14.4	14.383	7	285	Fe II		94.547	8	3	Be I					
	-14.315	100r	1	Si I		94.250	(5)	57	Fe I	74.1				
					94.0	93.998	(6)	* 62	Fe I					
13.5	13.328	(5)	Uncl	Fe I	93.2	93.269	12	161	Fe II					
						93.174	12	*161	Fe II		73.156	(3)	8	Fe I
										72.9	-72.910	12R	9	Fe I
	12.513	5	343	Fe II							72.875	(5)	9	Fe I
	12.361	(5r)	8	Fe I						72.4	72.426	5	179	Fe II
12.2	12.280	--	5	Na I	92.2	92.341	4	243	Fe II		72.343	5	*59	Fe I
	12.128	--	5	Na I		92.146	2000R	1	Cu I		72.065	6	7	Ni I
11.8	11.759	10	161	Fe II		91.983	(8)	163	Fe I					
						-91.155	20R	9	Fe I					
10.9	10.871	30	18	Ni II	90.9	90.856	6	179	Fe II		70.961	(4)	* 63	Fe I
	-10.833	15R	7	Fe I		-90.642	30R	9	Fe I	70.6	70.661	7	179	Fe II
						89.826	8	207	Fe II					
					89.7	89.751	15r	9	Fe I	69.7				
											69.512	6	299	Fe II
	09.117	4	242	Fe II							69.407	40	31	Mn I
09.0										69.0				
	08.751	(5)	63	Fe I							68.876	4	59	Fe I
										68.2	68.292	4	*145	Fe II
	07.899	6	59	Fe I	88.1	88.143	40R	9	Fe I					
07.7	07.777	100R	*17	V I						67.7	67.730	(5)	62	Fe I
					87.3	87.368	(4)	10	Fe I					
						87.064	(12)	62	Fe I					
06.8	06.896	150r	1	Si I							66.811	7	179	Fe II
	06.569	(4)	163	Fe I		86.690	(10)	62	Fe I	66.7	66.670	7	179	Fe II
	06.474	70	15	Co II	86.4	-86.372	(10)	8	Fe I					
06.3	06.215	200	21	V II		86.143	7	208	Fe II	66.1				
	06.091	7	207	Fe II							65.911	7	208	Fe II
	05.627	(4)	Uncl	Fe I							65.263	2	5	Ni I
	05.483	(5)	Uncl	Fe I	85.2					65.1	65.194	7	148	Fe II
05.2	05.217	2	33	Fe II		85.076	0	34	Fe II		65.148	6	62	Fe I
											64.903	7	208	Fe II
	04.648	30	16	Nb I										
04.5	04.31	40r	31	Cr I	84.3	84.243	5	243	Fe II					
						84.186	15R	9	Fe I					
											64.007	7	208	Fe II
	03.560	5	*161	Fe II						63.8	63.728	(6)	65	Fe I
03.3	03.323	7	208	Fe II	83.4	83.531	10	62	Fe I					
						-83.270	60R	9	Fe I					
02.5	02.55	25r	32	Cr I							-62.645	10r	9	Fe I
	02.388	7	207	Fe II						62.5				
											62.178	4	9	Fe I
											61.282	8	209	Fe II
01.2	-01.130	40R	7	Fe I	81.0	81.044	3	243	Fe II	61.0	61.011	50	32	Mn I
	00.919	5	357	Fe II							60.887	40h	32	Mn I
						80.155	8	179	Fe II	60.3	60.453	5h	395	Fe II
											60.31	(4)	Uncl	Fe I

Table 2-Continued

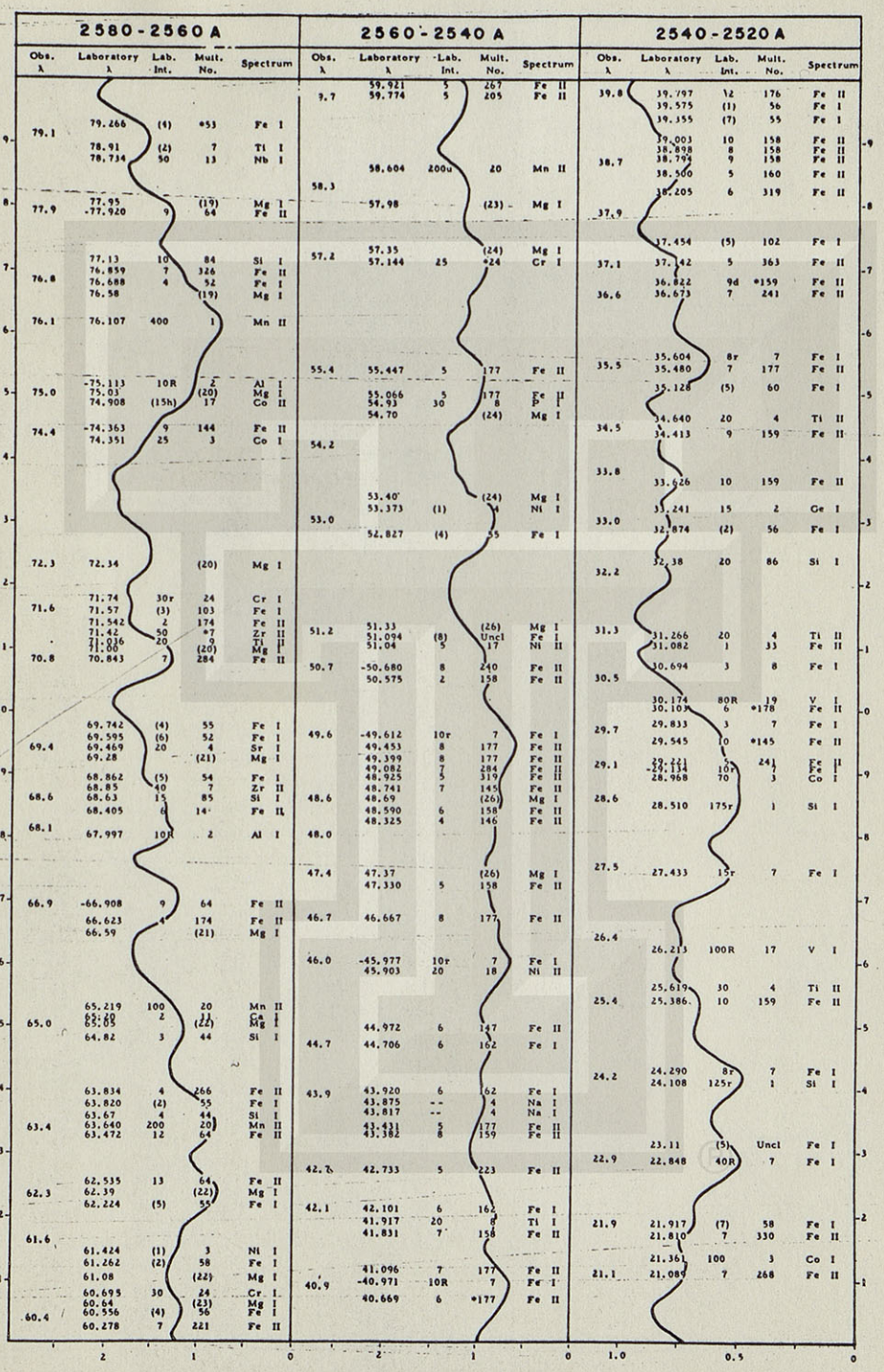

2580 - 2560 A					2560 - 2540 A					2540 - 2520 A				
Obs. λ	Laboratory λ	Lab. Int.	Mult. No.	Spectrum	Obs. λ	Laboratory λ	Lab. Int.	Mult. No.	Spectrum	Obs. λ	Laboratory λ	Lab. Int.	Mult. No.	Spectrum
						59.921	5	267	Fe II		39.797	½	176	Fe II
					59.7	59.774	5	205	Fe II		39.575	(1)	56	Fe I
											39.355	(7)	55	Fe I
79.1	79.266	(4)	*53	Fe I										
											39.003	10	158	Fe II
	78.91	(2)	7	Ti I							38.898	8	158	Fe II
	78.734	50	13	Nb I						38.7	38.794	9	158	Fe II
						58.604	200u	20	Mn II		38.500	5	160	Fe II
					58.3									
	77.95		(19)	Mg I		57.98		(23)	Mg I		38.205	6	319	Fe II
77.9	77.920	9	64	Fe II						37.9				
						57.35		(24)	Mg I		37.454	(5)	102	Fe I
	77.13	10	84	Si I	57.2	57.144	25	*24	Cr I					
	76.859	7	326	Fe II						37.1	37.42	5	363	Fe II
76.8	76.688	4	92	Fe I							36.822	9d	*159	Fe II
	76.58		(19)	Mg I						36.6	36.673	7	241	Fe II
76.1	76.107	400	1	Mn II										
											35.604	8r	7	Fe I
					55.4	55.447	5	177	Fe II	35.5	35.480	7	177	Fe II
	-75.113	10R	2	Al I							35.126	(5)	60	Fe I
75.0	75.03		(20)	Mg I		55.066	5	177	Fe II					
	74.908	(15h)	17	Co II		54.93	30	8	Fe I					
						54.70		(24)	Mg I		34.640	20	4	Ti II
74.4	-74.363	9	144	Fe II						34.5	34.413	9	159	Fe II
	74.351	25	3	Co I	54.2									
										33.8				
											33.626	10	159	Fe II
						53.40		(24)	Mg I					
						53.373	(1)	4	Ni I		33.241	15	2	Ge I
					53.0					33.0	32.874	(2)	56	Fe I
						52.827	(4)	55	Fe I					
72.3	72.34		(20)	Mg I										
										32.2	32.38	20	86	Si I
	71.74	30r	24	Cr I										
71.6	71.57	(3)	103	Fe I										
	71.542	2	174	Fe II										
	71.42	50	*7	Zr II	51.2	51.33		(26)	Mg I	31.3	31.266	20	4	Ti II
	71.036	20	9	Ti II		51.094	(8)	Uncl	Fe I		31.082	1	33	Fe II
	71.00		(20)	Mg I		51.04	5	17	Ni II					
70.8	70.843	7	284	Fe II							30.694	3	8	Fe I
					50.7	-50.680	8	240	Fe II	30.5				
						50.575	2	158	Fe II		30.174	80R	19	V I
											30.103	6	*178	Fe II
	69.742	(4)	55	Fe I							29.833	3	7	Fe I
	69.595	(6)	52	Fe I	49.6	-49.612	10r	7	Fe I	29.7				
69.4	69.469	20	4	Sr I		49.453	8	177	Fe II		29.545	10	*145	Fe II
	69.28		(21)	Mg I		49.399	8	177	Fe II					
						49.082	7	284	Fe II	29.1	29.221	5	241	Fe II
	68.862	(5)	54	Fe I		48.925	5	319	Fe II		-29.134	10r	1	Fe I
	68.85	40	7	Zr II		48.741	7	145	Fe II		28.968	70	3	Co I
68.6	68.63	15	85	Si I	48.6	48.69		(26)	Mg I	28.6				
	68.405	6	14	Fe II		48.590	6	158	Fe II		28.510	175r	1	Si I
68.1						48.325	4	146	Fe II					
	67.997	10r	2	Al I	48.0									
										27.5				
					47.4	47.37		(26)	Mg I		27.433	15r	7	Fe I
						47.330	5	158	Fe II					
66.9	-66.908	9	64	Fe II										
	66.623	4	174	Fe II	46.7	46.667	8	177	Fe II					
	66.59		(21)	Mg I						26.4				
											26.213	100R	17	V I
					46.0	-45.977	10r	7	Fe I					
						45.903	20	18	Ni II		25.619	30	4	Ti II
	65.219	100	20	Mn II						25.4	25.386	10	159	Fe II
	65.20	2	11	Ge I										
65.0	65.05		(22)	Mg I		44.972	6	147	Fe II					
	64.82	3	44	Si I	44.7	44.706	6	162	Fe I					
										24.2	24.290	8r	7	Fe I
											24.108	125r	1	Si I
	63.834	4	266	Fe II	43.9	43.920	6	162	Fe I					
	63.820	(2)	55	Fe I		43.875	--	4	Na I					
	63.67	4	44	Si I		43.817	--	4	Na I					
63.4	63.640	200	20	Mn II		43.431	5	177	Fe II					
	63.472	12	64	Fe II		43.382	8	159	Fe II					
											23.11	(5)	Uncl	Fe I
					42.8	42.733	5	223	Fe II	22.9	22.848	40R	7	Fe I
	62.535	13	64	Fe II										
62.3	62.39		(22)	Mg I										
	62.224	(5)	55	Fe I	42.1	42.101	6	162	Fe I					
						41.917	20	8	Ti I	21.9	21.917	(7)	58	Fe I
61.6						41.831	7	158	Fe II		21.810	7	330	Fe II
	61.424	(1)	3	Ni I							21.361	100	3	Co I
	61.262	(2)	58	Fe I		41.096	7	177	Fe II	21.1	21.084	7	268	Fe II
	61.08		(22)	Mg I	40.9	-40.971	10R	7	Fe I					
	60.695	30	24	Cr I		40.669	6	*177	Fe II					
	60.64		(23)	Mg I										
	60.556	(4)	56	Fe I										
60.4	60.278	7	221	Fe II										

Table 2-Continued

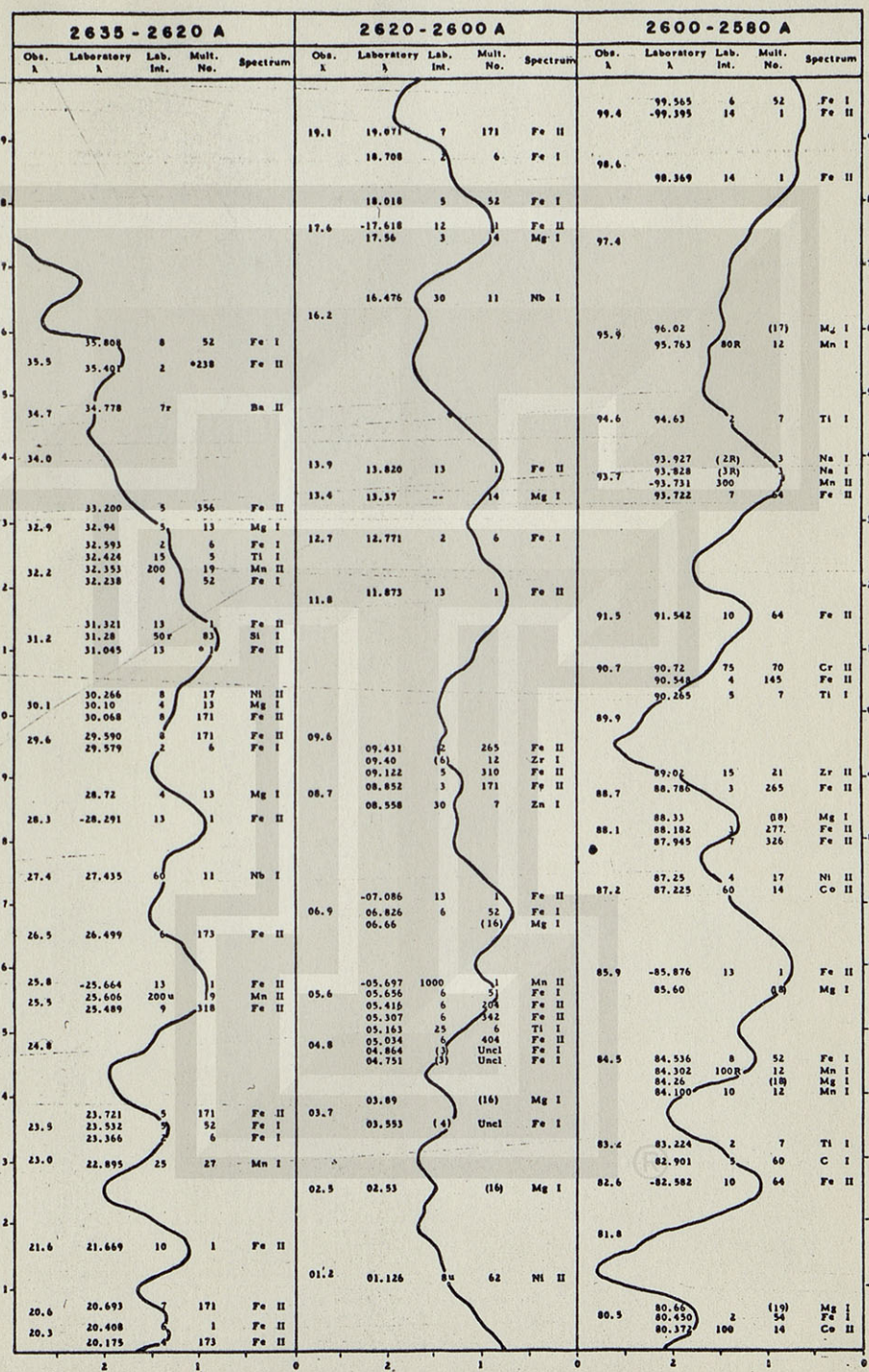

2635 - 2620 A					2620 - 2600 A					2600 - 2580 A				
Obs. λ	Laboratory λ	Lab. Int.	Mult. No.	Spectrum	Obs. λ	Laboratory λ	Lab. Int.	Mult. No.	Spectrum	Obs. λ	Laboratory λ	Lab. Int.	Mult. No.	Spectrum
											99.565	6	52	Fe I
										99.4	-99.395	14	1	Fe II
					19.1	19.071	7	171	Fe II					
						18.708	2	6	Fe I	98.6				
											98.369	14	1	Fe II
						18.018	5	52	Fe I					
					17.6	-17.618	12	1	Fe II					
						17.56	3	4	Mg I	97.4				
						16.476	30	11	Nb I					
					16.2									
	35.808	8	52	Fe I						95.9	96.02		(17)	Mg I
35.5	35.491	2	•238	Fe II							95.763	80R	12	Mn I
34.7	34.778	7r		Ba II						94.6	94.63	2	7	Ti I
34.0											93.927	(2R)	3	Na I
					13.9	13.820	13	1	Fe II	93.7	93.828	(3R)	3	Na I
					13.4	13.37	--	14	Mg I		-93.731	300	3	Mn II
	33.200	5	356	Fe II							93.722	7	64	Fe II
32.9	32.94	5	13	Mg I										
	32.593	2	6	Fe I	12.7	12.771	2	6	Fe I					
	32.424	15	5	Ti I										
32.2	32.353	200	19	Mn II										
	32.238	4	52	Fe I										
					11.8	11.873	13	1	Fe II					
	31.321	13	1	Fe II						91.5	91.542	10	64	Fe II
31.2	31.28	50r	83	Si I										
	31.045	13	• 1	Fe II						90.7	90.72	75	70	Cr II
											90.548	4	145	Fe II
	30.266	8	17	Ni II							90.265	5	7	Ti I
30.1	30.10	4	13	Mg I						89.9				
	30.068	8	171	Fe II										
29.6	29.590	8	171	Fe II	09.6									
	29.579	2	6	Fe I		09.431	2	265	Fe II					
						09.40	(6)	12	Zr I		89.02	15	21	Zr II
						09.122	5	310	Fe II					
	28.72	4	13	Mg I		08.852	3	171	Fe II	88.7	88.786	3	265	Fe II
28.3	-28.291	13	1	Fe II	08.7	08.558	30	7	Zn I		88.33		(8)	Mg I
										88.1	88.182	3	277	Fe II
											87.945	7	326	Fe II
27.4	27.435	60	11	Nb I										
											87.25	4	17	Ni II
						-07.086	13	1	Fe II	87.2	87.225	60	14	Co II
					06.9	06.826	6	52	Fe I					
						06.66		(16)	Mg I					
26.5	26.499	6	173	Fe II										
										85.9	-85.876	13	1	Fe II
25.8	-25.664	13	1	Fe II		-05.697	1000	1	Mn II		85.60		(8)	Mg I
25.5	25.606	200u	19	Mn II	05.6	05.656	6	5	Fe I					
	25.489	9	318	Fe II		05.416	6	204	Fe II					
						05.307	6	342	Fe II					
						05.163	25	6	Ti I					
24.8					04.8	05.034	6	404	Fe II					
						04.864	(3)	Uncl	Fe I					
						04.751	(3)	Uncl	Fe I					
										84.5	84.536	8	52	Fe I
						03.89		(16)	Mg I		84.302	100R	12	Mn I
											84.26		(18)	Mg I
											84.100	10	12	Mn I
	23.721	5	171	Fe II	03.7									
23.5	23.532	9	52	Fe I		03.553	(4)	Uncl	Fe I					
	23.366	2	6	Fe I										
										83.2	83.224	2	7	Ti I
23.0	22.895	25	27	Mn I							82.901	5	60	C I
					02.5	02.53		(16)	Mg I	82.6	-82.582	10	64	Fe II
										81.8				
21.6	21.669	10	1	Fe II										
					01.2	01.126	8u	62	Ni II					
20.6	20.693	7	171	Fe II							80.66		(19)	Mg I
20.3	20.408	5	1	Fe II						80.5	80.450	2	54	Fe I
	20.175	4	173	Fe II							80.372	100	14	Co II

Nitrogen Z=7.—N I lines are extremely weak in the sun. It is not surprising that the faint lines of high excitation potential of N II occurring in this region are not present.

Sodium Z=11.—The higher members of the principal series of Na I are masked; those in (3) by Mn II; (4) by Fe I; and (5) by Fe I and II.

Magnesium Z=12.—A number of higher series members of Mg I, (13) extended through (26), are entered in Table 1. Many of these are masked, but a considerable number offer the most probable identifications for observed lines.

Aluminum Z=13.—The first multiplet of Al I, 2660.393 A, 2652.484 A, is present in the spectrum reported by Wilson *et al.* (1954). Al I (2) is represented here by its two leading components, 2575.113 A and 2567.997 A. Multiplets (4) and (5) are somewhat blended. The coincident lines of Al (7) and (8) at 2204.627 A are present. Three members of Al I (11) are entered in Table 2, the others are masked. No lines of Al II have been found in this region. The raie ultime is at 1670.81 A and has been reported by Johnson *et al.* (1958) as probably present in emission.

Silicon Z=14.—Si I is present with great intensity. Almost all the lines occurring in this region have been found, though many of the fainter lines are blended. The entire multiplet (1) with raie ultime, 2516.109 A, is present and intense, as are multiplets (2), (3), and (4). Also present are the strong line at 2435.160 A (45), another at 2124.111 A (48), and the fainter singlet combination at 2122.99 A (49). Many lines from the $3p^2\ ^1S$ level are also present, but with less intensity.

Shenstone has revised and extended the analysis of Si II. From his unpublished data, received after preparation of Table 2, the multiplet $3p\ ^2P^o$–$3p^2\ ^4P$ should be considered; its lines are 2334.607 A, intensity 50; 2328.50 A, not listed by Shenstone but predicted; 2344.203 A, 20; 2334.402 A, 50; 2350.179 A, 30. The first and fourth lines are present, although blended with Ni II (20). The second explains an unidentified line. The third and fifth are masked by Fe II and Fe I, respectively. The leasing lines of Si II lie to shorter wave lengths.

Phosphorus Z=15.—P I (4) is present and unblended. Only one line of (8) is listed in Table 2, 2554.93 A, the rest being masked. Three lines of (3) are faint if present, and (9) is blended. P II (4) and (5) cannot be detected. The lines in (6) and (7) may coincide with unidentified solar features but require further confirmation.

Calcium Z=20.—Ca I lines in this region are faint and cannot be detected among solar lines otherwise identified. The pair of lines of Ca II (8) appears to be present, though the leading one is blended with Co I (20). Most of (9) is masked.

Titanium Z=22.—Ti is not well represented. Some lines of Ti I are listed by Wilson *et al.* (1954), but none are unblended. This is also true of the present region; here most of the lines are absent or masked, and only two lines, Ti I (7) 2594.63 A and 2583.224 A, match faint lines that are otherwise unidentified, and the leading line is masked. The stronger lines of Ti II longer than 2635 A are recorded by Wilson *et al.* (1954). The leading lines of Ti II (4) and (9) are present here but blended.

Vanadium Z=23.—The strongest V I multiplets are blended in the region short of 3000 A and are mostly minor contributors. Some lines of (17) and (19) are present. The line at 2435.518 A in (23) is not detected, but most of the other strong lines in this group appear to be present or blended. V II is represented to a greater degree than V I, in general. Here multiplets (7), (8), and (21) may contribute, but the leading line of (21), 2514.633 A, is probably masked. V II (123) may explain two unclassified lines in Table 2 at 2281 A.

Chromium Z=24.—Cr I is represented by all three lines in multiplet (1), which are very strong in the laboratory. The unidentified solar lines at 2307.2 A and 2314.7 A may be Cr II from multiplet (19), with the leading line 2297.17 A masked. Multiplets (23) and (70) are partially present.

Manganese Z=25.—The strongest Mn I lines in this region are present. Multiplets (2), (12), (32), (33), and (34) all have lines listed in Table 2; some lines are masked, and

many are blended. The raie ultime of Mn II, 2576.107 A, is present with great intensity, and the other two components of this multiplet are also present. No other lines are identified with certainty, but lines from (19) and (20) are entered as possibilities.

Iron Z=26.—Fe is the most abundant source of lines within this region, as it is to longer wave lengths. Both Fe I and Fe II are conspicuous. No Fe III has been detected.

Cobalt Z=27.—The strongest lines of Co I are present but not conspicuous. Many are blended or masked. The Co II raie ultime, 2286.165 A, is present with good intensity, as are several other lines of this multiplet. Multiplets (7) and (8) are represented by most of their stronger lines, and other strong lines are present.

Nickel Z=28.—Lines of Ni I and Ni II are strong in this region. For example, the strongest lines in each of multiplets (8), (9), and (10) of Ni I are conspicuous solar lines except for Ni I (8) 2337.484 A, which is in the wing of a strong line of Fe II. A number of other lines of lower laboratory intensity are also identified. Ni II is present with many lines. Eight of the nine listed components of (12) are present, including the raie ultime, and also the strongest lines of (11). All lines of multiplet (13) are present, likewise the strongest lines of (14), (15), and all of (20).

Copper Z=29.—Cu I is well represented. All the resonance lines within this region are present except Cu I (4), 2165.093 A, which is in the wing of a strong Ni II line. Several of the lines from the $4s^2\ ^2D$ level are present, but many are masked. The absence of 2263.079 A (24) is surprising. No lines of Cu II are identified; the raie ultime, 2135.976 A, if present, is blended with P I (4).

Zinc Z=30.—The raie ultime of Zn I, 2138.56 A, is blended with Fe I. The only other intense line of Zn I listed in this region, (7) 2608.558 A, is blended with Fe II.

Gallium Z = 31.—Although Ga I (3) 2624.82 A matches an unidentified line, this identification is considered improbable because of the absence of other strong lines.

Germanium Z = 32.—The raie ultime of Ge I, 2651.184 A, is present in the spectrum of Wilson *et al.* (1954). The present spectrum shows Ge I (11) 2198.73 A and possibly one or two other lines. Ge II has no strong lines in this region.

Arsenic Z=33.—The strongest lines in the present region are As I (6) 2288.12 A and 2349.84 A. The former is masked, and the latter, if present, is faint. In (5), 2381.18 A is absent, and and 2456.53 A, if present, is probably blended with Fe II (320) and Ru II (41) and (42.) It is concluded that the identification of As is not yet definite.

Selenium Z=34.—No lines of Se have yet been found in the solar spectrum. The leading lines of Se I lie short of 2085 A. Se I (20) 2547.98 has been rejected as an explanation for a weak unidentified solar line at 2548.0 A. The lines Se I (1) 2164.160 A and Se I (12) 2413.517 A, which are stronger in the laboratory, are not found.

Strontium Z=38.—In Sr II (2), 2425.17 and 2425.62 A are present, but both lines of (3) are masked.

Yttrium Z=39.—The strong line Y II (1) 2243.06 A is blended with Fe I; Y II (2) 2422.22 A is absent.

Zirconium Z=40.—A few of the strongest lines of Zr II have been included in Table 2; they are badly blended.

Niobium Z=41.—A few of the strong lines of Nb I are present. In Nb I (13), 2592.190 A and, in (21), 2247.997 A may be faintly visible in the tracing.

Heavy elements.—The Ultraviolet Multiplet Table, Section III, is in the course of preparation by Moore. Multiplet numbers are taken from the unpublished manuscript. Most of the following lines were considered, subsequent to the preparation of Table 2 and are not entered.

Molybdenum Z=42.—Two strong lines of Mo II, (8) 2538.444 A and (11) 2269.708 A, are, respectively, masked and absent.

Ruthenium Z=44.—Several strong lines of Ru II, multiplets (41) through (44), occur in this region. Ru II (41): 2402.72 A, 800, raie ultime; 2456.57 A, 500; 2498.58 A, 200; 24.55.53 A, 600; 2478.93 A, 500; and 2396.71 A. 600. Ru II (42): 2357.92 A, 600;

2342.85 A, 300; 2381.99 A, 400; 2358.79 A, 400; 2456.44 A, 500; 2407.92 A, 300; and 2375.63 A, 400. Ru II (43): 2268.14 A, 400; 2281.72 A, 300. Ru II (44): 2263.51 A, 300.

The raie ultime is blended with Fe II (36). Multiplets (41) 2456.57 A and (42) 2456.44 A probably contribute to the observed line at 2456.4 A and mask As I (5) 2456.53 A; (42) 2357.92 A is present, as is (43) 2281.72 A. The others are blended or masked.

Rhodium Z=45.—No lines of Rh II can be identified with certainty.

Palladium Z = 46.—A strong line of Pd I (2) occurs at 2476.43 A but probably does not contribute significantly to the observed line at 2476.4 A, which is considered to be produced mainly by Fe I. There is no evidence of the presence of Pd II.

Silver Z=47.—An unidentified solar line at 2246.4 A agrees in position with the raie ultime of Ag II, 2246.43 A. Other members of this multiplet (7) are masked, and lines having an excitation potential equal to zero lie below 1200 A. This identification needs confirmation.

Cadmium Z=48.—The strongest Cd I line in the present range is the raie ultime, 2288.018 A, which is masked by Fe I. The raie ultime of Cd II, 2144.41 A may explain the solar line at 2144.5 A. The other member of this multiplet (1), 2265.02 A, is masked by Fe I.

TABLE 3

Z	Spectrum	Laboratory Wave Length (A)	Z	Spectrum	Laboratory Wave Length (A)
43	Tc II	2543.24	48	Cd II	2144.41
44	Ru II	2402.72	52	Te I	2142.75
45	Rh II	2334.77	71	Lu II	2615.43
46	Pd II	2296.53	74	W II	2204.49
47	Ag II	2246.43	77	Ir I	2543.97
48	Cd I	2288.02	79	Au I	2427.95

Tin Z=50.—The strong lines of Sn I are badly masked.

Antimony Z=51.—Multiplet (1) of Sb I contains three intense lines: 2068.33 A, raie ultime; 2175.81, and 2311.47 A. The first is out of range, the second may be present, and the third is masked in the solar spectrum.

Barium Z=56.—Two multiplets of Ba II contribute to the solar lines. In (6), $6p\ ^2P^\circ$–$7d\ ^2D$, 2634.778 A is present. Lines in the next multiplet of the series are predicted at 2232.80, 2153.03, and 2235.32 A. The first and third of these lines are probably present, and the second line is probably masked.

Platinum Z=78.—The raie ultime of Pt I, 2659.44 A, is probably present in the spectrum of Wilson *et al.* (1954). This adds weight to the identification of a few Pt I lines in Table 2—(2) 2234.91 A, 2144.22 A, and others.

Gold Z=79.—An unidentified line, 2427.5 A, is not in close agreement with the raie ultime of Au I, (1) 2427.95 A. The second member of the multiplet, 2675.95 A, is blended, if present.

Mercury Z=80.—The Hg I 2536.517 A line was considered as possible explanation for an observed line at 2536.6 A. However, the presence of Fe II lines makes identification indefinite until greater resolution is achieved. The raie ultime is at 1849.50 A.

Table 3 lists the raie ultimes of the first and second spectra of elements heavier than Nb that occur in the present region. Of these lines, those of Tc II, Rh II, Pd II, Lu II, Cd I, Te I, and Au I cannot be detected in the present solar spectrum, and Ru II, W II and Ir I are masked. Those of Ag II and Cd II agree with unidentified solar features in

Table 2. Greater resolution is needed to settle definitely the question of these identifications. One of the most interesting future problems is the study of raie ultimes in the entire range of the vacuum ultraviolet solar spectrum.

REFERENCES

Clearman, H. E., Jr. 1953, *Ap. J.*, **117**, 29.

Dunkelman, L., and Scolnik, R. 1959, *J. Opt. Soc. America*, **49**, 356.

Durand, E., Oberley, J. J., and Tousey, R. 1949, *Ap. J.* **109**, 1.

Hopfield, J. J., and Clearman, H. E., Jr. 1948, *Phys. Rev.*, **73**, 877.

Johnson, F. S. 1956, *J. Opt. Soc. America*, **46**, 2, 101.

Johnson, F. S., Malitson, H. H., Purcell, J. D., and Tousey, R. 1958, *Ap. J.*, **127**, 1, 80.

Johnson, F. S., Purcell, J. D., and Tousey, R. 1954, *Studies of the Ozone Layer above New Mexico, Rocket Exploration of the Upper Atmosphere* (London: Pergamon Press), p. 189.

Johnson, F. S., Purcell, J. D., Tousey, R., and Watanabe, K. 1952, *J. Geophys. Res.*, **57**, 157.

Kachalov, V. P., Pavlenko, N. A., and Yakovleva, A. V. 1958, *Izvest. Akad. Nauk, S.S.S.R.*, Seriya Geofizicheskaya No. 9, p. 1099 (NRL Trans. No. 745).

———. 1959, *ibid.*, No. 8, p. 1177.

Minnaert, M., Mulders, G. F. W., and Houtgast, J. 1940, *Photometric Atlas of the Solar Spectrum* (Amsterdam).

Moore, C. E. 1950, 1952, *An Ultraviolet Multiplet Table* (National Bureau of Standards Circ. 488, Secs. I and II [Washington, D.C.] and, 1959, unpublished data from Sec. III).

Packer, D. M., and Lock, C. 1951, *J. Opt. Soc. America*, **41**, 10, 699.

Purcell, J. D. 1954, *J. Opt. Soc. America*, **44**, 679.

Stacey, D. S., Stith, G. A., Nidey, R. A., and Pietenpol, W. B. 1954, *Electronics*, **27**, 149.

Tousey, R. 1953*a*, "Solar Work at High Altitudes from Rockets," in *The Sun*, ed. G. P. Kuiper ("The Solar System," Vol. 1 [Chicago: University of Chicago Press]), p. 658.

———. 1953*b*, *J. Opt. Soc. America*, **43**, 245.

Wilson, N. L., Tousey, R., Purcell, J. D., Johnson, F. S., Moore, C. E. 1954, *Ap. J.*, **119**, 590.

Reprinted from Science, November 30, 1962, Vol. 138, No. 3544, pages 978-980

Visual Observations of Nightglow from Manned Spacecraft

Abstract. The luminous band around the horizon noted by J. Glenn in the first U.S. manned orbital flight is attributable to airglow. Dip-of-the-horizon measurements on the star γ Ursae Majoris showed that the band is centered at an elevation of 91 kilometers or somewhat higher. The edge-on brightness of the airglow layer was 6×10^{-7} candles per square centimeter.

The luminosity of the night sky in places remote from artificial illumination was discovered a long time ago and has been studied by many researchers in many countries. The sources of the light are radiations and scattered sunlight from interplanetary space, radiation and starlight from intersteller space, and atomic and molecular radiation from the earth's atmosphere, generally from above the ozonosphere. These atmospheric sources of light are either the aurorae or the night airglow. The physics of these phenomena has recently been comprehensively reviewed by J. W. Chamberlain (*1*). One of the most intense emissions of the nightglow is the strong oxygen green line at a wavelength of 5577 angstroms (Å). The height of this light has been measured, by various indirect means, from the ground. But the most reliable data, to date, come from direct measurements made in the 1950's from rockets passing through the nightglow layer at heights in the vicinity of 90 kilometers.

Glenn (*2*) reported from the first U.S. manned orbital flight (MA-6), observing with the naked eye a tan to buff luminous band some 6° to 8° above the horizon (*2*). It seemed to him that the starlight which passed through this layer might be reduced. This phenomenon was incorrectly attributed by O'Keefe to a reflection in the capsule window (*3*).

On the second U.S. orbital flight (MA-7) on 24 May 1962, this band was again observed. By means of an interference filter with a passband of 11 Å (half peak transmittance), centered at 5578 Å where transmittance was 44 percent, the luminous band was identified as attributable to the airglow, to which the emission at 5577 Å is a major contributor. At the moment of this observation, $17^h02^m39^s$ Universal Time, the sun was just rising on the third orbit and the horizon was illuminated. It was noted that, through the filter, the luminous band appeared bright, while the illuminated horizon was not seen.

Somewhat earlier in the flight, at $16^h48^m49^s$, it had been noted that the airglow band was approximately as bright as the horizon band, which was then illuminated by the moon, near last quarter. On the assumption that the atmosphere acts like a perfectly diffusing reflector and that the illuminance produced by the moon at last quarter is about 2×10^{-6} lumen/cm^2, it is found that the luminance (surface brightness) of the airglow layer is about 6×10^{-7} lumen/cm^2 per steradian (or 6×10^{-7} candle/cm^2). This is equivalent to about 30,000 Rayleighs if the radiation is assumed to be isotropic, a value consistent with previously reported visual measurements taken from the ground.

At about the same time it was noted that Phecda (γ Ursae Majoris) was about to pass through the airglow band, as seen from the capsule. From a replaying of the capsule tape, approximate times for apparent positions of Phecda have been determined as follows: Time just prior to entry into the airglow band, $16^h48^m49^s$; time of reaching approximate center of band, $16^h50^m8^s$; time of reaching apparent lower boundary of band, $16^h50^m41^s$.

From the tabulated latitude and longitude of the spacecraft it was possible to determine the angular zenith distance of Phecda for each minute of the relevant time interval. The orbital data were obtained from the Goddard Space Flight Center. The angular zenith distances shown in Table 1 were then interpolated, and capsule heights above the given feature were found from the standard formulas for the dip of the horizon.

The apparent angular elevation of the horizon, after allowance had been made for refraction, was approximtely 106°; it was thus only about 4° below the middle of the nightglow layer. This figure is supported by an observation as follows.

At $17^h03^m37^s$ the capsule happened to be rolled at such an angle that a reticle cross, scribed on the window, was seen against the background of the luminous band. The crossarm then spanned the angular distance from the luminous band to the horizon thus furnishing a measure of the angular distance. Subsequent measures show that the crossarm is 1.54 cm long and is at a distance of 26.2 cm from the observer's eye. At an angle of 45° it subtends a vertical arc of approximately 2.4°. This is reconcilable with the calculated arc of 4°, if it is assumed that the apparent horizon is produced by scattering and extinction of light in the atmosphere and is considerably above the true horizon.

The discrepancy between the measured height of 4° or less and the estimated heights of 6° to 10° above the horizon, estimated visually on both MA-6 and MA-7, may be attributable to the well-known illusion which makes the apparent diameters of the sun and moon seem largest near the horizon. If so, it is clear that this illusion can in no way be connected with the direction of gravity, as sensed by the inner ear.

These heights are somewhat lower than those previously reported from rockets (*4*). J. W. Chamberlain has kindly pointed out that observations made in the manner of the astronaut observations tend to give too low an estimate of the average height of the layer, for the following reason. A ray which passes through a thick uniform layer near the top lies within the layer only for a short distance, correspond-

Table 1. Angular zenith distances of Phecda and corresponding times, capsule heights, and heights of features of the airglow band.

Feature	Time (16^h +)	Angular zenith distances of Phecda (deg)	Capsule height (km)		Height of feature (km)
			Above feature	Above ground	
Outside layer	48^m49^s	100.86	118	237	119
Middle of layer	50^m08^s	101.88	141	232	91
Lower boundary of layer	50^m41^s	102.22	149	230	81

ing to the chord of a short arc. For rays which penetrate the layer at greater depths the chord is longer, until we reach the ray which is tangent to the bottom of the layer. Beyond this point a piece will be cut out of the middle of the chord. The approximate formula for the distance which must be traversed is the real part of the equation:

$$s = (2R)^{\frac{1}{2}} [h^{\frac{3}{2}} - (h\text{-}h_o)^{\frac{3}{2}}]$$

where R is the radius of the earth, h is the distance below the tip of the layer and h_o is the thickness of the layer. The second term is to be taken equal to zero until $h > h_o$. Then the distance s will be a maximum where $h = h_o$—that is, for a ray tangent to the bottom of the layer. Hence, this discussion implies that if the layer is 10 kilometers thick, the astronaut will find maximum luminance at a zenith distance which corresponds to a level 5 kilometers below the middle of the layer. In this way it is possible to explain the difference between the height reported here and that derived by rocket measurements.

The absorption in this layer which was suggested by the observations of Glenn in the MA-6 flight was not found in the MA-7 flight. In the latter, the passage of Venus through the layer was observed; there was no noticeable dimming. Fainter objects became more difficult to see, but it is our feeling that this is a contrast effect and not a true absorption.

Although time did not permit careful scrutiny of the band around the horizon, it was nevertheless possible to examine sections about 30° in length as they crossed the window. No structure, either vertical or horizontal, was noticed.

MALCOLM SCOTT CARPENTER
Manned Spacecraft Center, Houston, Texas
JOHN ALOYSIUS O'KEEFE III
LAWRENCE DUNKELMAN
Goddard Space Flight Center, Greenbelt, Maryland

References

1. J. W. Chamberlain, *Physics of the Aurora and Airglow* (Acadmic Press, New York, 1961).
2. J. H. Glenn, *Science* **136**, 1093 (1962).
3. J. A. O'Keefe, *ibid.* **136**, 1095 (1962).
4. M. Koomen, R. Scolnik, R. Tousey, *J. Geophys. Res.* **61**, 304 (1956); R. Tousey, *Ann. Geophys.* **14**, 186 (1958); J. P. Heppner and L. H. Meredith, *ibid.* **63**, 51 (1958).

15 November 1962

JOURNAL OF GEOPHYSICAL RESEARCH VOL. 69, NO. 13 JULY 1, 1964

Photographic Observations of the Airglow Layer

F. C. GILLETT, W. F. HUCH, E. P. NEY

University of Minnesota, Minneapolis

GORDON COOPER

Manned Spacecraft Center, Houston, Texas

Abstract. The night airglow photographs taken by Gordon Cooper during his orbital flight of May 15 and 16, 1963, are discussed. They show an airglow layer 24 ± 3 km thick and varying in height above the earth from 77 to 110 km. The measured brightness indicates a surface brightness in a vertical column through the airglow layer 0.4 Rayleigh/A in the vicinity of 5400 A and 0.6 Rayleigh/A at 4200 A.

The earth's airglow layer was first observed from above by Astronaut John Glenn in his orbital flight. Astronaut Scott Carpenter suggested that the brightness of the airglow layer observed in profile was approximately equal to the brightness of the earth illuminated by a quarter moon. Carpenter's observations have been discussed by *Carpenter et al.* [1962]. The astronauts recognize the airglow layer as an outstanding terrestrial phenomenon because they view it in profile from above. The layer is relatively thin and the gain in surface brightness in viewing it tangentially from above is approximately a factor of 35 compared with the surface brightness which would be observed looking vertically through the layer from below.

In Astronaut Cooper's flight on May 15 and 16, 1963, plans were made to study the brightness and geometry of the airglow layer. Most of the 16th orbit of this flight was used to obtain pictures of the earth's horizon, including the layer. The camera used had an angular field of view of 37°, a speed of f/1, and used 35-millimeter Ansco type 529 film. The photographs were taken during the nighttime part of the orbit that began over eastern Australia. They were taken in triads; 10-sec, 30-sec, and 2-min exposures looking backward in the orbit with the capsule positioned approximately in the re-entry mode. Altogether, fifteen useful pictures were obtained. In general, the shorter exposures do not produce enough photographic density for proper densitometry, and usually the longer exposures are smeared by spacecraft motions. It is possible, however, to use the short-exposure pictures to measure the angular height and the width of the airglow layer with some precision, and several of the long-exposure pictures allow three color densitometry of the airglow layer and the quarter moonlit illuminated earth. Several of the pictures are reproduced in black and white in Figures 1 through 5.

Figure 1 is a two-min exposure taken early in the satellite night as the spacecraft looked back over the eastern coast of Australia. The flashes in the foreground are presumed to be individual lightning discharges from four active regions in a storm. The successive flashes recede into the distance as the spacecraft moves away from the storm. Above these multiple flashes can be seen the airglow layer very much smeared by spacecraft motion.

Figure 2 is a 30-sec exposure showing the airglow layer as a sharp band with the horizon delineated by lightning strokes now seen at a great distance from the spacecraft.

Figure 3, the next exposure, although quite underexposed, shows a very sharp airglow line and one lightning stroke indicating the horizon.

In the subsequent pictures, the earth that is seen is a region of the Pacific Ocean illuminated by a quarter moon which has risen. In these pictures it is possible to compare the brightness of the moonlit illuminated earth and the airglow layer and to discern a sharp horizon.

Figure 4, which is a reproduction of photograph 35, shows the best 10-sec exposure of the moonlit earth and airglow layer. In the original transparencies the contrast of the airglow layer is very good and the sky viewed between the

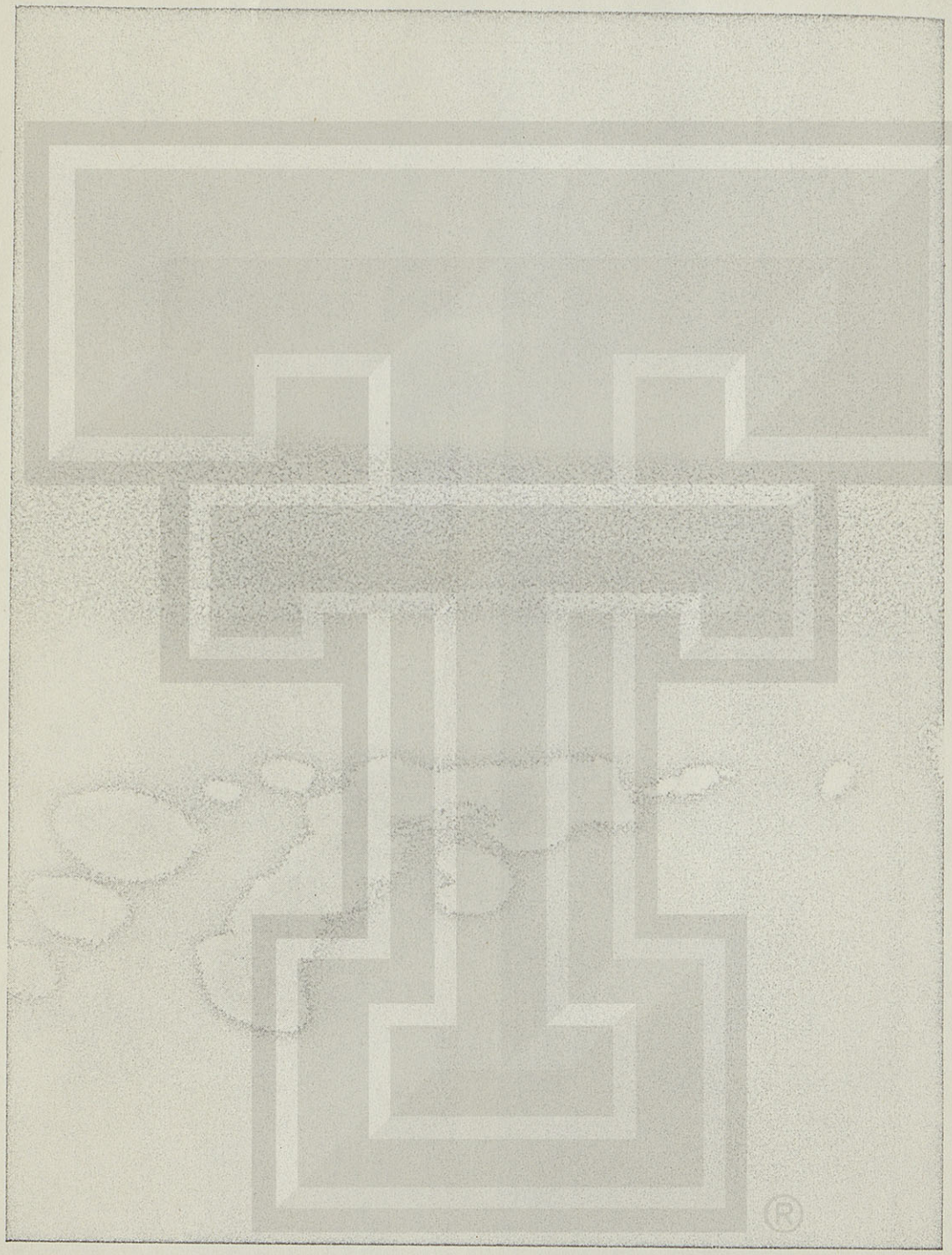

Fig. 1. A 2-min exposure of the airglow layer and the lightning storm taken over eastern Australia. Individual lightning discharges show the storm receding toward the horizon as the spacecraft moves east.

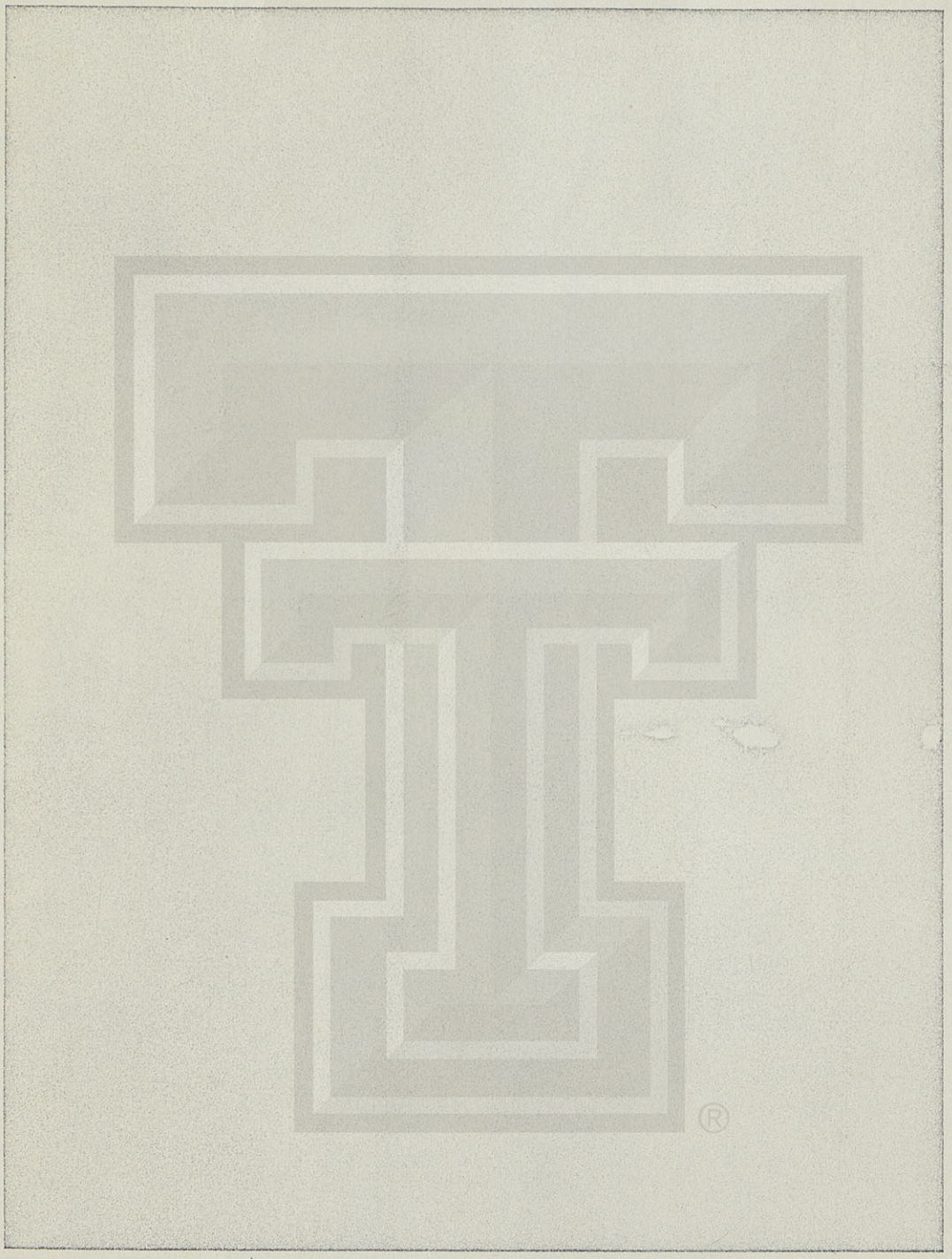

Fig. 2. The photograph taken with a 30-sec exposure immediately after the exposure of Figure 1. Three lightning discharges are visible on the horizon.

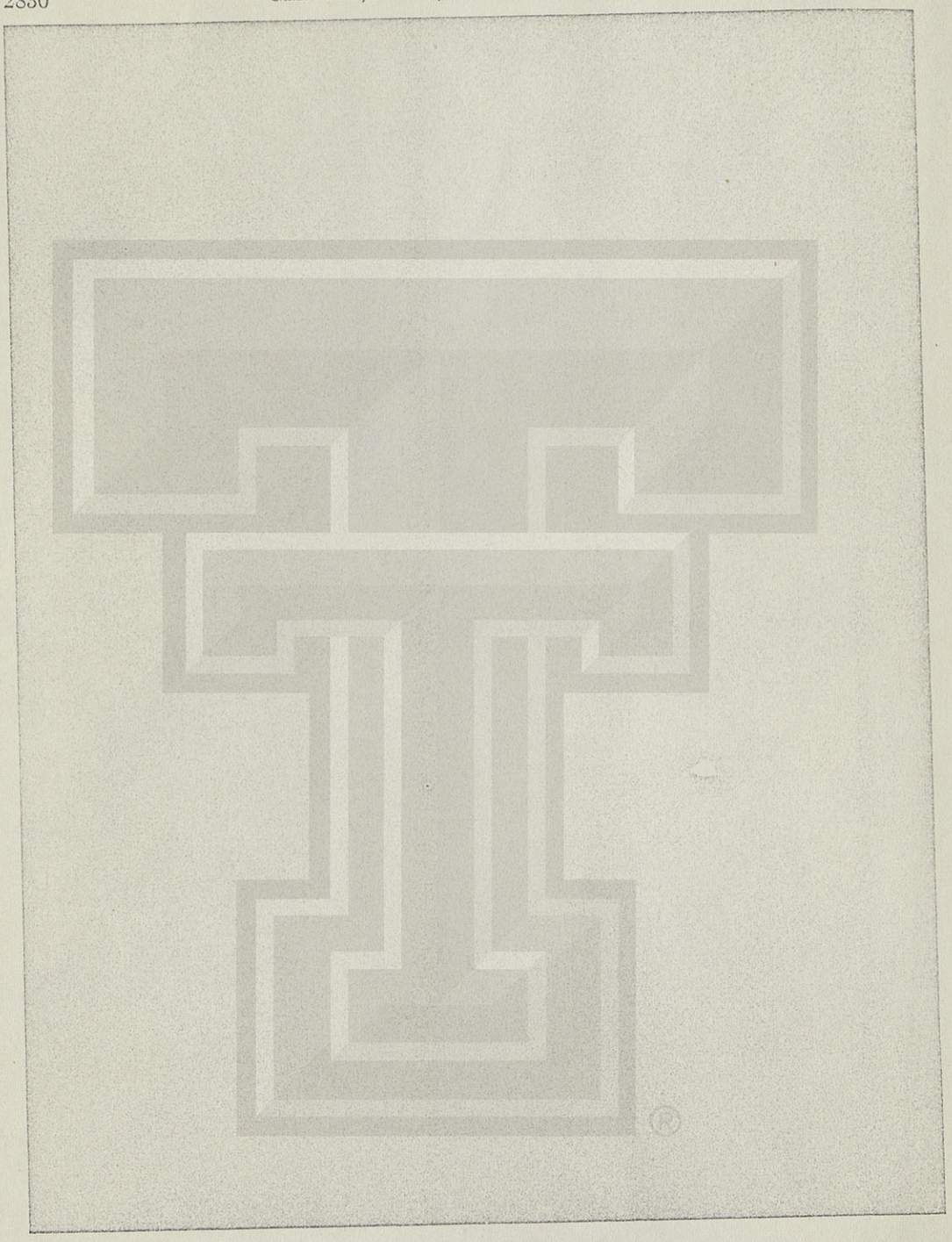

Fig. 3. The next exposure, 10-sec duration, shows one lightning discharge on the horizon and a sharp airglow layer.

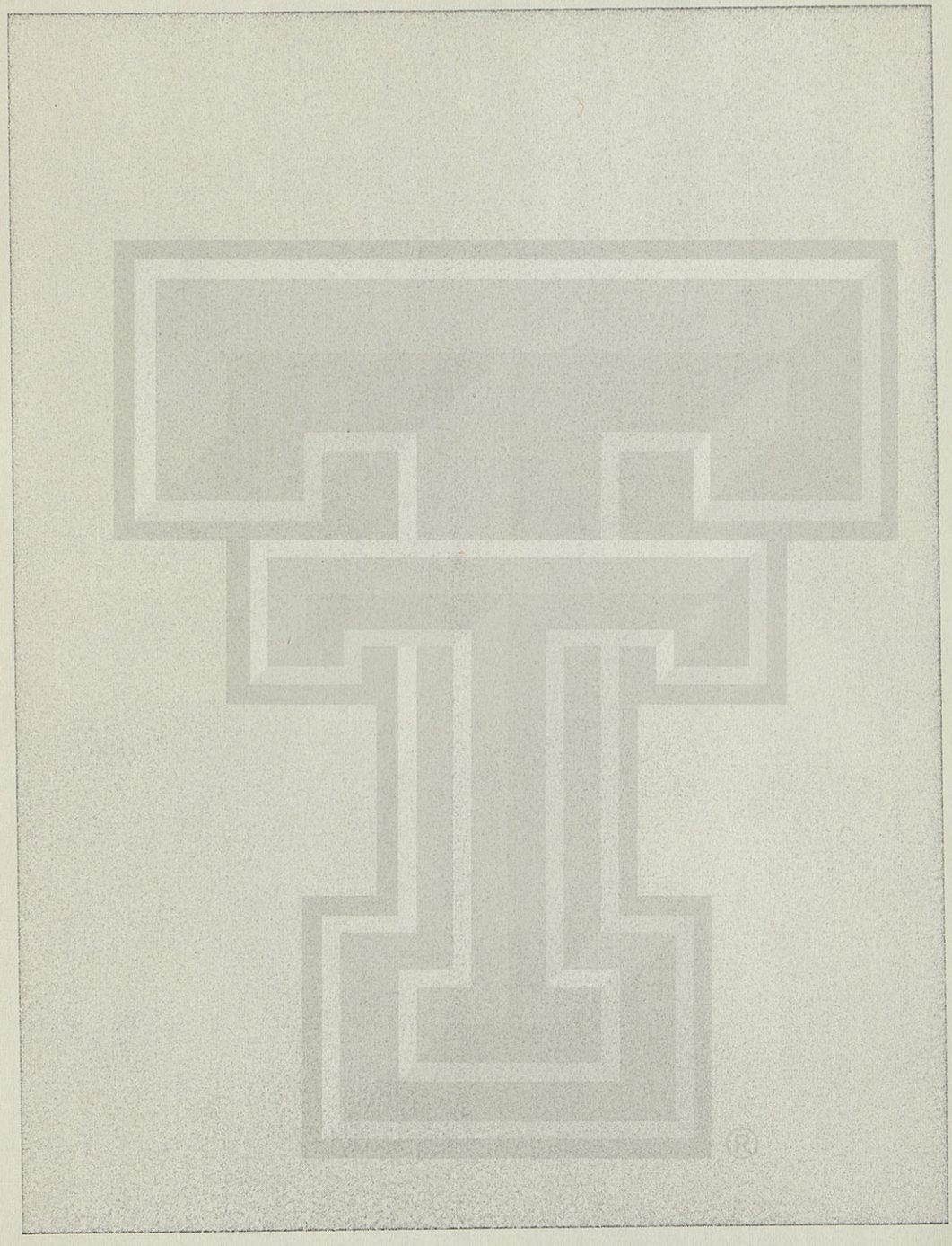

Fig. 4. A 10-sec exposure of the moonlit illuminated earth and the airglow layer.

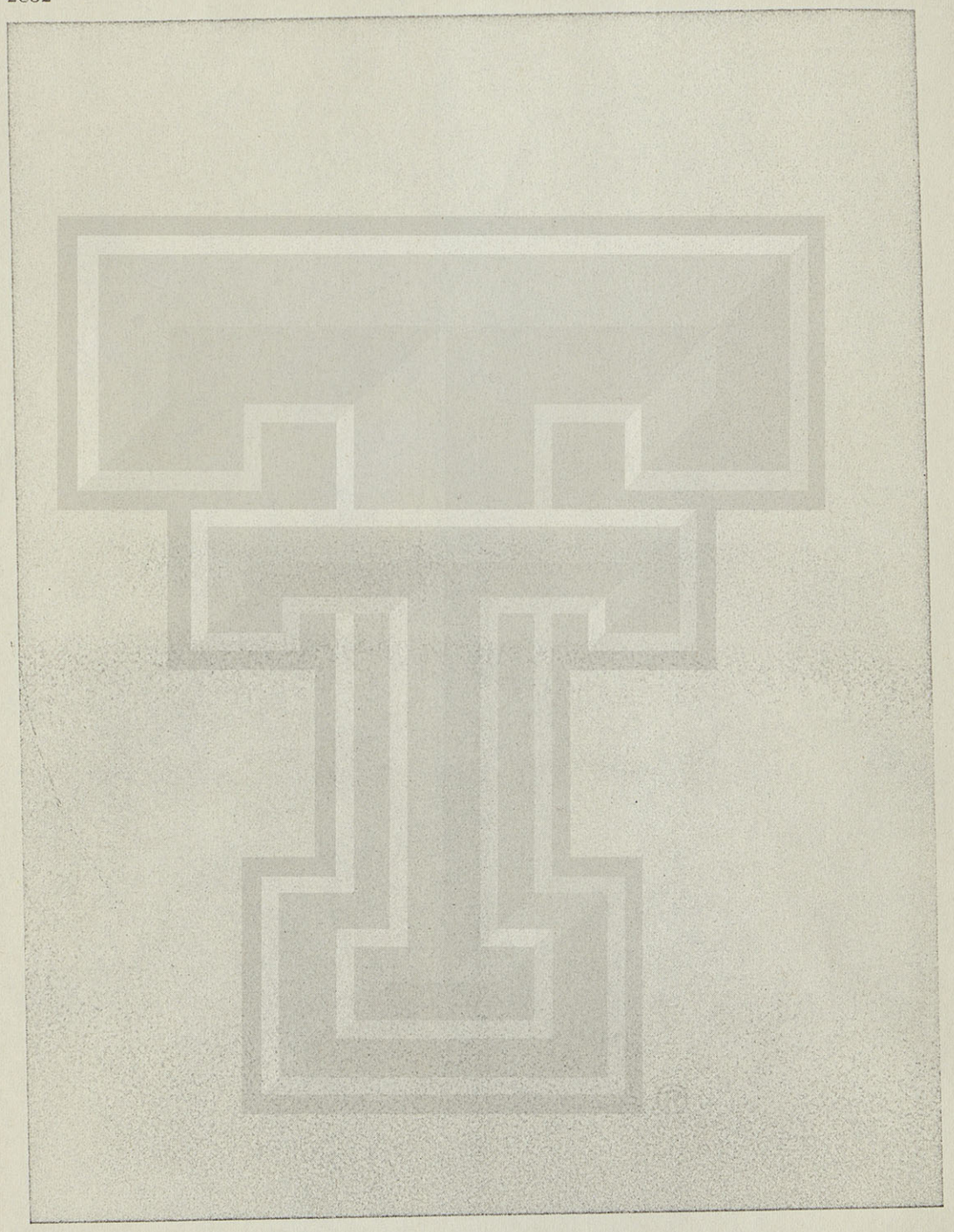

Fig. 5. A 2-min exposure smeared by spacecraft motion which was used for densitometry to determine the color of the airglow layer.

airglow layer and the earth is nearly as dark as the sky above the airglow layer.

Figure 5, a 2-min exposure, shows the smear associated with the longer exposures. This was the transparency densitometered to compare the color of the airglow and the moonlit earth.

Nine pictures could be used for measurement of height and width of the airglow layer. The data on these exposures are given in Table 1. These pictures covered times when the spacecraft altitude varied from 241 to 181 km above the surface and latitudes from 27° south to 8° north. In three of the photographs the lightning discharges were used to determine the horizon, and in the remainder the moonlit horizon was used. The height of the airglow layer so determined varied from 111 to 77 km, and the thickness of the layer measured to half intensity points was 24 ± 3 km. There appears to be a real change in height of the airglow layer during the experiment. It is impossible to say whether this change in height is due to a change in geographic position, local time, or latitude, although a change with latitude seems the most plausible. It should be pointed out that measurements of the height of the airglow layer by direct penetration with rocket-borne photometers have all been made at approximately the same latitude (33°N), i.e., the latitude of White Sands Proving Grounds [*Koomen et al.*, 1963].

In the preceding Mercury flight, Carpenter observed the airglow layer through a filter passing the green line of oxygen (5577 A) and concluded that a large fraction of the airglow was of this color. *Koomen et al.* [1963] subsequently published results from rocket flights which showed that only about a quarter of the airglow could arise from the green line. Densitometry of photograph 30 tends to support their conclusions. Because of the low exposures, it is not possible to give an accurate value for the ratio of green to blue, but it is possible to state categorically that the color of the airglow layer is not compatible with all 5577. Our densitometry would, however, be compatible with the value of 4 for the ratio of continuum to 5577 published by Koomen et al.

To get the absolute brightness of the airglow layer, it was necessary to use the observed brightness of the ground and cloud illuminated by the moon. While the pictures were taken, the moon was very nearly at third quarter. Using results of Rougier and Russell [*Kopal*, 1962] on brightness of the moon as function of phase and Fritz [*Danjon*, 1954, p. 732] on visual albedo of earth, clouds, and sky, we find that the observed brightness of airglow is about 3×10^3 10th mag. visual stars/deg^2 near 5400 A and 3.8×10^3 10th mag. photographic stars/deg^2 near 4200 A. This corresponds to zenith emission as seen from the ground of 0.4 R/A near 5400 A and 0.6 R/A near 4200 A.

TABLE 1. Pictures used for Geometrical Measurements

Picture No.	GMT*	Θ†	H‡, km	h§	λ‖	θ¶	Nominal Exposure Time
22	13h 42m 50s	3.62°	241	111	27°S	0.66°	30 sec
23	13h 43m 10s	3.26°	240	105	265°S	0.69°	10 sec
25	13h 46m 20s	3.00°	232	97	23°S	0.88°	30 sec
27	13h 49m 30s	2.26°	220	75	18°S	0.71°	120 sec
28	13h 50m 20s	2.40°	218	78	17°S	0.89°	30 sec
29	13h 50m 40s	2.41°	217	77	16.5°S	0.87°	10 sec
31	13h 55m 00s	2.66°	202	81	8°S	0.78°	30 sec
32	13h 55m 10s	2.65°	202	81	8°S	0.78°	10 sec
35	14h 01m 40s	3.20°	181	87	8°N	0.92°	10 sec
Avg.		2.86°		88		0.80°	

* Greenwich time.
† Θ is the angle between the earth's limb and the airglow line.
‡ H is the height of the spacecraft above the earth.
§ h is the height of the center of the airglow band.
‖ λ is the latitude at which the airglow is observed.
¶ θ is the angular width at half intensity of the airglow band.

An interesting and partly unsuspected result of the astronaut photographs is that more than 90 per cent of the light to which the film is sensitive arises in a layer less than 25 km thick. The principal airglow emission not at this altitude, namely the 6300 A line of atomic oxygen, does not contribute appreciably in our pictures. The 6300 A line could not arise in any intensity at 100 km because of the high collision frequency. The lifetime of the mestastable state for emission of 6300 A is 60 sec, and it is believed that 6300 A is emitted primarily at 400 km, where the time between collisions is approximately equal to the lifetime of the state.

The active layer of the atmosphere around 90 km, where we find the airglow maximum, has a number of interesting properties.

a. It is the region of emission of sodium *D* lines.

b. It is the region of emission of the 5577 A oxygen line.

c. It is the region in which the continuum airglow arises.

d. The atmospheric temperature probably reaches a minimum at this altitude.

e. Because of the temperature minimum, the region below this altitude must possess high winds, shear, and turbulence as shown by the twilight sodium experiments of *Blamont* [1959].

f. It is probably the region where the atomic oxygen number concentration reaches a maximum. It is possible that the atomic oxygen maximum is responsible for the emission of the light, clearly so in the case of 5577 A which probably arises from three-body collisions as *Chapman* [1931] suggested. The continuum emission may be a form of chemiluminescence produced by atomic oxygen.

It was originally suggested by *Link* [1933] that a layer of dust existed at approximately this same altitude. Several astronauts have observed that stars appeared to dim as they passed through the airglow layer. In two of our photographs a third-magnitude star passed through the airglow layer with no appreciable change in appearance. We feel it highly unlikely that the airglow layer contains a dust layer as well. In addition to the observations, we can make a physical argument that a dust layer should not form at these altitudes. It can be shown that the terminal velocity of particles of a few microns in diameter will be inversely proportional to the pressure in this region and that the fall velocity will be many centimeters per second. The dust should therefore not be affected by meteorological vertical motions and with a constant influx should distribute itself in constant mixing ratio with the air. The reason for the constant mixing ratio is that the number density is the flux divided by the fall velocity and the fall velocity is inversely proportional to the pressure.

To complement the astronaut's experiment, balloons carrying cameras were flown from Australia to photograph the zodiacal light and airglow. Comparison of the brightness of the airglow observed during Cooper's flight and during balloon flights, of which about thirty are available, shows that the airglow on the night of May 16 was less bright than the average. In future experiments of this type, we might expect to obtain airglow brightnesses approximately twice as great as that observed in MA-9.

Acknowledgments. We wish to express our appreciation to the Manned Spacecraft Program and especially to Dr. Jocelyn Gill for the help in carrying out this experiment. We would also like to thank Professor Victor Hopper and Mr. Jim Sparrow for making the balloon flights in Australia.

References

Blamont, J. E., Nuage artificiels de sodium. Vitesse du vent, turbulence et densité de la haute atmosphère, *Compt. Rend., 249,* 1248, 1959.

Carpenter, Malcolm Scott, J. A. O'Keefe, III, and Lawrence Dunkelman, Visual observations of nightglow from manned spacecraft, *Science, 138,* 978, 1962.

Chapman, S., Some phenomena of the upper atmosphere, *Proc. Roy. Soc. London, A, 132,* 353–374, 1931.

Danjon, André, Albedo, color, and polarization of the earth, in *The Earth as a Planet,* vol. 2 of *The Solar System,* edited by Gerard P. Kuiper, pp. 726–738, University of Chicago Press, Chicago, 1954.

Koomen, M. J., Irene S. Gulledge, D. M. Packer, and R. Tousey, Night airglow observations from orbiting spacecraft compared with measurements from rockets, *Science, 140,* 1087–1089, 1963.

Kopal, Zdenek, editor, *Physics and Astronomy of the Moon,* Academic Press, New York, p. 100, 1962.

Link, F., Photometric theory of lunar eclipses, *Comp. Rend., 196,* 251, 1933.

(Manuscript received March 30, 1964.)

JOURNAL OF GEOPHYSICAL RESEARCH VOL. 69, NO. 13 JULY 1, 1964

Middle Ultraviolet Day Radiance of the Atmosphere[1]

J. P. HENNES, W. B. FOWLER, AND L. DUNKELMAN

Goddard Space Flight Center, Greenbelt, Maryland

Abstract. The day radiance of the atmosphere has been measured, photoelectrically, at two middle ultraviolet wavelengths by rocket-borne photometers. Filters and collimators provided an effective field of view of 1.4×10^{-2} ster, and bandpasses of approximately 100 A at 2600 A and 230 A at 2200 A. At a height of 146 km, nadir radiance values of about 0.5 erg/sec cm^2 ster 100 A were obtained at both wavelengths. There is good agreement between the radiance values measured and those which have been calculated on the basis of single Rayleigh scattering in the presence of ozone. From the radiance data an atmospheric diffuse reflectivity of about 8×10^{-4} at 2600 A has been calculated. This can be contrasted with 1957 rocket observations of Mars and Jupiter which yielded albedos at 2700 A of 0.24 and 0.26, respectively.

Introduction. If the earth's sunlit side is viewed from space it exhibits a bright appearance in the visible part of the spectrum. In contrast, the appearance of the sunlit earth in the ultraviolet wavelength region below about 3100 A can be expected to be rather dim and relatively uniform. In the visible region the upward flux out of the atmosphere is made up of Rayleigh-scattered sunlight, sunlight reflected directly from clouds or from the earth's surface, light scattered from atmospheric dust, and a relatively small amount of resonant and fluorescent scattered sunlight or day airglow. In the middle ultraviolet region from 2100 to 3000 A, however, because of the totally absorbing ozone region from approximately 10 to 40 km, the day radiance will be produced only by Rayleigh scattering of sunlight in the thin upper atmosphere above the ozone region and by fluorescent scattered sunlight or ultraviolet dayglow. The combination of a thin atmosphere and strong ozone absorption produces a correspondingly low albedo. The absence of contributions from reflections by clouds and surface features and the strong wavelength dependence of Rayleigh scattering will produce a relatively uniform appearance.

The spherical albedo of a planet is the ratio of the total flux emitted in all directions by the planet to the total flux incident on the planet from the sun. Both quantities are being measured over the same wavelength interval. The earth's visual, spherical albedo has been experimentally determined, by studies of earth light on the moon, to range from 0.29 to 0.56, depending on the season and on which side of the earth is facing the moon. The average value of these visual albedos is given as 0.39–0.40 [*Danjon,* 1954; *Dzhasybekova et al.,* 1960]. The major part of the earth's visual albedo comes from contributions by reflection from clouds. If atmospheric scattering is considered separately, assuming no clouds, calculations [*Kano,* 1958] show the spectral albedos due to Rayleigh scattering to be: infrared region, 0.0075; visible region, 0.096; and near ultraviolet region, 0.23. The weighted sum of these various spectral albedos for a Rayleigh atmosphere is given as 0.066 by *Kano* [1958] for the entire spectral region $\lambda > 2900$ A and has been independently calculated by *Coulson* [1959] to be 0.069. The contribution in these spectral regions from airglow is negligible except over narrow wavelength intervals near the more pronounced dayglow emission lines. The uses and difficulties of dayglow measurements have been summarized recently by *Chamberlain* [1963].

The calculations which have been made for scattered solar radiation in the near ultraviolet have included multiple scatterings, ozone distributions, and upward and downward fluxes [*Sekera and Dave,* 1961*a*; *Larsen,* 1959].

In the middle ultraviolet region calculations have assumed single Rayleigh scattering with ozone absorption [*Ban,* 1962; *Hubbard,* 1963; *Green,* 1964] (W. C. Hrasky and T. B. McKee, private communication, 1964). Multiple scattering or fluorescence has not been included. The

[1] Presented at the Second Western National Meeting of the American Geophysical Union, December 27–29, 1962.

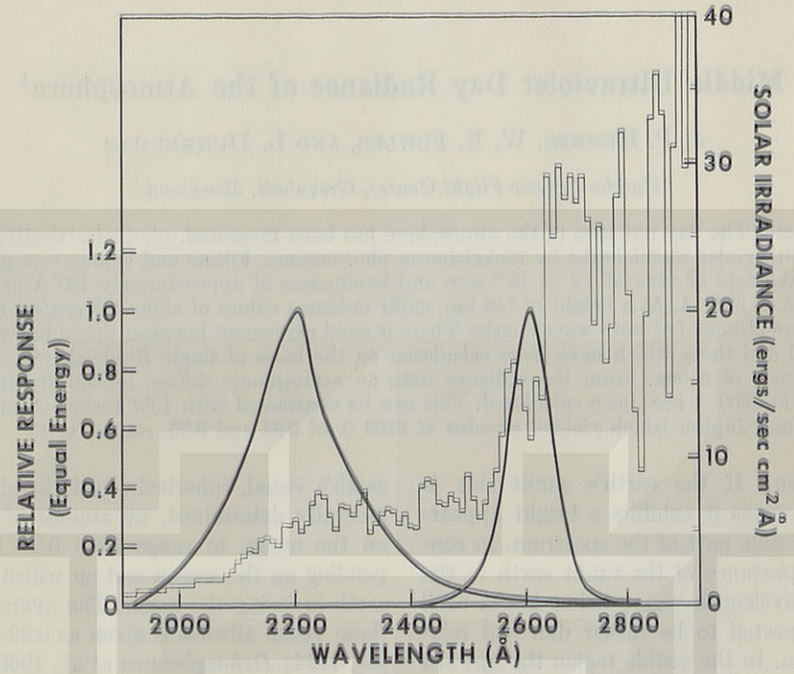

Fig. 1. Photometer response curves. Relative response of both photometers is shown on an equal energy basis. The solar spectrum, averaged over 10 A intervals, is also shown [*Wilson et al.*, 1954; *Malitson et al.*, 1960]. The 2200 A photometer response is provided by a combination of an interference filter and 4 mm $NiSO_4(H_2O)_6$ crystal. The 2600 A photometer combines an interference filter, Corning 7-54, 4 mm $NiSO_4(H_2O)_6$, Cation-X, and 2 mm Pb doped KCl : KBr crystal [*Childs*, 1961].

middle ultraviolet day radiance must originate in scattering above the ozone region. This insures a relatively small flux, since even the high-altitude ozone distribution is strongly absorbing in this spectral region. *Dalgarno* [1962, 1963] and *Chamberlain and Sobouti* [1962] have derived equations to show the effect of non-Rayleigh resonant and fluorescent scattering near atomic and molecular resonance lines, and point out that this effect could be significant in the ultraviolet where small Rayleigh-scattered fluxes are expected.

The experiment. At 1155 EST (1655 UT) on August 8, 1962, two middle ultraviolet photometers were included in an Aerobee rocket (NASA 4.60) launched from Wallops Island, Virginia. Measurements of the ultraviolet day radiance were taken continuously as the rocket climbed to a peak altitude of 150 km. Each photometer consisted of a mechanical collimator, a filter, and a photomultiplier sensitive only to ultraviolet radiation. The collimator produced an effective field of 1.4×10^{-2} ster (about a 7-deg square field). The filters were of the type described by *Childs* [1961]. The phototubes were type EMR 541F-05 photomultipliers with sapphire windows and cesium-tellurium cathodes [*Dunkelman et al.*, 1962].

The relative spectral response of these photometers is given in Figure 1 on an equal energy basis (amps/watt). Also included in Figure 1 is the solar spectrum, averaged over 10 A intervals, taken from data reported by *Wilson et al.* [1954] and *Malitson et al.* [1960]. The effective wavelengths of the photometers were at 2217 and 2610 A with effective bandwidths of 230 and 100 A, respectively.[2] The contribu-

[2] The effective wavelength λ_0 defined as

$$\lambda_0 = \int R(\lambda)\,\lambda\,d\lambda \Big/ \int R(\lambda)\,d\lambda$$

where $R(\lambda)$ is the relative spectral response of the photometer. The effective bandwidth W_0 is defined by the relation

$$W_0 R(\lambda_0) = \int R(\lambda)\,d\lambda$$

tion from the long wavelength region beyond 2800 A has been examined and found to be much less than the magnitudes of the radiance measurements made.

During the flight the rocket pitched through a wide range of zenith angles. Its motion, however, was confined by an attitude control system to a single plane having an azimuth of 175° passing through the zenith and the sun. The sun was at a zenith angle of 22°. The photometers, which were pointed out of the side of the rocket, toward the nose, approximately in the pitch plane and at an angle of 122° with the rocket axis, swept from the nadir up to a zenith angle of about 80° in both the north and south sky at various times.

Results. The data are shown in Figure 2; curve *a* gives the zenith angle of the photometers as a function of both flight time and altitude. The aspect data were obtained from solar sensing aspect cells, magnetometers, and the attitude control system error signals and pitch-rate signals. During the flight the rocket's attitude control system malfunctioned to the extent that, although controlled in two axes, the vehicle pitched through much larger angles than those for which the aspect instruments had been designed. Pitch-rate signals were integrated to find approximate zenith angles outside the region of aspect sensor operation. These calculations could be checked by fitting with the aspect signals as the rocket periodically moved back through the sensor region.

The photometer data, reduced from the original telemetry record at one-second intervals, are shown in curves *b* and *c*. Relative intensity is plotted, with the data normalized to unity for nadir (180°) values. The scatter in the relative intensity values is produced by photometer noise introduced because the signal level was near the bottom of a three-decade logarithmic scale. The photometer sensitivity in this exploratory measurement had been set low to avoid the possibility of saturation due to either unexpectedly

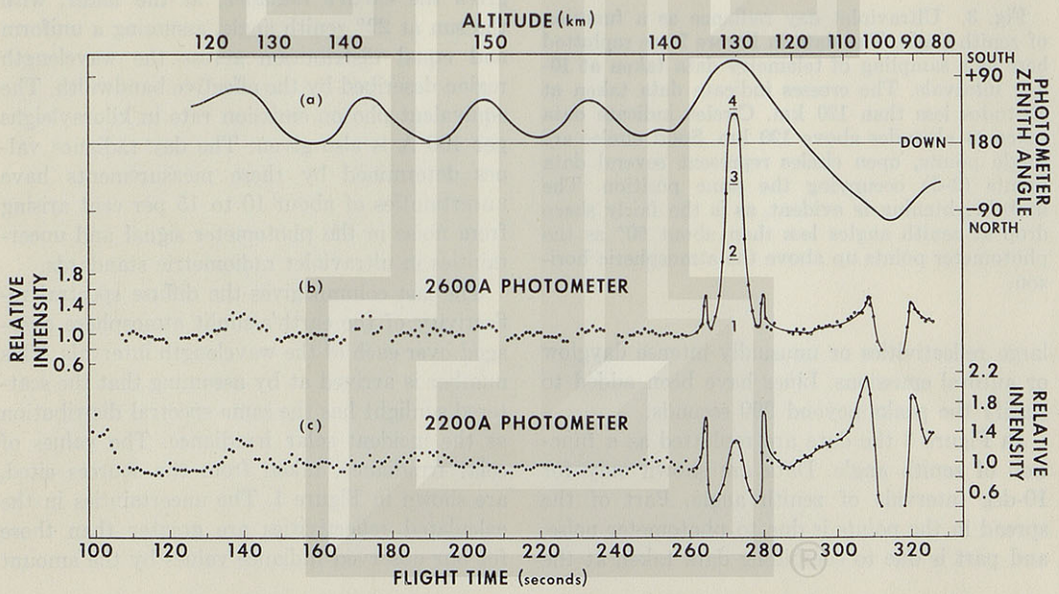

Fig. 2. Rocket flight data. Curve *a* is the zenith angle of the photometer direction as a function of time. Curves *b* and *c* are a sampling of the reduced telemetry data plotted in terms of the relative intensity received by the photometer. The points show scatter produced by photometer noise and a small amount of structure as a function of zenith angle. The peaks after 260 seconds correspond to the horizon limb brightening. The large peak at 273 seconds, which is extraneous, is produced by sunlight reflected off the photometer entrance with the photometers pointed above the horizon in the south. Without this sunlight effect the record would appear as it does at 310–320 seconds with the photometers pointed above the horizon in the north.

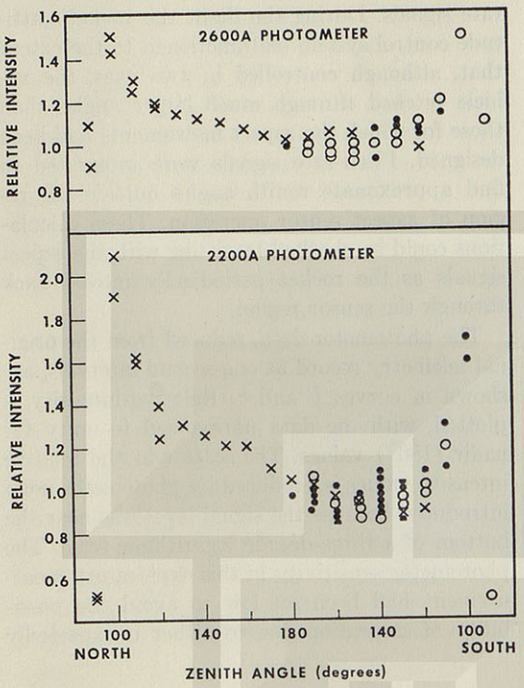

Fig. 3. Ultraviolet day radiance as a function of zenith angle. The data in Figure 2 are replotted here as a sampling of telemetry data taken at 10-deg intervals. The crosses indicate data taken at altitudes less than 120 km. Circles indicate data taken at altitudes above 120 km. Solid circles are single points, open circles represent several data points (2–5) occupying the same position. The limb brightening is evident, as is the fairly sharp drop at zenith angles less than about 90° as the photometer points up above the atmospheric horizon.

large reflectivities or unusually intense dayglow or auroral emissions. Lines have been added to clarify the peaks beyond 260 seconds.

In Figure 3 the data are replotted as a function of zenith angle. Data are shown only for 10-deg intervals of zenith angle. Part of the spread in the points is due to photometer noise, and part is due to combining data taken at the same zenith angles but from different altitudes.

The values of day radiance measured during this flight are notable for the lack of features seen over a large range of zenith angles. Even the horizon brightening is only a factor of 2 times the nadir radiance. The photometer field of 1.4×10^{-2} ster would, of course, diminish the effect of any increased radiance that extended over only a relatively narrow field.

The peaks at about 272 seconds in Figure 2 represent direct sunlight reflected off the photometer entrance. The photometer was pointed up in the southern sky at that point at a zenith angle of about 70 deg. The magnitude of the reflected solar signal under those conditions was determined by laboratory measurements to be about 10^{-5} that of direct sunlight. Note that this scattered light signal is still larger than the earth radiance signal. The problem of making measurements in the presence of direct sunlight is emphasized by this result.

The radiance values measured by the photometers are given in Table 1. The third column gives the earth's radiance, at the nadir, with the sun at 22° zenith angle, assuming a uniform and equal distribution across the wavelength region described by the effective bandwidth. The equivalent photon emission rate in kilorayleighs per 100 A is also given. The day radiance values determined by these measurements have uncertainties of about 10 to 15 per cent arising from noise in the photometer signal and uncertainties in ultraviolet radiometric standards.

The last column gives the diffuse spectral reflectivity of the earth's sunlit atmosphere averaged over each of the wavelength intervals. This number is arrived at by assuming that the scattered sunlight has the same spectral distribution as the incident solar irradiance. The values of solar irradiance, taken from the sources cited, are shown in Figure 1. The uncertainties in the calculated reflectivities are greater than those for our observed radiance values by the amount

TABLE 1. Ultraviolet Day Radiance Measurements of the Earth Taken August 8, 1962, at 146 km, with Photometers Pointed at the Nadir; Solar Zenith Angle 22°

Nominal Wavelength, A	Effective Bandwidth, A	Radiance, erg/sec cm² ster 100 A	Emission Rate, kilorayleigh/100 A	Diffuse Reflectivity
2600	100	0.5	8×10^{2}	8×10^{-4}
2200	230	0.5	7×10^{2}	3×10^{-3}

of uncertainty in published absolute spectral solar intensities. If we make the further assumption that the entire earth is a diffuse Lambert reflector, then the diffuse reflectivity of about 8×10^{-4} at 2600 A becomes the earth's spherical albedo. This number can be contrasted with the earth's total observable spherical albedo of 0.39–0.40, and with the calculated Rayleigh scattered albedo contribution in the near ultraviolet of 0.23 as given in the introduction.

Of interest also is a comparison of the earth's low middle ultraviolet effective albedo with measurements of the relatively high effective albedos of Mars and Jupiter made in 1957 with a photometer of about 300 A bandwidth centered at 2700 A [*Boggess and Dunkelman*, 1959]. They obtained values of about 0.24 for Mars and 0.26 for Jupiter.

We know of one other experimental observation of the middle ultraviolet day radiance. *Friedman et al.* [1963] have reported a satellite-borne photometer measurement of the day radiance with a spectral passband of 140 A centered at 2550 A. Their result, with the sun at a zenith angle of 49° and the detector pointed at the nadir with a field of 1.2×10^{-4} ster, showed an atmospheric radiance of 2.0 ± 0.3 ergs/sec cm^2 ster 100 A.

Table 2 gives the various measured and calculated middle ultraviolet day radiance values. The calculated values tend to support our results rather well. It should be kept in mind that the data were all taken or calculated using different parameters of altitude, solar zenith angle, ozone distribution, season, etc., so that the results cannot be compared too directly. The relatively large factor of 4 between the experimental results of Friedman et al. and ourselves is possibly explained by either a large change in the high-altitude ozone distribution between the time of the two measurements or the difficulties in maintaining calibration during the preparations for and launching of a satellite. The similarity of the various calculations and our measurements indicate that the simple approach to ultraviolet atmospheric radiance calculations, involving use of ozone distributions and single scattering with plane atmospheres [*Ban*, 1962; *Hubbard*, 1963; *Green*, 1964] or spherical atmospheres (Hrasky and McKee, private communication, 1964), is adequate for broad-band measurements. If higher spectral resolution were to be considered, the agreement might be strongly affected by resonant or fluorescent scattering.

The calculated results depend very strongly on ozone distribution, especially in the region around the peak of the ozone absorption curve at 2600 A, where the very high-altitude ozone has a dominant role. The ozone distribution at higher altitudes is relatively unknown, however,

TABLE 2. Comparison of Measured and Calculated Nadir Ultraviolet Day Radiance Values, Radiance in ergs/sec cm^2 ster 100 A

Source	2600 A Region: Average Radiance over Interval*	2600 A Region: Wavelengths, A	2200 A Region: Average Radiance over Interval*	2200 A Region: Wavelengths, A	Solar Zenith Angle
This work†	0.5	2560–2660	0.5	2100–2330	22°
Friedman et al. [1963]†	2.0	2480–2620			49°
Ban [1962]‡	0.5	2550–2650			0°
Hubbard [1963]‡	0.4§	2550–2650			0°
Green [1964]‡	0.5‖	2550–2650	0.7	2100–2330	0°
Hrasky and McKee, private communication‡	0.4	2550–2700	0.5	2000–2400	22°

* Values estimated or rounded off from data published by the referenced authors.

† Measured values.

‡ Calculated values.

§ A range of 0.05–0.8 is estimated, depending on the ozone distribution chosen. The radiance listed is taken from Figure 14, representing a 'standard' ozone curve.

‖ A range of 0.15–0.6 is estimated, depending on the ozone distribution chosen. The radiance listed is taken from Figure 6, representing an analytical fit to the same 'standard' ozone curve Hubbard used.

so that appreciable uncertainties may be introduced into the calculated values. At the shorter wavelength region around 2200 A and at longer wavelengths beyond 2800 A the ozone is much less absorbing, and incident solar radiation will penetrate more deeply into the atmosphere, thus permitting more scattering and producing higher albedos. By use of satellite-borne photometers with narrow spectral bandpasses, well removed from strong dayglow emission lines, and set at various middle ultraviolet wavelengths from 2100 and 3000 A, a profile of high-altitude ozone distribution should be obtainable. Such an idea was proposed in 1957 by *Singer and Wentworth* [1957], who considered only wavelengths at 2800 and 3000 A. *Twomey* [1961] carried out further calculations in this same wavelength region. The calculations in the near ultraviolet above 3000 A have been considered in detail by *Sekera and Dave* [1961*b*]. The altitudes above 50 km would require, however, use of wavelengths below 2800 A, where analysis should be much easier. The seasonal and latitudinal variations in upper-atmosphere ozone, so important to atmospheric heating processes, would thus be available.

Acknowledgment. We wish to express our appreciation to William Russell, Jr., of this Center who graciously provided support and the space for this experiment in one of the rockets under his supervision.

References

Ban, G. R., Scattered radiance in the middle ultraviolet region, in *Symposium on Military Applications of Ultraviolet Radiations, Rept. LAS-TR-199-37, Univ. Chicago, Lab. Appl. Sci.,* 1962.

Boggess, A., III, and L. Dunkelman, Ultraviolet reflectivities of Mars and Jupiter, *Astrophys. J., 129,* 236–237, 1959.

Chamberlain, J. W., Airglow and the physics of upper atmospheres, *Science, 142,* 921–924, 1963.

Chamberlain, J. W., and Y. Sobouti, Fluorescent scattering in planetary atmospheres, 1, Basic planetary considerations, *Astrophys. J., 135,* 925–937, 1962.

Childs, C. B., Broad band ultraviolet filters, *J. Opt. Soc. Am., 51,* 895–897, 1961.

Coulson, K. L., Characteristics of the radiation emerging from the top of a Rayleigh atmosphere, 2, Total upward flux and albedo, *Planetary Space Sci., 1,* 277–284, 1959.

Dalgarno, A., Spectral reflectivity of the earth's atmosphere, 3, The scattering of light by atomic systems, *Geophys. Corp. Am. Rept. 62-28-A,* 1962.

Dalgarno, A., Rayleigh scattering near an absorption line, *J. Opt. Soc. Am., 53,* 1222, 1963.

Danjon, A., Albedo, color, and polarization of the earth, in *The Earth as a Planet,* edited by G. P. Kuiper, pp. 726–738, University of Chicago Press, Chicago, 1954.

Dunkelman, L., W. B. Fowler, and J. P. Hennes, Spectrally selective photodetectors for the middle and vacuum ultraviolet, *Appl. Optics, 1,* 695–700, 1962.

Dzhasybekova, E. K., V. M. Kazachevskii, and A. V. Kharitonov, Determination of the earth's albedo, *Astron. Zh., 37,* 131–134, 1960 (translated in *Soviet Astron. AJ, 4,* 125–128, 1960).

Friedman, R. M., R. D. Rawcliffe, and G. E. Meloy, Radiance of the upper atmosphere in the middle ultraviolet, *J. Geophys. Res., 68,* 6419–6423, 1963.

Green, A. E. S., Attenuation by ozone and the earth's albedo in the middle ultraviolet, *Appl. Optics, 3,* 203–208, 1964.

Hubbard, E. L., Calculation of the intensity of light scattered in the atmosphere in the wavelength region 2300 A to 3100 A with absorption by oxygen and ozone considered, *Rept. LAS-TR-199-48, Univ. Chicago, Lab. Appl. Sci.,* September 1963.

Kano, M., The albedo of the earth's atmosphere, *Papers Meteorol. Geophys. Tokyo, 9*(2), 113–122, 1958.

Larsen, S. H. H., On the scattering of the ultraviolet solar radiation in the atmosphere with the ozone absorption considered, *Geofys. Publ., 21*(4), 1959.

Malitson, H. H., J. D. Purcell, R. Tousey, and C. E. Moore, The solar spectrum from 2635 to 2085 A, *Astrophys. J., 132,* 746–766, 1960.

Sekera, Z., and J. V. Dave, Diffuse transmission of solar ultraviolet radiation in the presence of ozone, *Astrophys. J., 133,* 210–227, 1961*a*.

Sekera, Z., and J. V. Dave, Determination of the vertical distribution of ozone from the measurement of diffusely reflected ultraviolet solar radiation, *Planetary Space Sci., 5,* 122–136, 1961*b*.

Singer, S. F., and R. C. Wentworth, A method for the determination of the vertical ozone distribution from a satellite, *J. Geophys. Res., 62,* 299–308, 1957.

Twomey, S., On the deduction of the vertical distribution of ozone by ultraviolet spectral measurements from a satellite, *J. Geophys. Res., 66,* 2153–2162, 1961.

Wilson, N. L., R. Tousey, J. D. Purcell, and F. S. Johnson, A revised analysis of the solar spectrum from 2990 to 2635 A, *Astrophys. J., 119,* 590–612, 1954.

(Manuscript received March 11, 1964.)

REPRINTED FROM:

SPACE RESEARCH III

PROCEEDINGS

OF THE THIRD INTERNATIONAL SPACE SCIENCE SYMPOSIUM

WASHINGTON, APRIL 30–MAY 9, 1962

EDITED BY

W. PRIESTER

1963

NORTH-HOLLAND PUBLISHING COMPANY—AMSTERDAM

MIDDLE ULTRAVIOLET PHOTOELECTRIC DETECTION TECHNIQUES

LAWRENCE DUNKELMAN, JOHN P. HENNES and WALTER B. FOWLER

Goddard Space Flight Center, National Aeronautics and Space Administration, Greenbelt, Md., USA

Abstract: Astronomical and geophysical observations from rockets in the ultraviolet region of the spectrum have been either spectral studies with dispersive optical systems or broad-band photometric measurements at particular wavelength regions of interest. In this paper non-dispersive optical techniques are described for the middle ultraviolet (3000–2000 Å). Band-pass (200–300 Å) and cut-off filters which may be used with conventional Cs-Sb photodetectors are described. When near ultraviolet and longer wavelength radiation must be rejected to a greater degree, higher work function "solar blind" photocathodes, such as the alkali tellurides, may be employed. These photodetectors, their calibration and applications are discussed.

Резюме: Астрономические и геофизические наблюдения с помощью ракет в ультрафиолетовой области спектра представляли собой или спектральные исследования при использовании дисперсионных оптических систем, или фотометрические измерения широких полос в длинах волн, которые представляли собой интерес. В данной работе описываются недесперсионные оптические приборы для среднего ультрафиолета (3000–2000 Å). Описываются полосы (200–300 Å) и порчи пропускания фильтров, которые можно использовать с Cs—Sb фотокатодами. Когда необходимо ослабить излучение в близком ультрафиолете или на большой длине волны, используются фотокатоды ("solar blind") с большой работой выхода, такие как щелочные теллуриды. Обсуждаются эти фотодетекторы, их калибровка и применение.

Optical measurements from rockets by the Goddard Space Flight Center have emphasized regions of the ultraviolet which cannot be observed from the ground due to absorption by the ozone layer located at about 25 km altitude. This and other absorbing layers block geophysical and astrophysical measurements at wavelengths shorter than 3000 Å. Measurements from rockets in the region below 3000 Å have been restricted to certain spectral bandpasses by limited development of filters and detectors. These ultraviolet wavelengths of interest may be divided into two regions: the middle and vacuum ultraviolet. In round numbers, the middle ultraviolet is from 3000 Å to 2000 Å. This paper will primarily be concerned with techniques of non-dispersive optics and will discuss filters, cathodes and calibration.

1. Filters

The variety of optical materials used in the visible part, of the spectrum is not available in the middle ultraviolet. Those materials which are useful can be put into three classes: long-wave pass filters which transmit all wavelengths longer than a short wavelength absorption edge; bandpass filters which transmit moderately well over broad regions of the middle ultraviolet; and absorption edge filters which have strong absorption over small wavelength intervals and are useful for producing sharp transmission cut-offs.

The first category of filter is used in photodetector envelopes, windows or trimmers to produce the short wavelength cut-off in spectral response. Fig. 1 shows materials which are available for such use. Corning 9700 glass,

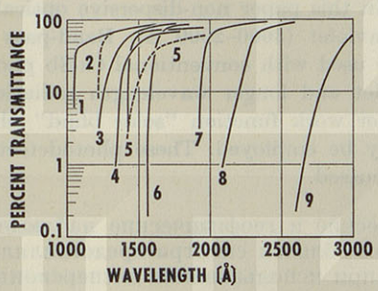

Fig. 1. Window transmittance cut-offs in the UV region. 1-LiF (1 mm); 2-CaF_2 (1 mm); 3-NaF (1 mm); 4-BaF_2 (1 mm); 5-sapphire (1 mm); 6-fused silica (1 mm); 7-$NiSO_4(H_2O)_6$ (3 mm); 8-Corning 7910 glass (9–54); Corning 9700 glass (2 mm). The two curves numbered 5 indicate the variation in UV transmission qualities of commercial materials.

with a transmittance of less than 0.05 % at 2537 Å, is useful for subtractive filter photometry such as with a low pressure mercury arc source. Corning 7910 (9–54), which is 96 % silica, is also useful for subtractive photometry techniques and can be compared with pure fused silica. The nickel sulfate hexahydrate crystal * is not strictly a cut-off filter since it has an absorption region from 3500–4500 Å. However its absorption edge at 1900 Å makes it a very useful solid for separating the middle from the vacuum ultraviolet, and it is included here for comparison.

The two curves marked 5 show different samples of commercial sapphire. The wide variation in ultraviolet transmittance is evident and indicates the problem which faces users of this material. The similar but smaller variations

* Supplied by Dr. W. R. McBride of the Naval Ordnance Test Station, China Lake, California.

in transmittance found in crystals shown in curves 1 to 4 are not found in the fused silica and other materials of curves 6 to 9. In choosing between fused silica (or cultured quartz) and sapphire as a phototube window, the advantages in transmission properties must be weighed along with those of sealing properties. For example, with fused silica a long graded seal is required while sapphire is readily sealed to glass without a graded seal.

Some of the curves in fig. 2 show the second category of filter materials,

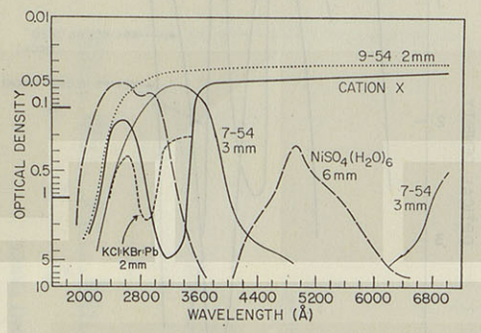

Fig. 2. Optical densities of typical samples of $NiSO_4(H_2O)_6$ crystal, KCl:KBr:Pb crystal, cation-X and Corning filters 9–54 and 7–54.

transmission bandpass. The $NiSO_4(H_2O)_6$ curve mentioned above is seen here to have two large transmission regions: one covering the middle ultraviolet; the other in the blue-green.

The dashed curve representing the optical density of a crystal of KCl:KBr doped with 0.05 % Pb is an example of an absorption edge filter and is shown more clearly in fig. 3. The very sharp absorption edges of these crystals can be used to produce equally sharp edges of transmission filters when combined with other materials. A useful variation in the wavelength of this edge can be achieved by varying the amounts of KBr and KCl in the crystal.

The narrow bandwidth multilayer dielectric interference filters of the visible and IR regions have not been generally available in the UV. In the last five years, however, rocket measurements have been made using several broad-band ultraviolet filters. One of these is the chemical filter described by Dunkelman and Field in 1955 [1]. The transmission of this filter, which was developed to replace the liquid "chemical" filters described by Kasha [2], is shown in fig. 6, curve 13, along with a variety of photosurfaces discussed in the next section. This filter, however, is unstable in direct sunlight and its use has been restricted to measurements of the night airglow and stellar fluxes.

In 1960 several filters were assembled at GSFC which were quite stable

and which have been used for measurements of both solar and stellar fluxes. These filters, described in a recent paper by Childs [3], are made up of the solid glasses and crystals shown in figs. 1–3. A typical filter is shown in figs. 4 and 5.

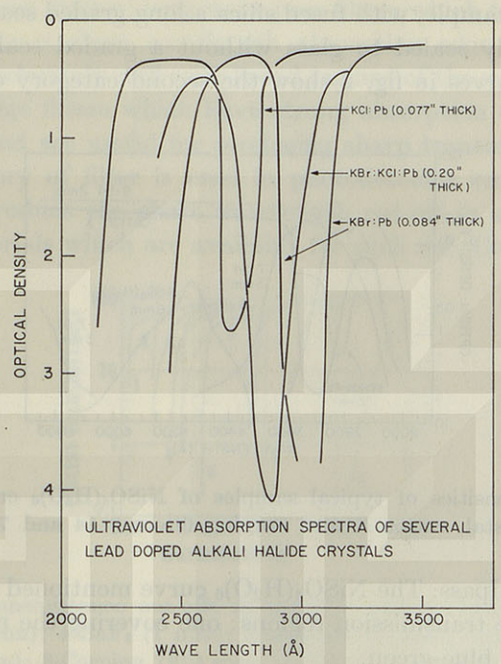

Fig. 3. Absorption curves showing how the absorption edge may be shifted from 2650 to 2900 Å by varying the amounts of KBr or KCl in the crystal.

Fig. 4 shows on a log scale the transmittance of a 2600 Å filter made up of lead doped KCl:KBr, a sheet of cation-X, a 3 mm crystal of nickel sulfate hexahydrate, a Corning 7–54 filter and a Corning 9–54 filter. This filter has an effective bandwidth of 200 Å and a peak transmittance of 23 %. Fig. 5 shows this filter normalized on a linear scale. The long wavelength and relatively minor "leaks" in these filters can be greatly reduced if necessary by using them with "solar blind" cathodes described below.

Broad-band interference filters for the middle ultraviolet can now be obtained commercially for wavelengths longer than 2100 Å. These are of the Fabry-Perot MDM type (metal-dielectric-metal). They have a 15 to 20 % peak transmittance with a 300 Å bandwidth at half peak. A somewhat narrower bandwidth can be obtained with lower peak transmission. For solar flux measurements selected optical materials described above have been

added to these interference filters for further trimming. Research on improved Fabry-Perot filters of the MDMDM type is being carried out by Turner [4] at Bausch and Lomb and Schroeder [5] at the University of Wisconsin. Here M represents aluminium and D a low index dielectric such as magnesium fluoride or chiolite (2 Na F · Al F_3).

Notable advances in multilayer interference filters have been reported abroad. Sokolova and Krylova [6] report an excellent transmission filter of ThO_2 and SiO_2 at wavelengths as short as 2200 Å. Sebire, Cojan, and

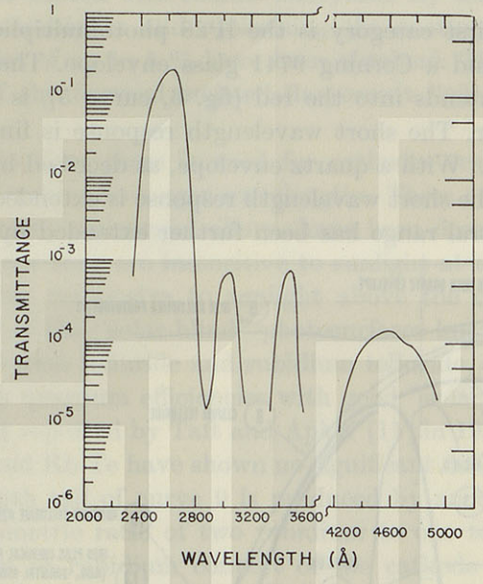

Fig. 4. Transmittance vs wavelength of a 2600 Å filter.

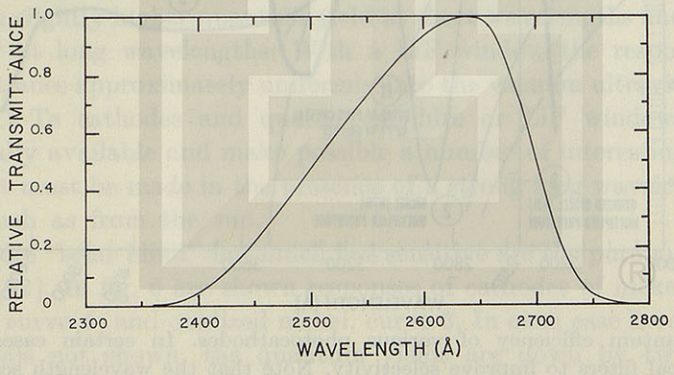

Fig. 5. Normalized transmittance of a 2600 Å filter.

Giacome [7] report a 2592 Å multilayer dielectric filter with 28 % peak transmission and 12 Å bandpass at half peak. Multilayers are of lead fluoride and cryolite ($Na_3Al\ F_6$).

2. Cathodes

Photocathodes can be divided into three spectral types. Those sensitive to both visible and ultraviolet wavelengths, those sensitive only to ultraviolet wavelengths below 3500 Å and those sensitive only to vacuum ultraviolet wavelengths.

Typical of the first category is the lP28 photomultiplier which contains a Cs-Sb cathode and a Corning 9741 glass envelope. The long wavelength response, which extends into the red (fig. 6, curve 5), is a property of the Cs-Sb photoemitter. The short wavelength response is limited by the glass envelope to 1800 Å. With a quartz envelope, as decribed by Dunkelman and Lock [8] in 1950, the short wavelength response is extended to below 1600 Å. Recently the spectral range has been further extended by means of a CaF_2

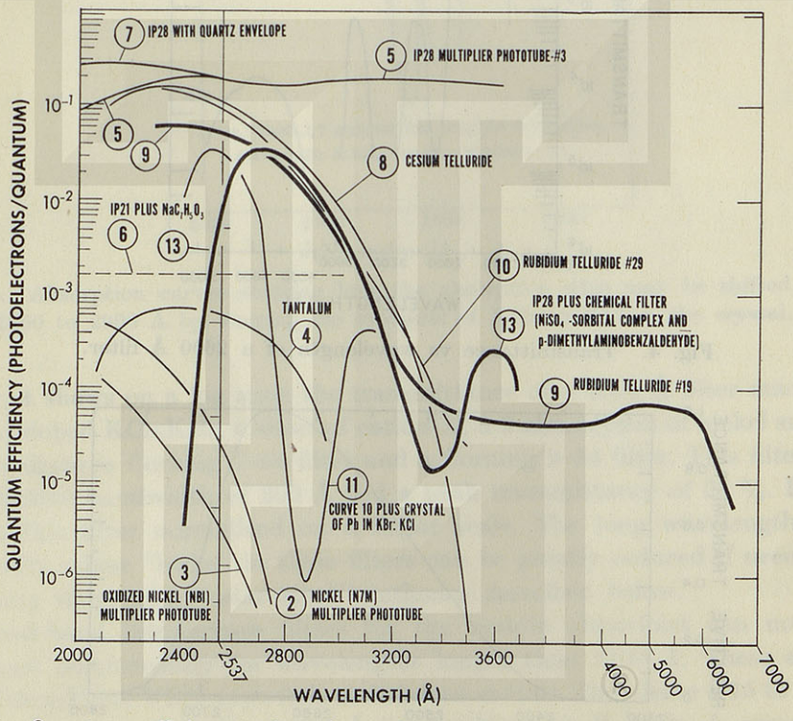

Fig. 6. Quantum efficiency of various photocathodes. In certain cases responses include optical filters to improve selectivity. Note that the wavelength scale changes at 4000 Å.

window. Such tubes have been studied at our laboratory [9], and the response found to be comparatively flat down to 1225 Å, the window cut-off.

Spectral response with more constant quantum efficiency can be obtained by coating the front face of a glass enveloped multiplier, such as the 1P21, with a layer of sodium salicylate ($NaC_7H_5O_3$). Sodium salicylate has been shown by Watanabe [10] to have a nearly constant quantum efficiency of fluorescence for excitation wavelengths from below 1000 Å to beyond 3000 Å; emission is in the blue-green. Curve 6 in fig. 6 shows a typical quantum efficiency of a 1P21 coated with sodium salicylate. By utilizing a high yield end-window photomultiplier and optimizing the coating thickness overall quantum efficiencies of up to 5 % have been obtained. The use of reflectors to collect some of the forward emitted fluorescent light can increase this figure somewhat.

For many applications there is need for cathodes responsive to middle ultraviolet but insensitive to longer wavelengths. These cathodes, which fall in the second category mentioned above, have been described by the term "solar blind" because they are insensitive to sunlight at the earth's surface. They are, of course, responsive to sunlight above the ozone layer.

The most useful of the "solar blind" photosurfaces known to date are the alkali tellurides. Cesium telluride and rubidium telluride, curves 8, 9 and 10 in fig. 6, offer high quantum efficiencies with good "solar blindness". These responses were first reported by Taft and Apker [11] in 1953. For the middle ultraviolet Cs-Te and Rb-Te have shown no significant difference in response. The long wavelength tail of curve 9 is produced by an excess of rubidium above the stoichiometric ratio of two rubidium to one tellurium atom. By varying the cesium or rubidium content of the cathode the manufacturer has some control over both the shape of the response curve in the 3000 Å region and the peak quantum yield. Increased proportions of cesium generally cause both slightly higher quantum yield at short wavelengths and increased sensitivity at long wavelengths. With a LiF window the response of the Cs-Te continues approximately uniformly into the vacuum ultraviolet. Tubes utilizing Cs-Te cathodes and quartz, sapphire or LiF windows are now commercially available and make possible a number of interesting measurements that must be made in the presence of a strong long wavelength background, such as from the sun.

Even more "solar blind" but much less sensitive are the pure metal photocathodes [12]. In fig. 6 are shown responses of cathodes of nickel, curve 2; tantalum, curve 4; and oxidized nickel, curve 3. In each case here, and with other metals not shown, the quantum yields are down by two or three decades from the alkali halide photosurfaces.

Applications using the second category of photocathodes described above often depend on selection of phototubes for "solar blindness" as well as quantum yield. One criterion for determining their merit is sensitivity to wavelengths below 2900 Å compared with the small but measurable response to sunlight. One such figure of merit, arbitrarily taken, is the irradiance at 2537 Å necessary to produce an anode current equal to that produced by full sunlight with skylight excluded. We have called this the "equivalent sunlight input." This measurement is admittedly not precise, since the intensity of short wavelength sunlight, to which the phototube is relatively most sensitive, depends on the altitude of the sun, the state of clarity of the sky and the amount of atmospheric ozone. Nevertheless, "equivalent sunlight input" has proved useful in comparing a wide variety of photodevices. Values for a number of cathodes are listed in table 1. Measurements were taken with the sun above 30 degrees altitude and with cloudless sky. The column to the right of the table lists the quantum efficiency at 2537 Å. Both the quantum efficiency and "solar blindness" should be considered,

TABLE 1

Solar blindness of various cathodes

Photo-cathode	Equivalent sunlight input * (watts of 2537 Å radiation/cm^2)	Quantum efficiency at 2537 Å	Remarks
Cs-Te	1.7×10^{-5}	5×10^{-2}	Semi-transparent cathode in a photodiode
Cs-Te	1.2×10^{-5}	2.7×10^{-2}	Semi-transparent cathode in a 14 stage photomultiplier
Cs-Te	8.5×10^{-6}	13×10^{-2}	Opaque cathode in a photodiode
Cs-Te	6.7×10^{-6}	1.4×10^{-2}	Semi-transparent cathode in a 14 stage photomultiplier
Ta	8×10^{-9}	6.5×10^{-4}	Opaque cathode in a photodiode
Oxidized Ni	6×10^{-9}	3.5×10^{-4}	Opaque cathode in a 9 stage photomultiplier
Ag	3×10^{-9}	1.5×10^{-5}	Opaque cathode in a 9 stage photomultiplier
Ni	1×10^{-9}	5×10^{-6}	Opaque cathode in a 9 stage photomultiplier
Cu Gauze	2×10^{-11}	2.8×10^{-7}	Photon counter

* Watts/cm^2 of 2537 Å radiation to give detector signal equal to signal produced by exposing detector to full sunlight (less sky background).